VOLUME 85 NO. ST8
OCTOBER 1959

# JOURNAL of the

# *Structural Division*

---

*PROCEEDINGS OF THE*


AMERICAN SOCIETY
OF CIVIL ENGINEERS

## BASIC REQUIREMENTS FOR MANUSCRIPTS

This Journal represents an effort by the Society to deliver information to the reader with the greatest possible speed. To this end the material herein has none of the usual editing required in more formal publications.

Original papers and discussions of current papers should be submitted to the Manager of Technical Publications, ASCE. Authors should indicate the technical division to which the paper should be referred. The final date on which a discussion should reach the Society is given as a footnote with each paper. Those who are planning to submit material will expedite the review and publication procedures by complying with the following basic requirements:

1. Titles should have a length not exceeding 50 characters and spaces.

2. A 50-word summary should accompany the paper.

3. The manuscript (a ribbon copy and two copies) should be double-spaced on one side of 8½-in. by 11-in. paper. Papers that were originally prepared for oral presentation must be rewritten into the third person before being submitted.

4. The author's full name, Society membership grade, and footnote reference stating present employment should appear on the first page of the paper.

5. Mathematics are reproduced directly from the copy that is submitted. Because of this, it is necessary that capital letters be drawn, in black ink, ⅛-in. high (with all other symbols and characters in the proportions dictated by standard drafting practice) and that no line of mathematics be longer than 6½-in. Ribbon copies of typed equations may be used but they will be proportionately smaller on the printed version.

6. Tables should be typed (ribbon copies) on one side of 8½-in. by 11-in. paper with a 6½-in. by 10½-in. invisible frame. Small tables should be grouped within this frame. Specific reference and explanation should be made in the text for each table.

7. Illustrations should be drawn in black ink on one side of 8½-in. by 11-in. paper within an invisible frame that measures 6½-in. by 10½-in.; the caption should also be included within the frame. Because illustrations will be reduced to 69% of the original size, the capital letters should be ⅛-in. high. Photographs should be submitted as glossy prints in a size that is less than 6½-in. by 10½-in. Explanations and descriptions should be made within the text for each illustration.

8. Papers should average about 12,000 words in length and should be no longer than 18,000 words. As an approximation, each full page of typed text, table, or illustration is the equivalent of 300 words.

Further information concerning the preparation of technical papers is contained in the "Technical Publications Handbook" which can be obtained from the Society.

---



This Journal is published monthly by the American Society of Civil Engineers. Publication office is at 2500 South State Street, Ann Arbor, Michigan. Editorial and General Offices are at 33 West 39 Street, New York 18, New York. $4.00 of a member's dues are applied as a subscription to this Journal. Second-class postage paid at Ann Arbor, Michigan.

Subject and author indexes, with abstracts, are published at the end of each year for the Proceedings of ASCE. The index for 1958 was published as Proc. Paper 1891; indexes for previous years are also available.

Journal of the

STRUCTURAL DIVISION

Proceedings of the American Society of Civil Engineers



CONTENTS

October, 1959

Papers

| | Page |
|---|---|
| Matrix Solution of Beams with Variable Moments of Inertia by Ming L. Pei | 1 |
| Reinforced Concrete Folded Plate Construction by Charles S. Whitney, Boyd G. Anderson and Harold Birnbaum | 15 |
| Laterally Deflected Columns by John Sherman | 45 |
| Theory and Test Results on the Fatigue of Metals by F. Stuessi | 65 |
| Bending Moments on Shell Boundaries by H. H. Bleich and M. G. Salvadori | 91 |
| The Design of Folded Plates by Eliahu Traum | 103 |
| Alpha-Gamma "Hot" Cells for Entry by Personnel by John M. Ruddy | 125 |
| Discussion | 135 |

Journal of the
STRUCTURAL DIVISION
Proceedings of the American Society of Civil Engineers

# MATRIX SOLUTION OF BEAMS WITH VARIABLE MOMENTS OF INERTIA

Ming L. Pei,[1] M. ASCE

## SYNOPSIS

Using finite differences and matrix algebra, new formulas are developed which permit the direct computation of bending moments, moment influence coefficients, deflections, and deflection influence coefficients of simply supported beams with variable moments of inertia. These formulas are explicit in the desired quantities and are especially suitable for use in digital computer programs.

## I. Matrix Formula for Bending Moment

Consider a simply supported beam subjected to an arbitrary transverse loading function $q = q(x)$, as shown in Fig. 1. The bending moment in the beam, $M = M(x)$, is governed by the differential equation,

$$\frac{d^2M}{dx^2} = q \tag{1}$$

together with the two boundary conditions,

$$\begin{aligned} &\text{at} \quad x = 0, \qquad M = 0 \\ &\text{at} \quad x = L, \qquad M = 0 \end{aligned} \tag{2}$$

Let us divide the span length L of the beam into n equal intervals of h each; and designate the equally spaced points as Points 0, 1, 2, 3, . . . n-2, n-1, and n. Points 0 and n are at the left and right support respectively. Eq. (1) may be expanded into finite difference equations.

Note: Discussion open until March 1, 1960. To extend the closing date one month, a written request must be filed with the Executive Secretary, ASCE. Paper 2218 is part of the copyrighted Journal of the Structural Division, Proceedings of the American Society of Civil Engineers, Vol. 85, No. ST 8, October, 1959.

1. Associate Prof., The City College, New York, N. Y.

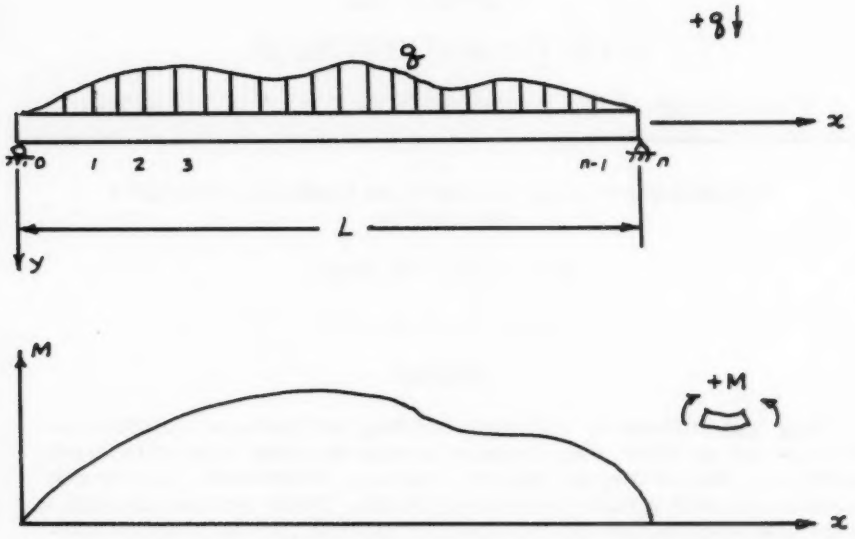


FIG 1

$$\frac{M_{i-1} - 2M_i + M_{i+1}}{h^2} = q_i$$

One such equation may be written for each of the points 1, 2, . . . , n-1, giving a total of n-1 equations.

$$M_{i-1} - 2M_i + M_{i+1} = q_i h^2 \qquad i = 1,2,3,..,n-1 \qquad (3)$$

The boundary equations become,

$$M_0 = 0 \quad \text{and} \quad M_n = 0 \qquad (4)$$

After substitution of Eq. (4) into Eq. (3) in order to eliminate $M_0$ and $M_n$, we have n-1 simultaneous linear algebraic equations containing n-1 unknown moments $M_i$. Writing out these equations in full, we have,

$$
\begin{aligned}
-2M_1 + M_2 &= q_1h^2 \\
M_1 - 2M_2 + M_3 &= q_2h^2 \\
M_2 - 2M_3 + M_4 &= q_3h^2 \\
&\cdots\cdots\cdots\cdots \\
&\cdots\cdots\cdots\cdots \\
M_{n-3} - 2M_{n-2} + M_{n-1} &= q_{n-2}h^2 \\
M_{n-2} - 2M_{n-1} &= q_{n-1}h^2
\end{aligned}
\tag{5}
$$

The set of n-1 simultaneous equations can be condensed into a single matrix equation.

$$[B][M] = [Q] \tag{6}$$

where [B] is a square matrix and M and Q are two column matrices, defined by the following:

$$[B] = \frac{1}{h}\begin{bmatrix} -2 & 1 & & & & \\ 1 & -2 & 1 & & & \\ & 1 & -2 & 1 & & \\ & & \cdots\cdots & & & \\ & & & \cdots\cdots & & \\ & & & & 1 & -2 & 1 \\ & & & & & 1 & -2 \end{bmatrix} \tag{7}$$

$$[M] = \begin{bmatrix} M_1 \\ M_2 \\ M_3 \\ \cdot \\ \cdot \\ \cdot \\ M_{n-1} \end{bmatrix} \tag{8}$$

$$[Q] = h\begin{bmatrix} q_1 \\ q_2 \\ q_3 \\ \cdot \\ \cdot \\ \cdot \\ q_{n-1} \end{bmatrix} \tag{9}$$

The basic differential equation (1) together with the boundary conditions (2) are now replaced by a single matrix equation (6). To solve Eq. (6) for the moment matrix M, we pre-multiply both side of the equation by the inverse of matrix [ B ].

$$[B]^{-1}\,[B][M] = [B]^{-1}[\,Q\,]$$

or,
$$[M] = [B]^{-1}[\,Q\,] \tag{10}$$

As the matrix $[B]^{-1}$ appears frequently in the following paragraphs, we shall designate it as matrix A.

$$[M] = [A][Q] \tag{11}$$

The matrix A is independent of the load matrix Q, and can be evaluated once and for all. In fact, it is easy to show by matrix algebra that matrix A is given by the following:

$$[A] = \frac{h}{n}\begin{bmatrix} n-1 & n-2 & n-3 & \cdots & 3 & 2 & 1 \\ & 2(n-2) & 2(n-3) & \cdots & 6 & 4 & 2 \\ & & 3(n-3) & \cdots & 9 & 6 & 3 \\ & & & \cdots\cdots & & & \\ & & & \cdots\cdots & & & \\ & \text{symmetrical} & & & & 2(n-2) & n-2 \\ & & & & & & n-1 \end{bmatrix} \tag{12}$$

In particular, matrix A for three different n values are given below.

For n = 5,
$$[A] = \frac{h}{5}\begin{bmatrix} 4 & 3 & 2 & 1 \\ 3 & 6 & 4 & 2 \\ 2 & 4 & 6 & 3 \\ 1 & 2 & 3 & 4 \end{bmatrix}$$

For n = 6,
$$[A] = h/6\begin{bmatrix} 5 & 4 & 3 & 2 & 1 \\ 4 & 8 & 6 & 4 & 2 \\ 3 & 6 & 9 & 6 & 3 \\ 2 & 4 & 6 & 8 & 4 \\ 1 & 2 & 3 & 4 & 5 \end{bmatrix}$$

For n = 10,
$$[A] = h/10\begin{bmatrix} 9 & 8 & 7 & 6 & 5 & 4 & 3 & 2 & 1 \\ 8 & 16 & 14 & 12 & 10 & 8 & 6 & 4 & 2 \\ 7 & 14 & 21 & 18 & 15 & 12 & 9 & 6 & 3 \\ 6 & 12 & 18 & 24 & 20 & 16 & 12 & 8 & 4 \\ 5 & 10 & 15 & 20 & 25 & 20 & 15 & 10 & 5 \\ 4 & 8 & 12 & 16 & 20 & 24 & 18 & 12 & 6 \\ 3 & 6 & 9 & 12 & 15 & 18 & 21 & 14 & 7 \\ 2 & 4 & 6 & 8 & 10 & 12 & 14 & 16 & 8 \\ 1 & 2 & 3 & 4 & 5 & 6 & 7 & 8 & 9 \end{bmatrix}$$

Eq. (11) is the general solution of the bending moment of a simple beam in matrix form. Given any loading condition, the multiplication of the two known matrices A and Q gives at once the values of the bending moments at the n-1 equally spaced points along the beam. Eq. (11) is not a new method to be learned and mastered, but is a formula explicit in the unknown bending moments.

When the load function is a series of concentrated loads, it is represented exactly by the load matrix Q. In this case, Eq. (11) gives the exact solution of moments in the beam. When the load function cannot be represented exactly by the load matrix Q, i.e., as in the case of a nonuniformly distributed load, the bending moments obtained by Eq. (11) are only approximate. The approximation, of course, can be improved without limit by choosing larger values of n.

Example 1

Compute the bending moments of a simple beam due to the set of loads shown in Fig. 2.

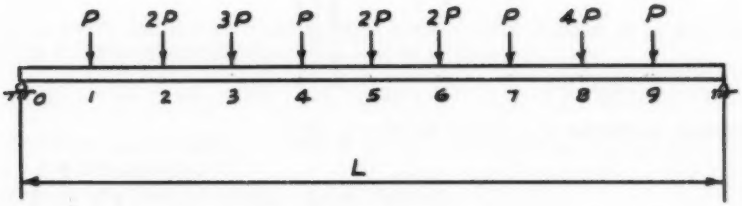


FIG 2

The element in the load matrix Q, qh, represents the magnitude of the concentrated load in the interval h.

$$[Q] = P\begin{bmatrix} 1 \\ 2 \\ 3 \\ 1 \\ 2 \\ 2 \\ 1 \\ 4 \\ 1 \end{bmatrix}$$

From Eq. (11), we have,

$$[M] = [A][Q] = Ph/n \begin{bmatrix} 9 & 8 & 7 & 6 & 5 & 4 & 3 & 2 & 1 \\ 8 & 16 & 14 & 12 & 10 & 8 & 6 & 4 & 2 \\ 7 & 14 & 21 & 18 & 15 & 12 & 9 & 6 & 3 \\ 6 & 12 & 18 & 24 & 20 & 16 & 12 & 8 & 4 \\ 5 & 10 & 15 & 20 & 25 & 20 & 15 & 10 & 5 \\ 4 & 8 & 12 & 16 & 20 & 24 & 18 & 12 & 6 \\ 3 & 6 & 9 & 12 & 15 & 18 & 21 & 14 & 7 \\ 2 & 4 & 6 & 8 & 10 & 12 & 14 & 16 & 8 \\ 1 & 2 & 3 & 4 & 5 & 6 & 7 & 8 & 9 \end{bmatrix} \begin{bmatrix} 1 \\ 2 \\ 3 \\ 1 \\ 2 \\ 2 \\ 1 \\ 4 \\ 1 \end{bmatrix}$$

$$= \frac{PL}{n^2} \begin{bmatrix} 9+16+21+6+10+8+3+8+1 \\ 8+32+42+12+20+16+6+16+2 \\ 7+28+63+18+30+24+9+24+3 \\ 6+24+54+24+40+32+12+32+4 \\ 5+20+45+20+50+40+15+40+5 \\ 4+16+36+16+40+48+18+48+6 \\ 3+12+27+12+30+36+21+56+7 \\ 2+8+18+8+20+24+14+64+8 \\ 1+4+9+4+10+12+7+32+9 \end{bmatrix} = PL/100 \begin{bmatrix} 82 \\ 154 \\ 206 \\ 228 \\ 240 \\ 232 \\ 204 \\ 166 \\ 88 \end{bmatrix}$$

**Example 2**

Compute the bending moments in a simple beam due to a uniformly distributed load q applied over the entire beam. In this case the load matrix is simply the following.

$$[Q] = qh \begin{bmatrix} 1 \\ 1 \\ 1 \\ 1 \\ 1 \\ 1 \\ 1 \\ 1 \\ 1 \end{bmatrix}$$

The bending moments are computed by Eq. (11).

$$[M] = [A][Q] = qh^2/n \begin{bmatrix} 9 & 8 & 7 & 6 & 5 & 4 & 3 & 2 & 1 \\ 8 & 16 & 14 & 12 & 10 & 8 & 6 & 4 & 2 \\ 7 & 14 & 21 & 18 & 15 & 12 & 9 & 6 & 3 \\ 6 & 12 & 18 & 24 & 20 & 16 & 12 & 8 & 4 \\ 5 & 10 & 15 & 20 & 25 & 20 & 15 & 10 & 5 \\ 4 & 8 & 12 & 16 & 20 & 24 & 18 & 12 & 6 \\ 3 & 6 & 9 & 12 & 15 & 18 & 21 & 14 & 7 \\ 2 & 4 & 6 & 8 & 10 & 12 & 14 & 16 & 8 \\ 1 & 2 & 3 & 4 & 5 & 6 & 7 & 8 & 9 \end{bmatrix} \begin{bmatrix} 1 \\ 1 \\ 1 \\ 1 \\ 1 \\ 1 \\ 1 \\ 1 \\ 1 \end{bmatrix}$$

$$= qL^2/100 \begin{bmatrix} 45 \\ 80 \\ 105 \\ 120 \\ 125 \\ 120 \\ 105 \\ 80 \\ 45 \end{bmatrix}$$

It can easily be verified that the elements in the moment matrix M are the exact bending moments at the nine points.

## II. Moment Influence Coefficient Matrix

The moment influence coefficient, $a_{ij}$, is defined as the bending moment in

the beam at Point i, due to a unit load applied at Point j. If the beam is divided into n equal segments, there will be $(n-1)^2$ of these coefficients. Arranging them in a square array, we have the moment influence coefficient matrix. To compute these coefficient, we apply unit load at Points 1, 2, 3, . . . successively. Carrying out the computation in one operation, we use a unit matrix as the load matrix.

$$[Q] = [I] = \begin{bmatrix} 1 & & & & & & & & 0 \\ & 1 & & & & & & & \\ & & 1 & & & & & & \\ & & & 1 & & & & & \\ & & & & 1 & & & & \\ & & & & & 1 & & & \\ & & & & & & 1 & & \\ & & & & & & & 1 & \\ 0 & & & & & & & & 1 \end{bmatrix}$$

By Eq. (11), we compute the moment influence coefficient matrix.

$$[M] = [A][Q] = [A][I] = [A] \tag{13}$$

Thus it is seem that the moment influence coefficient matrix is simply equal to matrix A. For example, the third row of matrix A,

$$[7 \quad 14 \quad 21 \quad 18 \quad 15 \quad 12 \quad 9 \quad 6 \quad 3]\ L/100$$

gives the bending moments at Point 3 due to a unit load applied at Points 1, 2, 3, . . . . 9 successively.

Matrix A is a symmetrical matrix. That is,

$$a_{ij} = a_{ji} \tag{14}$$

This is a direct consequence of the Maxwell's Reciprocal Theorem which states that "the moment at i due to a unit load at j is equal to the moment at j due to a unit load at i."

The moment influence coefficient matrix of a simple beam may be useful in the analysis of truss members under live loads,(5) in which case the panel length of the truss should be taken as h.

## III. Matrix Formula for Deflections

The deflection, y of a simple beam with variable moments of inertia is governed by (see Fig. 1),

$$\frac{d^2y}{dx^2} = \frac{M}{EI} \tag{15}$$

$$\begin{aligned} &\text{at} \quad x = 0, \quad && y_o = 0 \\ &\text{at} \quad x = L, \quad && y_n = 0 \end{aligned} \tag{16}$$

Again expanding Eq. (15) into finite difference equations and taking into consideration of Eq. (16), we have,

$$y_{i-1} - 2y_i + y_{i+1} = \frac{M_i}{EI_i} h^2 \qquad i=1, 2, .., n-1 \tag{17}$$

The n-1 equations in Eq. (17) are condensed into one matrix equation.

$$[B][Y] = [Mh/EI] \tag{18}$$

where matrix B has been defined previously by Eq. (7). The deflection matrix and the [Mh/EI] are both column matrices.

$$[Y] = \begin{bmatrix} y_1 \\ y_2 \\ . \\ . \\ . \\ y_{n-1} \end{bmatrix} \tag{19}$$

$$[Mh/EI] = \begin{bmatrix} M_1/EI_1 \\ M_2/EI_2 \\ .... \\ .... \\ .... \\ M_{n-1}/EI_{n-1} \end{bmatrix} \tag{20}$$

The elements of the matrix [Mh/EI] represent the area of the familiar M/EI diagram within the interval h. Solving Eq. (18) for the deflections, as have,

$$[Y] = [A][Mh/EI] \tag{21}$$

where matrix A is the same matrix previously defined by Eq. (12). With Eq. (21), one can compute the deflections by direct substitution.

Example 3

Compute the deflections of a simple beam with constant moment of inertia subjected to two equal and opposite moments applied at its ends.

$$[Mh/EI] = \begin{bmatrix} 1 \\ 1 \\ 1 \\ 1 \\ 1 \\ 1 \\ 1 \\ 1 \\ 1 \end{bmatrix} M_o/EI$$

$$[Y] = [A][M_h/EI] = \begin{bmatrix} 9 & 8 & 7 & 6 & 5 & 4 & 3 & 2 & 1 \\ 8 & 16 & 14 & 12 & 10 & 8 & 6 & 4 & 2 \\ 7 & 14 & 21 & 18 & 15 & 12 & 9 & 6 & 3 \\ 6 & 12 & 18 & 24 & 20 & 16 & 12 & 8 & 4 \\ 5 & 10 & 15 & 20 & 25 & 20 & 15 & 10 & 5 \\ 4 & 8 & 12 & 16 & 20 & 24 & 18 & 12 & 6 \\ 3 & 6 & 9 & 12 & 15 & 18 & 21 & 14 & 7 \\ 2 & 4 & 6 & 8 & 10 & 12 & 14 & 16 & 8 \\ 1 & 2 & 3 & 4 & 5 & 6 & 7 & 8 & 9 \end{bmatrix} \begin{bmatrix} 1 \\ 1 \\ 1 \\ 1 \\ 1 \\ 1 \\ 1 \\ 1 \\ 1 \end{bmatrix} \frac{h}{n} \frac{M_o h}{E I}$$

$$[Y] = M_o L^2/10^3 EI \begin{bmatrix} 45 \\ 80 \\ 105 \\ 120 \\ 125 \\ 120 \\ 105 \\ 80 \\ 45 \end{bmatrix}$$

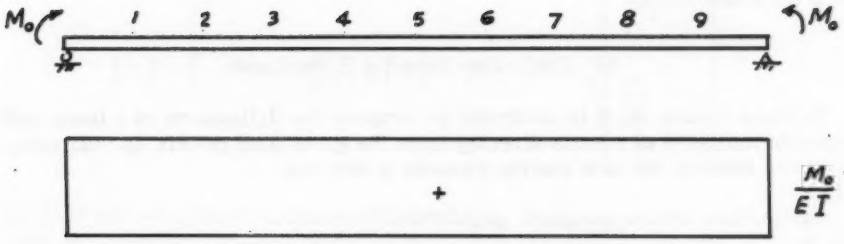


FIG 3

Example 4

Calculate the deflections at nine points along the beam carrying the loads as shown in Ex. 1. The flexural rigidity of the beam is given in Fig. 4.

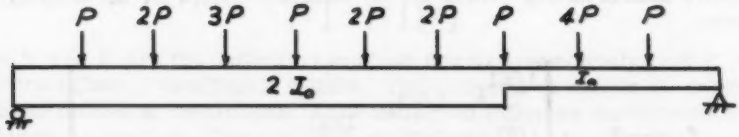


FIG 4

$$[M] = [A][Q] = PL/100 \begin{bmatrix} 82 \\ 154 \\ 206 \\ 228 \\ 240 \\ 232 \\ 204 \\ 166 \\ 88 \end{bmatrix}, \quad [Mh/EI] = PL^2/10^3 EI_o \begin{bmatrix} 41 \\ 77 \\ 103 \\ 114 \\ 120 \\ 116 \\ 136 \\ 166 \\ 88 \end{bmatrix}$$

$$[Y] = [A][Mh/EI] = PL^3/10^5 EI_o \begin{bmatrix} 4,282 \\ 8,154 \\ 11,256 \\ 13,328 \\ 14,260 \\ 13,992 \\ 12,564 \\ 9,776 \\ 5,328 \end{bmatrix}$$

The matrix multiplications required in this example can be easily carried out on a desk calculator.

## IV. Deflection Directly From Load

In some instances, it is desirable to compute the deflections of a beam with variable moments of inertia directly from the given load matrix Q. Utilizing previous results, the new matrix formula is derived.

$$\begin{aligned} (EI\ y'')'' &= q \\ EI\ y'' &= [M] = [A][Q] \\ y'' &= [1/EI][A][Q] \\ [Y] &= [A][h/EI][A][Q] \end{aligned} \tag{22}$$

where the matrices Y, A, and Q have been defined in Eqs. (19), (12) and (9). The flexural rigidity matrix [h/EI] is a diagonal matrix. A diagonal matrix is a square matrix having zeroes for all elements except for the diagonal elements.

$$[h/EI] = h \begin{bmatrix} 1/EI_1 & & & & \\ & 1/EI_2 & & & \\ & & 1/EI_3 & & \\ & & & \cdots & \\ & & & & 1/EI_{n-1} \end{bmatrix} \tag{23}$$

Eq. (23) is the most important equation derived in this paper. With it, one can calculate the deflections from given loads and moments of inertia by direct matrix multiplications.

Example 5

Calculate the deflections of the beam shown in Ex. 4 by means of Eq. (22). The given data are the load matrix Q, and the flexural rigidity matrix [h/EI].

$$[Q] = P \begin{bmatrix} 1 \\ 2 \\ 3 \\ 1 \\ 2 \\ 2 \\ 2 \\ 4 \\ 1 \end{bmatrix}, \qquad [h/EI] = h/EI_o \begin{bmatrix} 2 & & & & & & & & \\ & 2 & & & & & & & \\ & & 2 & & & & & & \\ & & & 2 & & & & & \\ & & & & 2 & & & & \\ & & & & & 2 & & & \\ & & & & & & 1.5 & & \\ & & & & & & & 1 & \\ & & & & & & & & 1 \end{bmatrix}$$

Substituting the above matrices into Eq. (22),

$$[Y] = [A][h/EI][A][Q] = PL^3/10^5EI_o \begin{bmatrix} 4,282 \\ 8,154 \\ 11,256 \\ 13,328 \\ 14,260 \\ 13,992 \\ 12,564 \\ 9,776 \\ 5,328 \end{bmatrix}$$

Eq. (22) involves three matrix multiplications. Because matrix multiplications are associative, the order in which these multiplications are carried out is immaterial.

## V. Deflection Influence Coefficient Matrix

The deflection influence coefficient, $c_{ij}$, is defined as the deflection of the beam at Point i due to a unit load applied at Point j.

$$y_i = c_{ij}P_j \tag{24}$$

Written in matrix notation, Eq. (24) becomes,

$$[Y] = [C][Q] \tag{25}$$

where Y and Q are the deflection and load matrix respectively, and C is the deflection influence coefficient matrix. The elements of matrix C are the deflection influence coefficients. (The deflection influence coefficients are also known as the flexibility influence coefficients.(6)) Comparing Eq. (25) with Eq. (22), it is seen at once that,

$$[C] = [A][h/EI][A] \tag{26}$$

Eq. (26) is the general formula of deflection influence coefficient matrix for beams with variable moments of inertia. For beams with constant moment of inertia, Eq. (26) may be simplified.

$$[h/EI] = h/EI\,[I]$$

$$[C] = h/EI\,[A][I][A] = h/EI\,[A]^2 \qquad (27)$$

Several $[A]^2$ are given in Appendix I for easy reference.

Example 6

Find the deflection influence coefficient matrix for a beam of constant moment of inertia. Using the value of $[A]^2$ given in Appendix I, for n = 10,

$$[C] = h^3/100EI \begin{bmatrix} 285 & 480 & 595 & 640 & 625 & 560 & 455 & 320 & 165 \\ 480 & 880 & 1120 & 1220 & 1200 & 1080 & 880 & 620 & 320 \\ 595 & 1120 & 1505 & 1680 & 1625 & 1520 & 1245 & 880 & 455 \\ 640 & 1220 & 1680 & 1960 & 2000 & 1840 & 1520 & 1080 & 560 \\ 625 & 1200 & 1675 & 2000 & 2125 & 2000 & 1675 & 1200 & 625 \\ 560 & 1080 & 1520 & 1840 & 2000 & 1960 & 1680 & 1220 & 640 \\ 455 & 880 & 1245 & 1520 & 1675 & 1680 & 1505 & 1120 & 595 \\ 320 & 620 & 880 & 1080 & 1200 & 1220 & 1120 & 880 & 480 \\ 165 & 320 & 455 & 560 & 625 & 640 & 595 & 480 & 285 \end{bmatrix}$$

For example, the coefficient for the deflection at the midspan due to a unit load at the mid-span is,

$$c_{55} = 2125\ h^3/100EI = 0.02125\ L^3/EI = L^3/47.06EI$$

Compared with the exact answer of $L^3/48EI$, the error is about 2%.

Example 7

Determine the deflection influence coefficient matrix for the beam shown in Fig. 5.

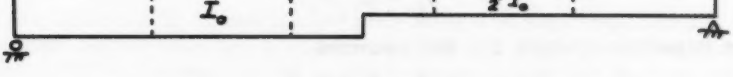


FIG 5

For the sake of simplicity, we shall divide the beam into five equal segments and carry out the computations in detail. By Eq. (26),

$$[C] = [A][h/EI][A] = \frac{h}{n}\frac{h}{EI}\frac{h}{n} \begin{bmatrix} 4 & 3 & 2 & 1 \\ 3 & 6 & 4 & 2 \\ 2 & 4 & 6 & 3 \\ 1 & 2 & 3 & 4 \end{bmatrix} \begin{bmatrix} 1 & & & \\ & 1 & & \\ & & 2 & \\ & & & 2 \end{bmatrix} \begin{bmatrix} 4 & 3 & 2 & 1 \\ 3 & 6 & 4 & 2 \\ 2 & 4 & 6 & 3 \\ 1 & 2 & 3 & 4 \end{bmatrix}$$

$$= L^3/n^5EI \begin{bmatrix} 4 & 3 & 2 & 1 \\ 3 & 6 & 4 & 2 \\ 2 & 4 & 6 & 3 \\ 1 & 2 & 3 & 4 \end{bmatrix} \begin{bmatrix} 4 & 3 & 2 & 1 \\ 3 & 6 & 4 & 2 \\ 4 & 8 & 12 & 6 \\ 2 & 4 & 6 & 8 \end{bmatrix}$$

$$= L^3/5^5EI \begin{bmatrix} 35 & 50 & 50 & 30 \\ 50 & 85 & 90 & 55 \\ 50 & 90 & 110 & 70 \\ 30 & 55 & 70 & 55 \end{bmatrix}$$

Thus with little effort, mental or computational, we have obtained sixteen deflection influence coefficients. The results are, of course, not very precise, as only five segments were taken. $c_{22}$, for example, has an error of about 10.5%.

## CONCLUSIONS

There are many excellent methods for the calculation of beam deflections. Among the most well-known are the conjugate beam method,[7] Newmark's method,[8] and the relaxation method.[L],[9] With any of these methods, one can compute beam deflections systematically and efficiently. Their only drawback, if it can be called a drawback, is that one must learn and memorize the particular procedure involved. Unfortunately the procedures can be easily forgotten, unless one uses them fairly regularly. This is probably the main reason why Newmark's method did not have the popularity it rightfully deserves among the engineers.

With the matrix formulas developed in this paper, the deflection computations are reduced to a mere routine. All one needs to know are the formulas and the rule for matrix multiplication. It would be possible, for example, to explain how to use the formulas to an engineering aide in, say, half an hour. Thereafter, he will be able to crank out deflections on a desk calculator as fast as anyone.

None of the existing methods are particularly suitable for use on digital computer, because of the long and involved programming required. With the matrix formulas developed in this paper, one can write a short, possibly the shortest, subroutine for beam deflections on any digital computer. The matrix A can be fed into the computer as part of the subroutine. For medium capacity machines, such as the 650, G-15, or LGP-30, it is entirely feasible to use, say, 30 segments so as to attain a high degree of accuracy. Or it may be desirable to let the computer generate matrix A internally, for any value of n.

The extension of the matrix formulas to compute stiffness matrix, buckling load, and the natural frequency of beams with variable moments of inertia will be treated in a subsequent paper.

## APPENDIX I

For n = 3,

$$[A]^2 = L^2/3^4 \begin{bmatrix} 5 & 4 \\ 4 & 5 \end{bmatrix}$$

For n = 4,

$$[A]^2 = L^2/4^4 \begin{bmatrix} 14 & 16 & 10 \\ 16 & 24 & 16 \\ 10 & 16 & 14 \end{bmatrix}$$

For n = 5,

$$[A]^2 = L^2/5^4 \begin{bmatrix} 30 & 40 & 35 & 20 \\ 40 & 65 & 60 & 35 \\ 35 & 60 & 65 & 40 \\ 20 & 35 & 40 & 30 \end{bmatrix}$$

For n = 6,

$$[A]^2 = L^2/6^4 \begin{bmatrix} 55 & 80 & 81 & 64 & 35 \\ 80 & 136 & 114 & 116 & 64 \\ 81 & 144 & 171 & 144 & 81 \\ 64 & 116 & 144 & 136 & 80 \\ 35 & 64 & 81 & 80 & 55 \end{bmatrix}$$

For n = 10,

$$[A]^2 = L^2/10^4 \begin{bmatrix} 285 & 480 & 595 & 640 & 625 & 560 & 455 & 320 & 165 \\ 480 & 880 & 1120 & 1220 & 1200 & 1080 & 880 & 620 & 320 \\ 595 & 1120 & 1505 & 1680 & 1675 & 1520 & 1245 & 880 & 455 \\ 640 & 1220 & 1680 & 1960 & 2000 & 1840 & 1520 & 1080 & 560 \\ 625 & 1200 & 1675 & 2000 & 2125 & 2000 & 1675 & 1200 & 625 \\ 560 & 1080 & 1520 & 1840 & 2000 & 1960 & 1680 & 1220 & 640 \\ 455 & 880 & 1245 & 1520 & 1675 & 1680 & 1505 & 1120 & 595 \\ 320 & 620 & 880 & 1080 & 1200 & 1220 & 1120 & 880 & 480 \\ 165 & 320 & 455 & 560 & 625 & 640 & 595 & 480 & 285 \end{bmatrix}$$

Journal of the
STRUCTURAL DIVISION
Proceedings of the American Society of Civil Engineers

# REINFORCED CONCRETE FOLDED PLATE CONSTRUCTION

Charles S. Whitney,[1] F. ASCE, M. IABSE,
Boyd G. Anderson,[2] F. ASCE and
Harold Birnbaum[3]

---

This paper is one of the group of papers which were the bases for oral presentations at the Joint ASCE-IABSE Meeting in New York, October 1958. The entire group, including those published in CIVIL ENGINEERING, will be reprinted in one volume.

---

## SYNOPSIS

This paper presents design methods and discusses experience with the construction of reinforced concrete folded plate thin shells for the roofs and floors of hangars, auditoriums, warehouses and other buildings. Quantities of materials and costs are compared with other types of structures.

## INTRODUCTION

Reinforced concrete folded plates, or as they are sometimes called, prismatic shells or hipped plates, provide a useful and economical method of construction for roof and floor systems in a wide variety of structures. It is often competitive with other construction methods for short spans and has proven exceptionally economical where relatively large spans are needed as for auditoriums, gymnasiums, industrial buildings, hangers, department stores and parking garages.

The materials required are usually much less than needed for flat slab, beam and slab, or other conventional systems and are little more than

Note: Discussion open until March 1, 1960. Separate Discussions should be submitted for the individual papers in this symposium. To extend the closing date one month, a written request must be filed with the Executive Secretary, ASCE. Paper 2219 is part of the copyrighted Journal of the Structural Division, Proceedings of the American Society of Civil Engineers, Vol. 85, No. ST 8, October, 1959.

1. Partner, Ammann & Whitney, Cons. Engrs., New York, N. Y.
2. Partner, Ammann & Whitney, Cons. Engrs., New York, N. Y.
3. Engr., Ammann & Whitney, Cons. Engrs., New York, N. Y.

required for continuously curved shells, with the advantage of utilizing relatively simple formwork. In many cases, concrete folded plates will provide fire resisting structures at substantially less cost than structural steel framing.

Folded plate structures were first constructed in Germany during the 1920's for use as coal bunkers and similar structures where the ratio of span to width of plate is relatively small. Technical papers on the subject began appearing about 1930.

The first application in America may have been a warehouse in San Francisco designed by L. H. Nishkian, Consulting Engineer, and built about 1935. This was about 44 feet wide and 70 feet long. The roof consisted of three ribbed concrete flat segments with the center plate horizontal and the roof load carried to the end walls by the two sloping side plates. It is reported that a number of similar structures were subsequently built in California.

In recent years, concrete folded plates have been used for a large variety of structures and are of increasing importance in the building industry as the basis of a new system of construction.

## Applications of Folded Plates

Folded plate floor or roof construction consists of a series of repeated units, each of which is formed by two or more flat plates intersecting at an angle. The plates act as a continuous slab transversely and as beams in their own planes longitudinally.

The angle of the sloping plates is usually made 45° or less with the horizontal in order to facilitate placing of the concrete without top forms. The simplest form is a two-plate V-shaped unit. The disadvantage of this form is that it may provide an inadequate area of concrete at the top and bottom to resist the compressive flexural force or permit placement of the reinforcing steel.

The most useful and practical form of unit is developed by adding horizontal plates between the sloping plates at the top and bottom of sufficient width to keep the concrete compressive stress within proper limits and to accommodate the necessary reinforcing steel. The majority of the following examples are of this type.

Sometimes the bottom plate is placed vertically, forming a downward projecting beam instead of a horizontal flange. This has the disadvantage of greater height of structure and greater form cost.

The use of inclined plates which extend from top to bottom of the unit is usually more economical in both cost of construction and design than more complicated forms with intermediate folds.

Tapered or triangular plates may also be used where desired. In the Illinois dome, (Fig. 6) tapering makes possible the use of folded plates in the circular structure without excessive convergence and narrowing of the folds. In the roof of the American Concrete Institute office building[1] they are used for aesthetic reasons.

The folded plate units are usually symmetrical where the solid roof or floor is desired, but unsymmetrical units may be used to provide north-light roofs.[2]

A number of examples of folded plate construction will be illustrated on the following pages and drawings are presented showing typical cross sections.

The roofs of the social hall and chapel of the Temple Beth Sholem in Miami (Fig. 7) are formed of four-inch concrete slabs corrugated to a height of 2'-8". The spans were 80 feet and 40 feet respectively and the cost was comparable to the cost of much shorter spans using conventional framing.

The roof of the Sears Roebuck & Co. store in Tampa is also the simple type of corrugated construction (Fig. 1). It consists of two 125 foot continuous spans with cantilevers at the ends. The strength and rigidity of the construction is indicated by the fact that the roof supports a steel and concrete mezzanine floor with suspenders at 25 foot intervals leaving the 125 foot spans clear in the first story.

Temple Mishkan Tefila, Newton, Massachusetts (Fig. 12), has a 75 foot span. The horizontal plate has been omitted at the bottom forming units consisting of V's separated by narrow horizontal plates at the top. There is a vertical beam 12" by 4'-10" projecting below the V forming the bottom flange. The total height of the section is 10 feet.

The floors of the Wayne University conference building (Fig. 2) are of the simple V type with a level slab poured across the top forming the floor surface. The hollow triangular spaces were used for ventilating ducts.

The folded plate roof of the cold storage warehouse for the Central Warehouse Corporation at Albany (Fig. 10) were also leveled up with a top slab and the interior spans were used as cold air ducts for refrigeration. The operation of the plant has been very satisfactory.

Another example of the use of folded plate construction with a top levelling slab is in the central portion of the TWA hangar in Kansas City (Fig. 11). The upper floors were suspended from the roof with two 50 foot spans, leaving the ground floor open for the full width of 100 feet. The folded plate construction provided a shallower and more economical framing than could be obtained by using beams and girders.

Folded plate roofs have been used on several high schools in Milwaukee for gymnasiums, auditoriums, and other portions (Fig. 8). Examples of these are the John Muir High School (Eschweiler & Eschweiler, Architects),

Fig. 1. Sears Roebuck & Co. Store, Tampa, Florida

the John Marshall High School (Brust & Brust and Eschweiler & Eschweiler, Architects) and the John Audubon High School (Grassold & Johnson, Architects). In some cases the same unit cross section is used for several different spans in order to simplify the flasework and detailing. The roofs have been leveled with top slabs and the interior spaces used as plenum chambers for ventilating. The top slabs may be either precast or poured in place.

Another use of folded plate construction is in long span cantilever hangar roofs.(3) The first one to be built, the Trans World Airlines hangar at Kansas City, Burns & McDonnell, Architects, has a cantilever span of 150 feet and a continuous door length of over 800 feet. The building is 420 feet wide and 1000 feet long. Preliminary designs have been made for cantilever spans up to 250 feet which are perfectly feasible if needed.

A second hangar with a 150 foot cantilever has been completed for Trans World Airlines at New York International Airport, and one with a 130 foot span for Pan American World Airways at the same location. (Figs. 3 and 4) These three have steel bridge cables supporting the outer end. The latter two have the folded plate roof curved up to reduce the positive bending between the center building and the cable supports. They all have a 30 foot plate module poured in 60 foot widths which were grouted together after the cables were jacked up. In order to prevent lateral distortion of the units which were self supporting before being grouted into a continuous roof, lateral tie rods were cast into the corrugations at the top. Fig. 4 shows a sixty foot wide section of the Pan American hangar undergoing a load test. This also shows the lateral ties and the joint to be grouted between sections.

During the load test of the TWA hangar, a block of concrete weighing ten tons was accidentally dropped about two feet on the outer end of the cantilever without causing appreciable damage. Both load tests completely justified the design assumptions and methods.

More recently designed are the Mohawk Airlines hangar at Utica (Fig. 12) with a span of 120 feet and the National Airlines hangar at Miami (Fig. 5) with

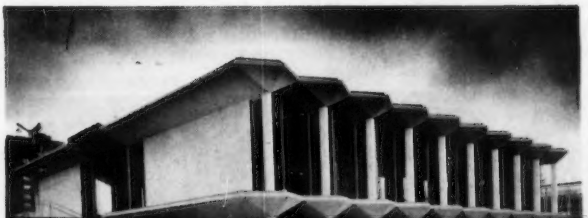

Fig. 2. Wayne University, McGregor Memorial Community Conference Center, Detroit, Michigan (Yamasaki, Leinweber & Associates, Architects)

Fig. 3. 130-ft. Cantilever Span Pan American World Airways Hangar, New York International Airport

Fig. 4. Load Test on Cantilever Roof Span Pan American World Airways Hangar, New York International Airport

a 111 foot cantilever span. These are built without the suspension cables or other prestressing. They also have a 30 foot module and the folded plate units are about 11 feet high at the support and three feet high at the outer ends.

In all five of these hangars, the simple corrugated plate arrangement was used with horizontal plates top and bottom between the diagonal plates. The plates of the two hangars at New York International Airport were increased one inch in thickness over that used at Kansas City and recommended by the designers because of a ruling by the Port of New York Authority regarding the minimum concrete cover required by the New York City building code.

The American Concrete Institute office building in Detroit has a cantilever roof built of tapered folded plates with a 4 foot module. The units for each side were precast and jointed together after erection by welding and grouting. Precasting instead of pouring in place was optional with the contractor.

Another interesting application of folded plate construction is the assembly hall now being designed for the University of Illinois. (Fig. 6) This will be a 400 foot diameter ribbed concrete saucer surmounted by a dome of thin tapered concrete folded plates. The saucer will be of folded plates with a top slab carrying the seating and the interior corrugation spaces used to carry heating and ventilating ducts. The rim of the saucer will be a precast concrete ring of sufficient strength to turn the thrust of the dome inward toward the central foundation.

The dome as well as the saucer will be cast in segments on rotating forms to reduce the cost. After both the saucer and the dome are concreted, the rim will be prestressed to give them both the proper camber.

The development of the structural design of all of the preceding examples has been the work of Ammann & Whitney, Consulting Engineers, who also did the architectural design where no other architect has been credited.

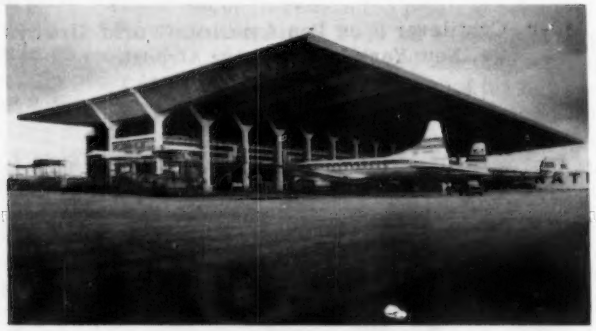

Fig. 5. 111-ft. Cantilevers
National Airlines Hangar, Miami International Airport
(Weed, Russell & Johnson, Architects)

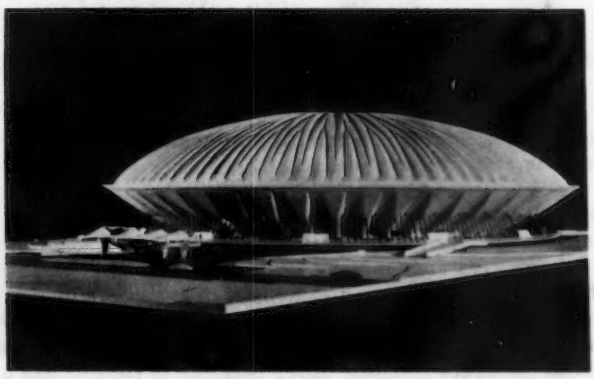

Fig. 6. 400-ft. diameter Dome
Assembly Hall, University of Illinois, Champaign-Urbana, Illinois
(Harrison & Abramovitz, Architects)

FIG. 7 TEMPLE BETH SHOLEM, MIAMI




FIG. 8 JOHN AUDUBON & JOHN MUIR HIGH SCHOOL, MILWAUKEE

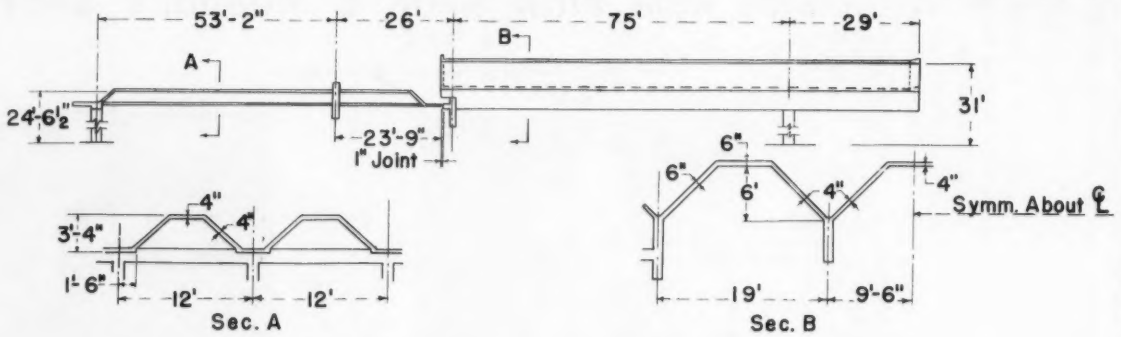


FIG. 9 TEMPLE MISHKAN TEFILA, NEWTON

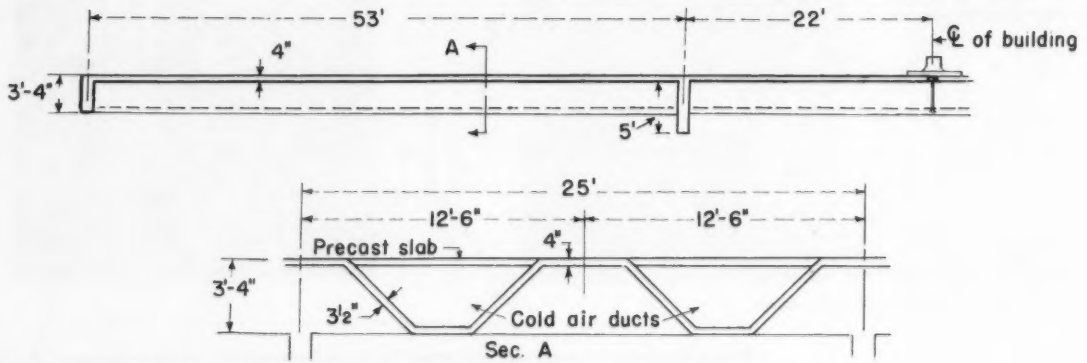


FIG. 10 COLD STORAGE WAREHOUSE - ALBANY

FIG. 10 COLD STORAGE WAREHOUSE - ALBANY

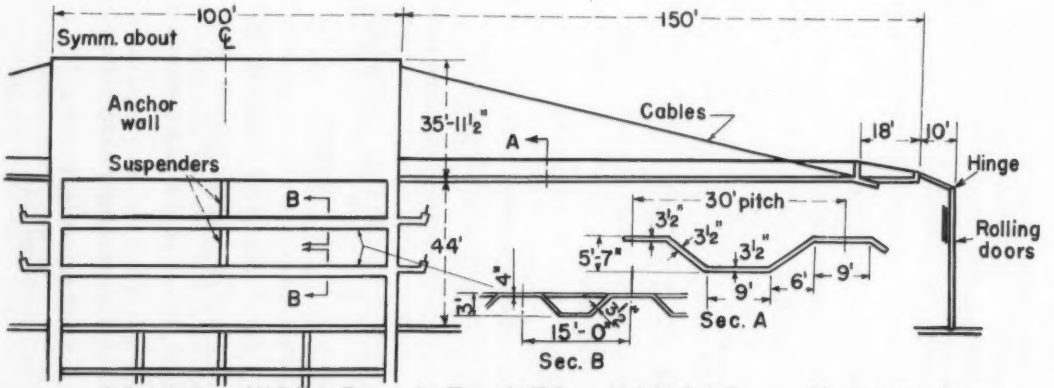


FIG. 11 TRANS-WORLD AIRLINES HANGAR - KANSAS CITY

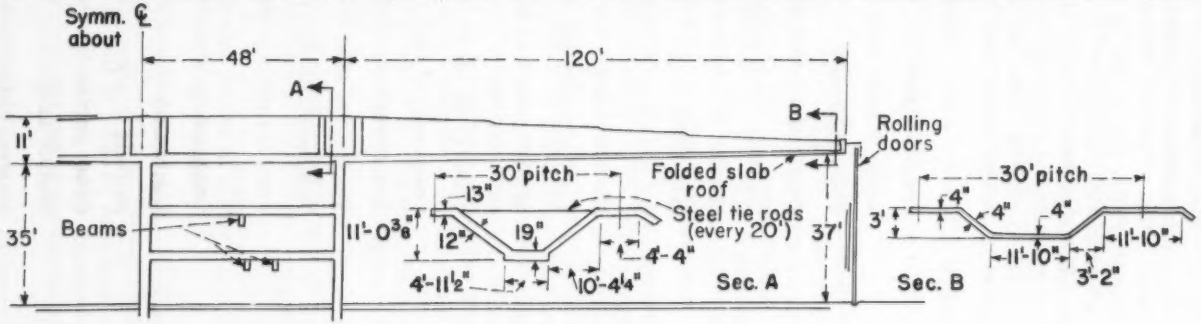


FIG. 12 MOHAWK AIRLINES HANGAR - UTICA, N. Y.

## Methods of Analysis

1. The following terminology, which is consistent with that used by Winter and Pei[5] will be used in this paper: Each individual planar element of the structure is called a "plate." The plate "length" is the dimension between transverse supports, its "width" is the transverse dimension between longitudinal edges and its "thickness" is the perpendicular dimension between surfaces. The structure "height" is the vertical dimension between the upper and lower extremes of a transverse crossection. Bending of individual plates in their planes is called "plate action" and bending of individual plates out of their planes is called "slab action." Following is a list of the symbols used:

| Symbol | Definition |
|---|---|
| L | Length of plate between transverse supports |
| $\omega$ | Width of plate between longitudinal edges |
| d | Plate thickness |
| H | Height of a folded plate unit |
| x | Distance from support along length of plate |
| B | Spacing of a folded plate unit |
| b | Horizontal projection of plate width, $\omega$ |
| $\phi$ | Angle of plate to horizontal |
| $\gamma$ | Change in angle $\phi$ between adjacent plates |
| q | Load intensity per unit area of horizontal projection |
| p | Approximation of load intensity (First term of Fourier sine series) |
| P | Transverse slab reaction due to approximate applied load, p |
| S | Component of slab reaction, P, in plane of plate |
| m | Transverse moment at plate edge |
| $\Delta P$ | Transverse slab reaction due to transverse moments, m |
| $\Delta S$ | Component of slab reaction $\Delta P$ in plane of plate |
| R | Total transverse plate load (resultant of S &$\Delta$S acting on a plate |
| t | Longitudinal shear intensity per unit length along plate edge |
| T | Summation of longitudinal shear intensity, t |
| $M_o$ | Moment in plate caused by transverse load |
| A | Cross sectional area of plate |
| Z | Section modulus of plate for "plate action" |
| I | Moment of inertia of plate for "plate action" |
| E | Modulus of Elasticity |
| $\Delta$ | Deflection of plate for "plate action" |

| Symbol | Definition |
|---|---|
| $\Theta$ | Change in slope of slab at a joint as caused by load, q |
| $\Psi$ | Change in slope of slab at a joint as caused by transverse moments, m |
| v | Deflection of slab at joint as caused by plate deflection $\Delta$ |
| J | Moment of inertia of a unit length of plate for "slab action" |
| k | Subscript indicating symbol is applicable at $k^{th}$ joint or plate |
| T | Subscript referring to tie between plates |
| — | When shown over symbol indicates a value at mid span |

The notation is taken from Girkmann[4] but has been revised to conform to certain usages common in the United States.

2. Transversely, the structural action of a folded plate system is similar to that of a series of continuous frames on elastic supports. The sections that would be isolated by a series of transverse cuts through the structure spaced at a unit distance, may be considered as elastic frames which are supported at the intersections of the longitudinal plates. The frame reactions are supplied by the plates acting in their own planes. (See Fig. 13) These reactions are affected by the displacements of the plates' intersections.

3. Where the ratio of length to height is small, the "elastic support" is relatively rigid and the frame action is not modified by the comparatively small deflections. Stress distribution in the folded plate can be computed by the equations of statics and an equation of compatible longitudinal stress at plate intersections. A relatively simple method of analysis for this condition is that proposed by Winter & Pei.[5] A relaxation technique, analogous to moment distribution, is used to compute the stress variation across the plate cross section. Although the method is set up for simply supported plate systems it can also be applied to continuous spans with some modifications.

4. For intermediate ratios of length to height it is necessary to consider deflections as well as compatibility of longitudinal stresses. This problem can be solved by either one of the following:

a. a modification of the Winter-Pei solution extended to include joint displacements.[6] The solution involves n-1 simultaneous equations, where n is the number of plates.

b. an equivalent method[7] which involves a series of simultaneous algebraic or differential equations including all effects.

5. When the ratio of length to height is large, and there is a series of repetitions of the folded plate unit, the stress variation is closely approximated by treating the transverse cross section as that of a beam, assuming no change in geometry of the section. Stresses are then determined by standard methods of beam design. In this case plates at the end of the series should be investigated for the effects of deflection.

The stress variation can be determined by using the beam theory for length to height ratios as low as 2 when the folded plate unit is triangular  or trapezoidal 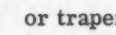 . As the number of plates per unit is

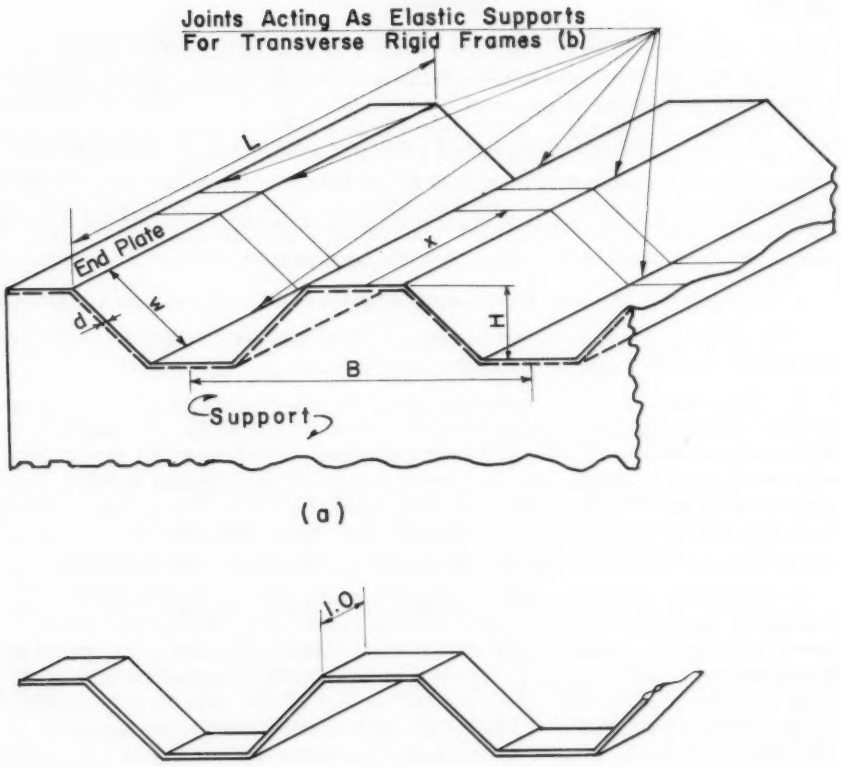


Fig. 13

increased and their arrangement becomes more complicated, the lower limit of length to height ratio at which the ordinary beam theory is applicable for a given configuration cannot be completely defined beforehand. However, a definition of the range of applicability for a specific folded plate system was derived by Craemer[7] and a study of his findings indicates that a lower limit which is applicable for the vast majority of designs can be determined. He found that this lower limit of the length to height ratios could be expressed as $\frac{L}{H} = \alpha\sqrt{w/d}$ where $\alpha$ is a constant, dependent upon the folded plate system and the remaining terms are as indicated in Fig. 13. For the ratio of $\omega/d = 20$, which is usual in reinforced concrete structures, and for Craemer's configuration, the beam theory is applicable to a single folded plate unit with the ratio $L/H = 9.9$. For a repetitive folded plate structure the beam theory is applicable when $L/H = 7.0$. Both of these values are much less than the ratio $L/H = 15$ which is sufficient to carry ordinary building loads. Therefore,

the use of L/H = 10 as a lower limit for a structure with symmetrical, repetitive folded plate units should ensure sufficiently accurate stress patterns in most building designs. This ratio will be lower than necessary for most structures. It should not be applied to unsymmetrical units such as "northern light" structures without further investigation.

When the ratio $L/H \geq 10$ the method of analysis by beam theory is as outlined below.

a. Estimate the unit dead plus live load.

b. Isolate a transverse strip of unit length and determine thickness and transverse reinforcing by treating the strip as a continuous beam rigidly supported at each of the slab folds. With this result the estimated dead load can be revised if required.

c. For one repetition of a folded plate unit (dimension B, Fig. 13), compute the maximum longitudinal moment.

d. For the selected section check the longitudinal concrete flexural stress and calculate the required tensile steel, either by straight line method or by ultimate strength equations. In either event the computation is similar to any "T" beam design.

e. Check the web section (diagonal plate) for the effect of shear using standard shear equations.

f. Increase the concrete dimensions as required for tensile or shear reinforcement.

g. Check effect of load on end plates at the discontinuous edge of the structure to determine the adequacy of the end plates. This analysis will be described below.

6. For the portion of the roof near the end plate an analysis similar to those described in previous references[4,6,7] should be used. The analysis described hereafter is an adaptation of one presented by Girkmann, however analyses could be derived from the other referenced sources.

Fig. 13 shows an end portion of a folded plate roof of Length L, where the roof contains a large number of folded units. The interior plates of this roof can be designed as outlined, but because of the lack of transverse restraint at the exterior edge of the end plate, there will occur disturbances that materially alter stresses and deformations in the end plate, becoming smaller for successive interior plates. Stress patterns in the plates affected by the edge disturbance are determined by isolating the first n exterior plates of the roof. These plates are then treated as a folded plate roof having zero shear force and zero transverse moment at the exterior edge of plate 1 (free end) and zero lateral deflection at the interior edge of the $n^{th}$ plate. The solution becomes more accurate but also more tedious as the number of plates included in the analysis is increased. It has been found that sufficiently accurate solutions are obtained when the number of plates included is equal to 1-1/2 units (6 plates in Fig. 13, one unit B consisting of 4 plates).

The analysis of the n end plates is based on a continuity of stress and deformation along the common edges of adjacent plates. At each joint, for any value of x (See Fig. 13), the change in joint angle caused by load, by transverse joint moments and plate deformations and rotations is expressed for

adjacent plates. Since the joint is rigid, the algebraic sum of the angle changes must be zero. For n plates it is possible to write n-1 equations involving n-1 unknown transverse joint moments.

If the width and thickness of the plates and the intensity of loading do not vary with x it is possible to greatly simplify the mathematics by approximating the uniform plate load q by the first term of the Fourier series. The approximate applied load p is

$$p_k = \frac{4q_k}{\pi} \sin \frac{\pi x}{L} \qquad (1)$$

When equation (1) is used, all plate stresses, moments, and deformations are expressed as sine functions of x, having maximum values at mid-span.

In brief, the analysis proceeds as follows:

a. Assume each plate to act as a simply supported slab spanning between adjacent plates and find the loads that would act along the joints (forces P in Fig. 14c) if the joints were continuously supported for their full length. Replace all joint loads by their components in the planes of the plates (forces S in Fig. 14c). Since the plates are much wider than they are thick, all longitudinal transfer of loads occurs by plate action.

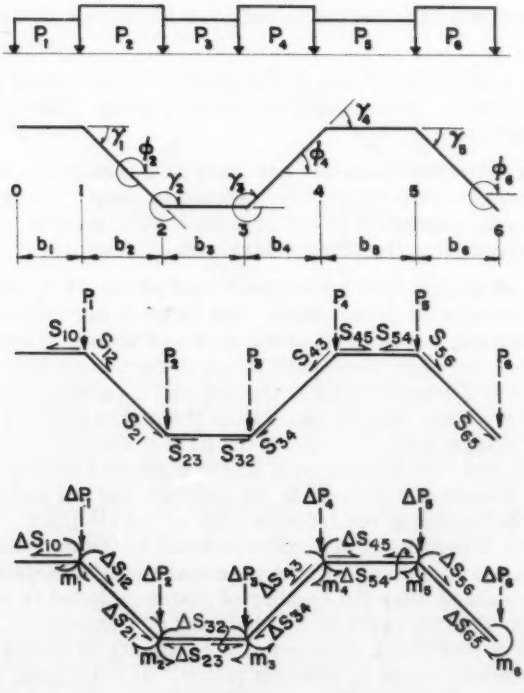


Fig. 14

b. Since the plates are in reality continuous across the longitudinal joints there will be transverse moments at the joints that will cause additional joint loads (moments m in Fig. 14d). Compute these additional joint loads ($\Delta S$ in Fig. 14d) in terms of unknown transverse moments at the plate edges.

c. Compute longitudinal edge shear forces (t & T in Fig. 15) for each plate as required for compatible stresses in adjacent plates at each joint. The transverse loading causing the direct stress are the loads computed in a and b.

d. Compute individual plate deflections caused by the transverse loads and longitudinal edge shear stresses found previously. These deflections will be in terms of load and unknown joint moments.

e. Express condition of zero angle change (Fig. 16) at each joint in terms of applied loads, transverse joint moments and plate deflections. When n plates are considered there will be n equations.

f. Solve equations from e for unknown transverse moments, and then solve preceding equations for stresses.

Fig. 14 is a cross section through the first six plates of the structure of Fig. 13 taken at a distance x from the near end. Also shown is the approximate load acting on a unit length of each plate. At plate k the vertical load is computed from equation (1). At $x = L/2$ the load intensity is $P_k = \frac{4q_k}{\pi}$. In Fig. 14c the simply supported transverse slab reaction at each joint, $P_k$, (when k = 1 to 6) is indicated by dashed lines. Also shown in Fig. 14c are the components of the slab reactions $S_{k,\,k-1}$ in the plane of the adjacent plates. These components are the plate loads. The expressions for $P_k$, $S_{k,\,k-1}$ and $S_{k,\,k+1}$, are given in equations 2 and 3. At $x = L/2$ the values of $\overline{P}_k$, $\overline{S}_{k,\,k-1}$ and $\overline{S}_{k,\,k+1}$ are obtained by setting $\sin\frac{\pi x}{L} = 1$

$$\left.\begin{aligned} P_1 &= p_1 b_1 + \tfrac{1}{2} p_2 b_2 = \tfrac{4}{\pi}\left[q_1 b_1 + \tfrac{1}{2} q_2 b_2\right]\sin\tfrac{\pi x}{L} \\ P_k &= \tfrac{4}{\pi}\left[\tfrac{1}{2} q_k b_k + \tfrac{1}{2} q_{k+1} b_{k+1}\right]\sin\tfrac{\pi x}{L} \end{aligned}\right\} \qquad (2)$$

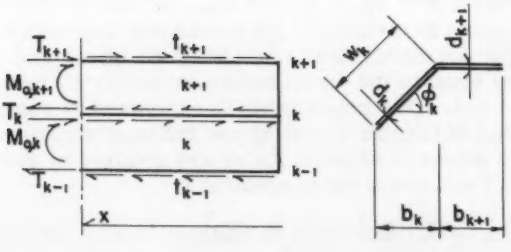


$w_k = b_k / \cos\phi_k$

$Z = d_k w_k^2 / 6$

$I = d_k w_k^3 / 12$

$A = d_k w_k$

$\overline{M}_{o,k} = \frac{L^2}{\pi^2}\overline{R}_k$

Fig. 15

$$S_{k,k-1} = P_k \frac{\cos\phi_{k+1}}{\sin\gamma_k}$$
$$S_{k,k+1} = P_k \frac{\cos\phi_k}{\sin\gamma_k} \qquad (3)$$

These forces can be easily obtained by a graphical resolution of force $P_k$ in the direction of the two plates k, k-1. The positive direction for $\phi$ and $\gamma$ are measured as indicated in Fig. 14b. As shown in Fig. 14d there acts along each joint k a transverse $m_k = \bar{m}_k \sin\frac{\pi x}{L}$ which has a maximum value at midspan of $\bar{m}_k$. Transverse moments cause changes in the resultant joint loads $\Delta P_k$, the expressions for which are given below.

$$\Delta P_1 = \left[\frac{\bar{m}_2 - \bar{m}_1}{b_2}\right]\sin\frac{\pi x}{L}$$
$$\Delta P_k = \left[\frac{m_{k+1} - m_k}{b_{k+1}} + \frac{m_{k-1} - m_k}{b_k}\right]\sin\frac{\pi x}{L} \qquad (4)$$

The torsional stiffness of the first plate is neglected and $\bar{m}_1$ is obtained by treating the first plate as a cantilever fixed at joint 1. The components of $\Delta P_k$ in the planes of the adjacent plates are computed by equations 5.

$$\Delta S_{k,k-1} = \Delta P_k \frac{\cos\phi_{k+1}}{\sin\gamma_k}$$
$$\Delta S_{k,k+1} = \Delta P_k \frac{\cos\phi_k}{\sin\gamma_k} \qquad (5)$$

The total transverse load in the plane of plate k, $R_k$, is obtained by summing equations 3 and 5.

$$R_k = \left[S+\Delta S\right]_{k,k-1} - \left[S+\Delta S\right]_{k-1,k} \qquad (6)$$

In the above equations S is positive when acting away from the joint and R is positive when acting toward the edge of lower order (i.e., $R_k$ is positive if acting toward edge k-1)

Fig. 15 shows two successive folded plates isolated along edges k-1 and k+1 and at a distance x from the support. $M_{o,k}$ and $M_{o,k+1}$ are the moments caused by transverse loads; $t_{k-1}$, $t_{k+1}$ and $t_k$ indicate the intensity of longitudinal shears along joint edges; and $T_{k-1}$, $T_k$ and $T_{k+1}$ are the summation of these shears from the support to section x. All forces and moments are positive as shown. At joint k the direct stress caused by all forces and moments on plate k must be equal to the direct stress caused by all forces and moments acting on plate k+1. This relationship is expressed by equation 7. If x is taken at L/2, T and M become $\bar{T}$ and $\bar{M}$ and the joint shears required for compatible direct stress in adjacent plates are obtained by rearranging terms in equation 7 and are given in equation 8.

$$\frac{6}{w_k^2 d_k}\left[M_{o,k} + \frac{w_k}{2}(T_k + T_{k-1})\right] - \frac{1}{w_k d_k}\left[T_k - T_{k-1}\right]$$
$$= \frac{6}{w_k^2 d_k}\left[M_{o,k+1} + \frac{w_{k+1}}{2}(T_k + T_{k+1})\right] - \frac{1}{w_{k+1} d_{k+1}}\left[T_k - T_{k+1}\right] \qquad (7)$$

$$T_{k-1}\frac{1}{A_k} + 2T_k\left[\frac{1}{A_k} + \frac{1}{A_{k+1}}\right] + T_{k+1}\frac{1}{A_{k+1}} = -\frac{1}{2}\left[\frac{M_{o,k}}{Z_k} + \frac{M_{o,k+1}}{Z_{k+1}}\right] \quad (8)$$

In Equation 8 $T_o = 0$ and $T_n$ can be determined from the assumption of no lateral motion of joint n. Equation 8 is written for n successive joints containing n-1 unknown values of $\overline{T}_k$ and n unknown values of $\overline{m}_k$.

The plate deflections, $\Delta$ which are obtained by twice differentiating the expression for $M_x$ are given in equation 9. At mid span $\Delta_k = \overline{\Delta}_k$

$$\Delta_k = \frac{1}{EI_k\left(\frac{\pi}{L}\right)^4}\left\{\overline{R}_k + \left[\overline{T}_k + \overline{T}_{k-1}\right]\left(\frac{\pi}{L}\right)^2\frac{l_k}{2}\right\}\sin\frac{\pi x}{L} \quad (9)$$

A solution for unknown joint moments $\overline{m}_k$ is obtained by setting all angle changes at each joint equal to zero. Fig. 16 shows the angle changes at joint k as caused by load, moment, and deformation of adjacent plates, the sum of which must be zero. This is expressed in equation 10.

$$\overline{\theta}_{k,k-1} - \overline{\theta}_{k,k+1} + \overline{\psi}_{k,k-1} - \overline{\psi}_{k,k+1} + \frac{1}{w_k}\left[\overline{v}_{k,k-1} - \overline{v}_{k-1,k}\right] - \frac{1}{w_{k+1}}\left[\overline{v}_{k+1,k} - \overline{v}_{k,k+1}\right] = 0 \quad (10)$$

The angle change $\theta$ is caused by the load, the angle change $\psi$ is caused by moment and the angle change $\frac{1}{w}\left[\Delta v\right]$ is caused by translational deformations of the plate as a whole. The expressions for the various terms of equation 10 are given below.

$$\left.\begin{aligned}\overline{\theta}_{k,k-1} &= -q_k b_k^3/24EJ_k\cos^2\phi_k \\ \overline{\theta}_{k,k+1} &= +q_{k+1}b_{k+1}^3/24EJ_{k+1}\cos^2\phi_{k+1}\end{aligned}\right\} \quad (11)$$

$$\left.\begin{aligned}\overline{\psi}_{k,k-1} &= w_k\left[2\overline{m}_k + \overline{m}_{k-1}\right]/6EJ_k \\ \overline{\psi}_{k,k+1} &= w_{k+1}\left[2\overline{m}_k + \overline{m}_{k+1}\right]/6EJ_{k+1}\end{aligned}\right\} \quad (12)$$

$$\left.\begin{aligned}\left[\overline{v}_{k,k-1} - \overline{v}_{k-1,k}\right]/w_k &= \frac{1}{w_k}\left\{\overline{\Delta}_k\left[\cot\gamma_k + \cot\gamma_{k-1}\right] - \frac{\overline{\Delta}_{k+1}}{\sin\gamma_k} - \frac{\overline{\Delta}_{k-1}}{\sin\gamma_{k-1}}\right\} \\ \left[\overline{v}_{k+1,k} - \overline{v}_{k,k+1}\right]/w_{k+1} &= \frac{1}{w_{k+1}}\left\{\overline{\Delta}_{k+1}\left[\cot\gamma_{k+1} + \cot\gamma_k\right] - \frac{\overline{\Delta}_{k+2}}{\sin\gamma_{k+1}} - \frac{\overline{\Delta}_k}{\sin\gamma_k}\right\}\end{aligned}\right\} \quad (13)$$

The solution of equation 10 (expressed in terms of eqs. 11, 12 & 13) will yield n values of mid span joint moments with which, using equations 8 and 7, it is possible to evaluate plate stresses.

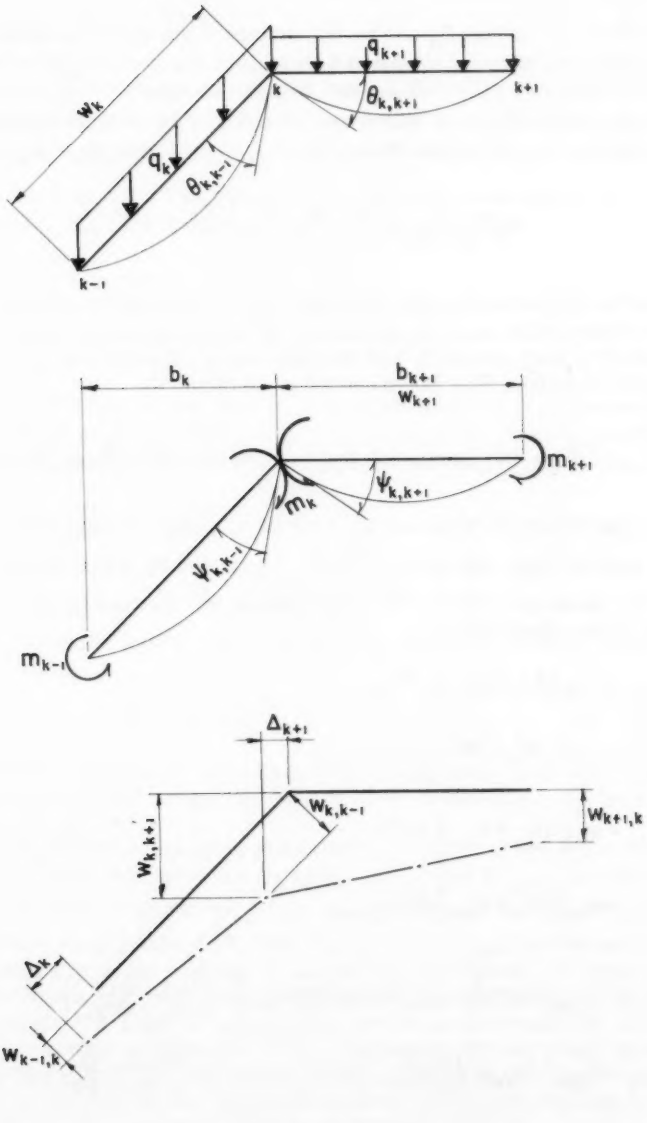
$w_k$
$q_k$
$\theta_{k,k-1}$
k-1
k
$q_{k+1}$
$\theta_{k,k+1}$
k+1
$b_k$
$b_{k+1}$
$w_{k+1}$
$m_{k+1}$
$\psi_{k,k+1}$
$m_k$
$\psi_{k,k-1}$
$m_{k-1}$
$\Delta_{k+1}$
$w_{k,k-1}$
$w_{k+1,k}$
$w_{k,k+1}$
$\Delta_k$
$w_{k-1,k}$

Fig. 16

Equation 10, when written at joint n-1 and n will require values of $\bar{m}_{n+1}$, $\bar{\Delta}_{n+1}$ and $\bar{\Delta}_{n+2}$. These values can be obtained from an analysis of the typical interior folded plate unit. A measure of the accuracy of the solution is given by a comparison of the value obtained for $\bar{m}_n$ from equations 10 and that obtained at the same joint in a typical interior unit.

This analysis requires the solution of 2 sets of simultaneous equations each involving n unknowns. The solutions proposed by Gaafar[6] or when applied to this problem each require the solution of only one set of simultaneous equations of n unknowns. However in addition n sets of "moment distributions" must be performed to evaluate deflection effects and the total labor would appear to be greater than that for the method proposed here.

7. When the stress in the end plate exceeds the permissible value a reduction of stress can be obtained, either by increasing the size of the end plate, or by supplying additional transverse support. The increase in the width of the end plate is limited by the transverse moment capacity at joint 1. Where the end plate is horizontal, as in Fig. 14, it may be possible to supply restraint against vertical deflection at joint 0 by the use of intermediate columns along line 0. The addition of these columns would cause a reduction in $m_1$, thus allowing an increase in $b_1$.

For the folded plate section shown in Fig. 14 the end plate disturbance can be reduced by the introduction of intermittent ties between plates 1 and 5. If a single tie were added at mid span the change in deflection of plates 1 and 5 is as given below.

$$\bar{\Delta}_{1T} = -\frac{P_T L^3}{48 E I_1} \tag{14}$$

$$\bar{\Delta}_{5T} = \frac{P_T L^3}{48 E I_5} \tag{15}$$

$$P_T = \frac{A_T E_T}{L_T}\left[\bar{\Delta}_1 + \bar{\Delta}_{1T} - \bar{\Delta}_5 - \bar{\Delta}_{5T}\right] \tag{16}$$

The force in the tie is obtained from equation 16.

In the above equations $P_T$ is the force in the tie and $A_T$, $L_T$ and $E_T$ are the crossectional area, length and modulus of elasticity of the tie respectively. With the addition of the tie an approximate solution for plate stress is obtained by substituting $\bar{\Delta}_1 + \bar{\Delta}_{1T}$ and $\bar{\Delta}_5 + \bar{\Delta}_{5T}$ for the original values of deflection in equation 13. A revised solution for joint moments and plate stresses can then be obtained.

## Standards and Practice

Except for a few provisions particularly pertinent to folded plate construction, practice in connection with aggregates, material and product, tests, concrete quality, allowable unit stresses, the mixing and placing of concrete, forms and details of construction, etc., should follow the normal requirements of codes such as the Building Code Requirements for Reinforced Concrete (ACI 318-56).

Folded plate design will vary from what is specified in the typical code in regard to methods of analysis, precautions against buckling instability, camber and deflection controls, permissible combined flexural, shear and axial unit stresses, corrosion control and fire protection requirements.

Folded plates, like shells, utilize thin sections with the concrete distributed over large surfaces. The load carrying capabilities of these sections, because of thinness, depend on the local as well as the general stability of the section. Readily available methods of analysis for buckling stability of plates with varying types of edge support may be used. Somewhat higher factors of safety are recommended than normally required in metal construction. On most concrete folded plates a factor of safety of 5 to 6 can be provided by small variations in the thickness and geometry of the folds without affecting the economy of the structure. Structures designed to this criteria have behaved well under severe overload and test conditions. Designs based upon ultimate strengths for safety under overload should also consider the local effects of stress transfer to ascertain that the assumed configuration will either be maintained at ultimate loads or, if distortion occurs, that the reduced capacity is adequate to provide the necessary factor of safety. Changes in stress caused by geometrical displacements should be included in the design.

Camber and deflection controls follow those prevalent for beam and slab design. Overall deflection can generally be determined on the basis of the gross crossectional area for computing the moment of inertia. For longtime loads the effective modulus may be approximated by using 750,000 psi for stone concrete and 500,000 psi for lightweight aggregate concrete. Where sag becomes a problem, a small amount of compression steel will be very effective in controlling deflections. Other local deflection additives may be approximated by consideration of the effects of transverse distortions as described in the methods of analysis. In case the plate width is narrow compared to the span and the break in the surface at the connecting edges is small, strains in the plane of the plate may cause large local displacements, loss of edge support and consequent buckling of the member. Rules accounting for the latter motions are difficult to formulate because of the infinite combinations possible in different configurations, but for angles over 25° on plates 1/20 or more of the span, the effect may be considered small.

Care must be exercised so as not to introduce curves into tension chords during the cambering process as the introduced radial force components will tend to force the edges into straight lines. Such cambers are useless for correcting overall elastic and plastic deflections.

Unit stresses can be governed by usual code requirements, however, care must be exercised to relate maximum stress to buckling stress by adequate factors of safety. Except where governed by buckling, direct design stresses in the flange up to $0.45f'_c$ and shearing stresses (with web reinforcement) to 200 psi have been used numerous times without signs of distress.

The usual practices relating to corrosion protection are applicable to folded plate construction. While the cracking in the deep corrugated sections may be less than in slender conventional beams, the light reinforcement is somewhat more difficult to hold to fine tolerances, particularly on the sloped sections and there appears no justification for reducing cover required by the ACI code in buildings of comparable construction. Carefully controlled precast folded plates with accurately placed reinforcing steel and rich concrete

steel coverage should be governed by the presently established ACI requirements for Thin Skin Precast Concrete.

Numerous inadvertent tests have proven that folded plate structures with the usual ACI covers behave well under severe fires. Intensities high enough to spall and strip the cover over the bars have not caused collapse, disturbing deflections or, as demonstrated by subsequent load test, a reduction to the safe capacity of the member. Assuming the use of suitable aggregate, cover sufficient to satisfy corrosion protection requirements should be sufficient for fire protection. Where fire causes spalling, subsequent protection of reinforcing steel can be provided by use of gunite patching or other suitable remedial measures.

At points of restraint such as stiffener ribs, frames and end beams special consideration should be given to the plate design. Ordinarily the folded plates are able to accommodate volumetric changes by slight sidesways and small flexural adjustments. However these thin plates are subject to rather quick and intense volume changes and the sections invariably will crack where these motions are restrained by thicker slower acting frames and rigid beams. At these restraint points, the slab must be reinforced at the juncture to resist and distribute cracking.

Both lightweight and stone concrete have been used extensively for folded plate roofs. Both provide the strengths required for any normal design. While the modulus of the lightweight concretes may only be one half to two thirds that of stone concrete, this usually does not cause deflections which cannot be provided for in the design.

## Construction Procedures

Formwork and Falsework - Forming details for folded plate construction have been as varied as the applications that can be made of folded plates. A majority of the simple span falseworks have consisted of a light wood or tubular working platform on which is set self-contained surface units shaped to the fold configuration. Space may be provided at the platform so that the upper sections can be dropped as an integral unit by means of a jack assembly located at ground level. In one installation small construction holes were left in the folded shell. When the concrete had obtained sufficient strength the top sections were supported from the shell through these holes while the lower platform was moved forward, after which the top sections were lowered to ground level by means of cranes and subsequently rolled forward at that level. This procedure added to the number of operations but obviated more complicated raising and lowering operations at either the platform top, or ground levels.

On large, deep folded plates the form sections are more intricate and heavier and it is usually necessary to provide a mobile falsework accommodating the greater weights and the deeper sections.(8) Various schemes have worked satisfactorily and it is doubtful whether even the contractors have sufficient cost data to evaluate any appreciable savings of one scheme over the others.

Because of the desirability of obtaining maximum re-use of the falsework without excessive delays to progress of the work it is customary to permit decentering of the formwork within 3 to 5 days from the day of the pour. Decentering is controlled by stripping cylinders which are required to show

minimum specified strengths prior to the decentering. These strengths ordinarily are established to assure a minimum modulus and a strength of at least 2500 psi at the time of stripping.

Decentering of the falsework ordinarily does not invoke particular difficulties but requires solely that the steps of the operation are recognized. The falsework must be designed so that strains caused by any part of the pour will not damage concrete already reaching the set stage. The decentering can usually be done using visual reference to line or level points as the concrete structure will usually be much stiffer than the supporting falsework. At this time the concern is limited to obtaining a gradual easing of individual post loads such that excessive load concentrations are not induced in individual framing and supports which could overload the falsework locally, buckle individual posts, or provide reactions to the plate structure that were not considered in the design.

Joint and Edge Details - Construction joints at the edges of the plate pours usually are not critical because the flexibility of the edges usually permits closure of succeeding pours by shoring or clamping of adjacent edges into one plane. One common method of making the joints is to decenter several sections and then connect the adjacent sections by means of a narrow cast joint. In some cases, where falsework area is available, the edge of the previous pour is shored to the theoretical position and the new concrete is cast against the previous section. The latter method will result in load transfer between sections but the folded plate unit is usually too flexible in bending and torsion to reduce the ultimate load capacity of the sections.

The edge configuration may be handled in many ways depending on the span of the folded sections and the desired architectural treatment. On many types of folded plate structures a vertical or horizontal edge plate will effectively terminate the sides of the building. For large spans the width of horizontal plate needed to restrain the edge of the adjacent plate will require thick sections and heavy reinforcement to carry its own weight as a cantilever. In this case it is often advisable to cut down the required width by tieing the exterior plate back to interior plates and thus reducing the "plate action" bending. The temporary edges at construction joints can be treated in the same manner. Columns may be placed under the edges for vertical support if properly considered in the design.

Reinforcing - Reinforcing steel is likely to be light and closely spaced to distribute such cracking as may occur in the concrete. Because of this lightness and the difficulties added by the sloped plates, the steel in place should be protected by walkways and working platforms. The steel patterns are likely to appear complicated on the drawings but only because the steel is usually more elaborately detailed than for more conventional slab construction.

Folded plate structures are usually long with simple steel patterns. This results in arrangements ideally adaptable to ground fabrication of much of the heavier steel into mats. These mats can be placed in large sections by means of crane operations. In such cases careful attention should be given to the location of each layer of bars so that the fabricated systems will mesh properly at all points without lacing of the bars.

Casting Techniques - Casting techniques for folded plate construction are not particularly difficult or different from that for conventional construction. The overall section is usually so effective that the slabs are insensitive to local flaws or weaknesses except possibly in the areas of maximum shear transfer at the support points. In the transverse direction between folds, the

strength requirements are similar to those of normal slab construction except that the span is usually so short that the flexural stresses are low. Accordingly the folded plates can be cast employing the same concrete handling techniques utilized for normal concrete joist, waffle and flat slab construction, in spite of the thinness of construction and some difficulties added by the sloped surfaces.

As the slope of the surfaces approaches 45° care must be exercised to achieve the desirable compactness and smoothness. In the experience of the writers most sloping plates up to 45° have been poured without the use of top forms. To accomplish this, the bottom plates are usually placed ahead of the rest of the pour. This is followed by feeding the concrete down the slope from the top and working the concrete around horizontal bars on the slope. Concrete slumps maintained between 1-1/2 to 2-1/2 inches are stiff enough for slopes up to 45°. Higher slumps than these will result in flow of the concrete down the slope while lower slumps are unnecessary and too unworkable to allow reasonable production speed. Bars closely spaced, which is desirable for stress distribution and reduced plate thickness, will also support the wet concrete and help prevent it from slumping down the slope. Spading is preferable to excessive vibration which may initiate sag in the finished concrete immediately behind the pour operation.

In other projects, methods of pouring sloping surfaces have included the use of modified top forms. Examples of these range from light ply-wood panels attached to the lower surface to large size crane-handled sectional frames covered by an open mesh surface. These double forming methods allow vibration compaction, the open mesh being particularly effective in restraining the concrete while permitting escape of entrapped air and water. Methods such as these utilizing the lower form surface for alignment and support are inexpensive, running from $0.05 to $0.12 psf.

A more general method of pouring utilizes a rack or ladder section with longitudinal dividers set above the concrete surfaces (Fig. 17). The section progresses with the pour and forms a ladder-platform for the workmen which also restrains the concrete from slip or flow during the vibration.

On a new job, the techniques of concrete control, slump regulation and vibration are usually mastered in the first three or four hours of the first pour, after which the pouring operation proceeds as smoothly as in other construction.

## Protective Cover and Insulation

A wide variety of covers and insulations have been used on folded plate structures with varying degrees of success. Among the coverings are included reinforced bitumens, cold bitumens, bituminous roofing felts, asphalt and reinforced asphalt, vinyls, acryllics and acryllic plasters. Unfortunately the experience record is too short on most of these roofing types to offer more than comment and such recommendations as are believed to be sound on the basis of limited experience.

The folded reinforced concrete sections are inherently a tight waterproof type of construction. Usually the supporting structure of these roofs offers little restraint in the direction of the long span and the folded slab is flexible in the transverse direction so they are not subject to the usual shrinkage and temperature cracking inherent in restrained slab construction. When

Fig. 17. Placing of Concrete

prestressed in the main span direction and reinforced to distribute local cracking at stiffener restraint points, the shells are watertight and have been tested up to six foot water heads without leakage. With non-prestressed reinforcing, minor cracking will occur in the bottom plates of simple spans and also along the top plates at points of restraint or in cantilevered areas. Again these cracks are limited if the reinforcing is well distributed and worked at normal unit stresses. However, in spite of the good experience with bare plate roofs, the practice of leaving the concrete devoid of insulation and covering invites larger motions and water penetration and is highly questionable where the class of construction warrants a cover.

Normal multiple felt roofing laid over insulation and anchored to wood strips will assure protection and can be furnished with 10, 15 and 20 year roofing bonds. The cost will range between $0.30 to $0.50 psf.

Vinyls are available in a variety of rich colors suitable for exciting architectural effects. Experience has indicated that these vinyls will behave satisfactorily except over wide or working cracks that open after the coating is applied. Such cracks, incidently, can be covered by vinyl reinforced with glass fabric. However, vinyls form a membrane sealing the surface of the concrete with the possible entrapment of moisture and consequent blister problems. Adequate thicknesses (30 to 40 mils) must be used and the cost will likely range from $0.50 to $0.75 psf.

The experience with acrylics has been both good and bad depending on the circumstances. Placed under specified conditions on a clean surface, the bond has been good as observed over several years and this material can

supply an acceptable cheap roof. Placed over wet concrete in areas where water ponds, on dusty surface or applied during low temperatures, this covering has been known to strip badly over large areas. The colors available are good. Solvent type and water emulsion types are available with the advantage appearing to be with water emulsion because of the probable moisture content of the concrete. The acrylic coatings will not bridge cracks formed after application of the surfacing. The cost is very low, being only about a third of felt ply roofing. Acrylics reinforced with glass fabric may be a good cheap roofing solution but no experience record is available on such an installation.

A good solution where insulation is not required above the slab surface appears to be the use of asphaltic coating with a powdered aluminum surface and reinforced with glass fabric. The reinforcing is flexible enough to bridge small cracks. Aluminum green, blue and limited red colors are available with all apparently reducing to aluminum in time. The cost is somewhat less ($0.20 to $0.35 psf) than that of ply roofs. Ten year guarantees at a lower cost and 15 year bond at higher cost will be furnished by certain manufacturers.

Insulation materials have been applied to both the inside and outside of folded plate slabs. Exterior insulation is desirable in that it reduces volumetric strains in the concrete and keeps the dew point temperature outside of the concrete surface. Such insulation is usually set between wood nailers and covered with felt roofing.

Insulation on the undersurface of the concrete has been used in many installations with reported good results. In many cases this inside insulation has served the double purpose of acting as the form surface or dual purpose of insulation and acoustical material. Inner insulations permit the use of roofing membranes offering a wider selection of colors.

## Economics

Basic data on typical material quantities are presented in Figs. 18 and 19. This information is based on particular folded plate units, section heights, control joints and type of beam framing. The expansion of this information to estimated building costs, as shown in Fig. 20, furnishes an interesting comparison with joist construction. These serve to illustrate the possibilities of folded plate construction. Fig. 20 also reflects contractors' bid prices for specific designs built in widely separate locations utilizing varied construction methods.

The average quantity of concrete required per square foot of floor area for folded plate structures will obviously depend on the configuration of the folded plate utilized in the design. Average thicknesses based on some 15 preliminary designs and checked against a number of final designs are shown in Fig. 18. These designs are largely for plates folded into a corrugated form similar in shape to that of the Central Warehouse roof. (Fig. 10) For simple spans the ratio of span to height ranges from 13 to 25. For cantilever spans the ratio of span to height is approximately 10.

For short spans the thickness of the folded plate is controlled by the criteria established for protection of reinforcement. For the designs used in cost comparisons a minimum cover of 3/4 in. on transverse steel and 1-1/2 inches on main steel was selected. Minimum steel and these covers governed the plate thickness in spans less than about 60 ft. where flexural and shear stress requirements begin to govern the design.

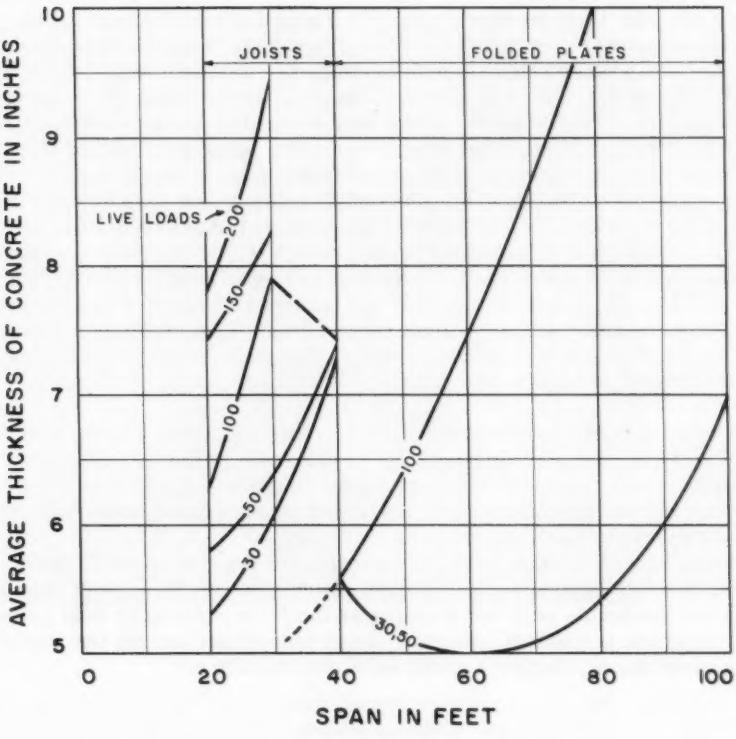


Fig. 18

It was assumed that the folded plates terminate on continuous beams at each end of each span. Inasmuch as these beams vary only slightly in total dimension with increases in the span, the average thickness (of slab plus edgebeam) actually decreases with increase in span up to an optimum point. This variation is reflected in the plot of the average thickness curves.

As the span increases beyond the point of minimum materials for the given sectional height, a lesser quantity of materials could be obtained than shown on the curves by decreasing the span-to-height ratio. However the entire configuration of the plates used on any given project is so controlled by many other factors such as esthetics, building volume, roofing and pouring costs, etc., that refinements were considered beyond the scope of this paper.

The reinforcing steel requirements are relatively low for folded plate construction, Fig. 19. This results from the unusually large lever arm furnished by the folds in the direction of the main span as compared to flat slab or concrete joist construction, and the usually very short transverse span between foldedges. Furthermore the bulk of the concrete is dispersed into areas and geometrical positions where it is highly efficient in carrying the developed stresses.

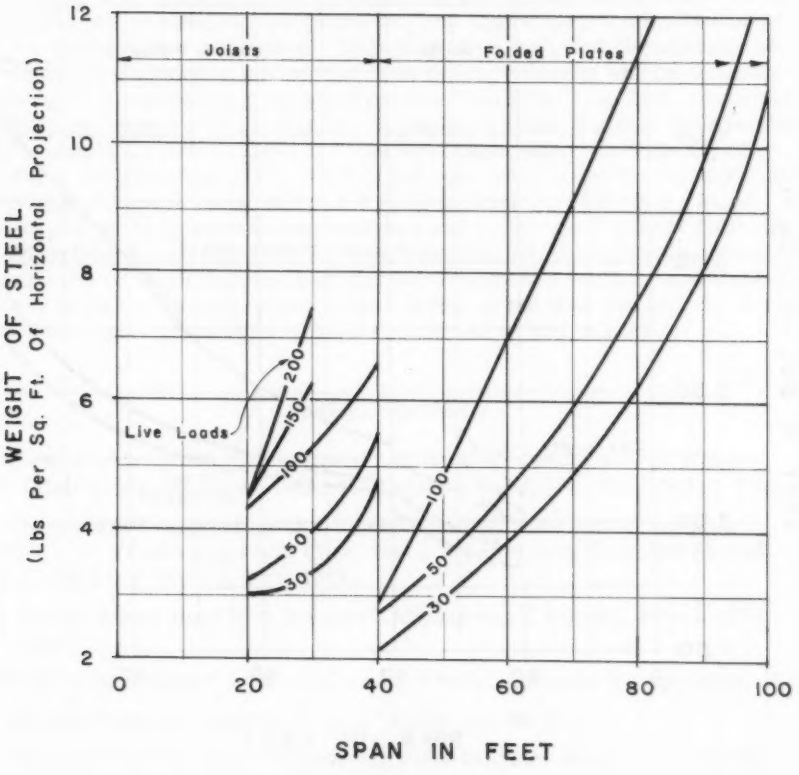


Fig. 19

The cost of concrete placement is similar to that for flat slab and joist construction with the exception of some additional time required for the handling and compaction of the concrete on the inclined surfaces. As an example, on the first and always most difficult pour of a 4 ft. high, 80 ft. span, a pour section covering 3200 square feet of roof area of folded plate and edge-beams used 73 c.y. of concrete. A crew consisting of one foreman, ten laborers, and two cement finishers placed and finished all work on the roof in 7-1/2 hours. A crane with operator and two mixers and a four man crew mixed and delivered the material to the roof.

Cost estimates for folded plates of a corrugated configuration are shown and compared with similar estimates for concrete joist construction in Fig. 20. The unit prices used in the cost buildup are as follows:

| | Joist | Folded Plate |
|---|---|---|
| Concrete | $22/Yd. | $37/Yd. |
| Reinforcing | $0.16/# | $0.16/# |
| Formwork | $0.60/SF | $0.85/SF |

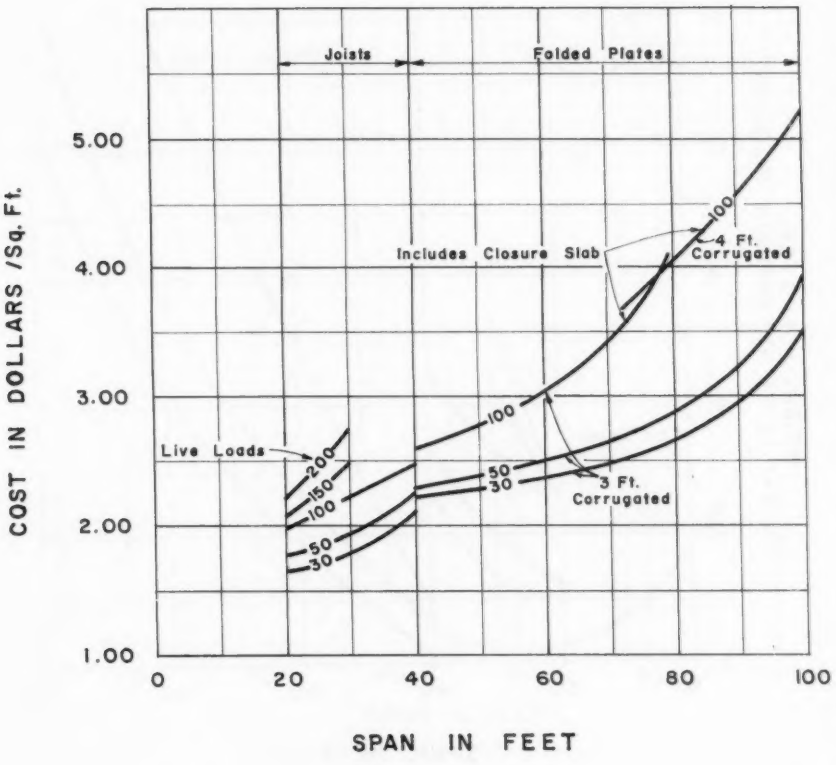


Fig. 20

These estimates show that generally the conventional framing is practical to spans up to 30 to 40 ft. Beyond this the cost increases rapidly and difficulties are introduced due to weight and deflections which limit further increase in span. The folded plate spans however can increase to 80 ft. or more at a cost of only $0.40 to $0.50 per square foot over the cost of the short spans utilizing conventional framing. This is true for both lightly loaded roofs and heavily loaded floors. The flat surfaces and geometrical form in many cases permit utilization of the exposed concrete surface for architectural treatment. This results in the elimination of suspended ceilings and savings thus effected may be more than the increase of the long span folded plate construction as compared with short conventional spans.

Another saving achieved in certain installations has resulted from the utilization of closed cells as ducts to distribute conditioned air. The savings shown by contractors' prices for alternate schemes with and without metal ductwork on one particular project showed savings great enough to pay for a substantial part of the total cost of the roof. The results experienced on this building over several years operation utilizing the structural system as the duct lines were exceptionally good because the area and volume of the ducts

were larger than could be afforded in normal mechanical installations. This resulted in low pressures, low velocities, and draft-free rooms with almost uniform temperature throughout. Estimates have indicated the economy of this framing in special applications. This is illustrated by one installation involving 50 ft. spans carrying a 250 psf live load (Fig. 11). Here numerous preliminary designs in structural steel, concrete beam and slab construction, and composite structural steel and concrete emphasized the difficulty of building a structure which would allow passage of the large ductwork systems needed for air conditioning within a 3 ft. total height. A 3 ft. high closed folded plate on 15 ft. module was designed and constructed without difficulty.

Where folded plates are used in roof construction, care must be exercised to shape the roofs so that drainage can be accomplished without multitudinous headers to relieve local trapped areas. If this is not done the added plumbing costs will tend to price the overall structure out of competition.

## REFERENCES

1. "Cantilevered Folded Plate Roofs ACI Headquarters" by C. S. Whitney, Journal of the American Concrete Institute No. 4, Vol. 30, October 1958.
2. "Design and Construction of a Folded Plate Roof Structure" by Milo S. Ketchum, Proceedings Am. Conc. Inst., Vol. 51, 1954-5, p. 449 (see also Architectural Forum, Feb. 1955).
3. "Folded Plates Roof New Hangars" Architectural Record, March 1958, p. 223.
4. "Flachentragwerke" by K. Girkmann, 2 Aufl., Apringer Verlag Wien, 1948.
5. "Hipped Plate Construction" by G. Winter and M. Pei.
6. "Hipped Plate Analysis Considering Joint Displacements" by I. Gaafar, ASCE Proceedings, April 1953.
7. "Design of Prismatic Shells" by H. Craemer, ACI Journal, Feb. 1953.
8. "Concrete Hangars Spread Folded Slab Wings" Eng. News-Record, Vol. 160, 1958, p. 46.

Journal of the
STRUCTURAL DIVISION
Proceedings of the American Society of Civil Engineers

# LATERALLY DEFLECTED COLUMNS

John Sherman,[1] F. ASCE

## SYNOPSIS

Column formulae in current specifications(1) are based on the assumption that the unbent axis of the column remains in its original position for all conditions of loading. It is the object of this paper to consider the case of a column of which the unbent axis is rotated about one end due to the deflection of the other end, a condition which occurs in portals and bents when subjected to lateral loading, and in truss members due to the deflection of the truss. For the purpose of this paper a column which deflects as described above will be called a laterally deflected column.

The simplest case of a laterally deflected column has both ends fixed to prevent roration. When the column is loaded with an axial compressive force P, and a horizontal shearing force H is applied at the top of the column, the deflection of the column can be considered to be made of two parts, 1 the deflection due to H, and 2 the deflection due to the displacement of the force P. The deflection due to P produce additional bending which increases the deflection, this phenomena continuing until the deflection reaches a final value. It will be shown how the value of this final deflection can be determined from the differential equation of the elastic curve of the column.

The moments at the ends of the column, which are equal for the fixed end column, can be closely approximated as follows. If the deflection due to P is ignored and the deflection due to H is $\delta'$, then the bending moments at the ends of the column become

$$M = \frac{HL}{2} + P\delta' \qquad (1)$$

in which M is the bending moment and L is the length of the column. Eq. (1) forms the basis of the approximate method which will be discussed in this paper.

Note: Discussion open until March 1, 1960. To extend the closing date one month, a written request must be filed with the Executive Secretary, ASCE. Paper 2221 is part of the copyrighted Journal of the Structural Division, Proceedings of the American Society of Civil Engineers, Vol. 85, No. ST 8, October, 1959.

1. Engr., American Bridge Div. U. S. Steel Corp., Roanoke, Va.

## NOTATION

The letter symbols adopted for use in this paper are defined where they first appear, in the text or illustrations, and are arranged alphabetically for convenience of reference in the appendix.

---

## INTRODUCTION

Column action has long been a matter of great interest and the present formulae used in design closely approximate the results obtained from mathematical investigations and loading tests. For the case where the axial compressive force P is eccentrically applied to the ends of the column the secant formula is applicable.

Considering the axial compressive force P as a load, the secant formula covers the following conditions of application of the load P.

1. The eccentricity of application of the load is the same at each end of the column.
   (a) The eccentricities lie on the same side of the column.
   (b) The eccentricities lie on opposite sides of the column.
2. The eccentricity of application of the load is larger at one end of the column than at the other end.
   (a) The eccentricities lie on the same side of the column. This is the general case of the secant formula which can be stated as follows; there is a magnitude of the load which will be denoted by $P_1$ which will produce a moment at a point in the column, near the end where the large eccentricity is applied, equal to the moment at that end of the column. Therefore, any load larger than $P_1$ will produce a larger moment at an interior point of the column than the moment at the end where the large eccentricity is applied.
   (b) The eccentricities lie on opposite sides of the column. In this case the maximum moment occurs at the end which has the largest eccentricity.
3. The column is subjected to lateral loads in addition to the load P. In this case the eccentricities are taken to be equal and on the same side of the column.

In all of the above cases of the secant formula the unbent axis of the column is assumed to remain in position, therefore, the secant formula unless modified is not applicable to the columns of the laterally loaded portals shown in Fig. 1.

The column bases in Fig. 1 are fixed, and as the portal deflects the columns rotate about the bottom panel point of the portal relieving the moment at this point and increasing the moment at the base of the columns.

If the location of the point of contraflexure and the deflection $\delta$ of this point are calculated from the moments due to the shearing force H, then an approximation of the moment at the base of the column is

$$M = HmL + P\delta \qquad (2)$$

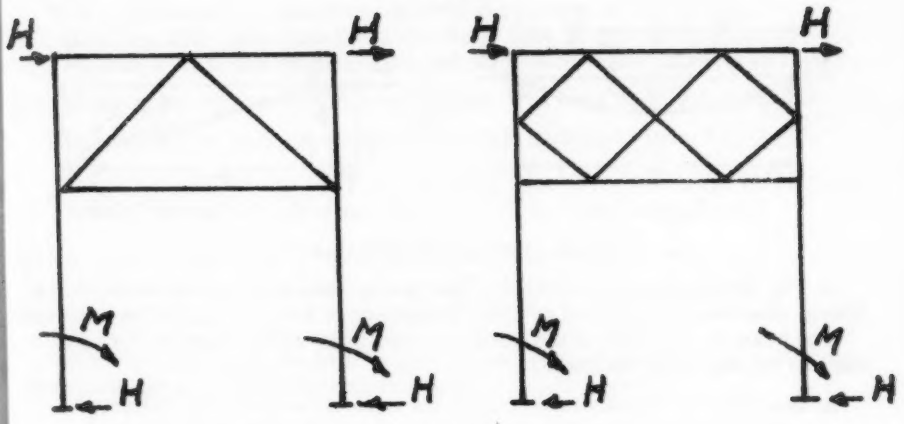


a. b.

Fig. 1. Showing Typical Portals.

in which mL is the distance from the base of the column to the point of contraflexure.

The portal shown in Fig. 1(b) has shorter panels than the portal shown in Fig. 1(a) and has smaller moments at the bases of the columns. Therefore, by using stiff portals the effect of lateral buckling can be controlled in design.

This paper will be restricted to the analysis of columns such as shown in Fig. 1, for which the following assumptions will be made;

(a) The unit stresses in the portal bracing is small and the rotation of the portal can be neglected. Therefore, the panel points of the portal will be assumed to remain in a vertical line during deflection.

(b) Since the columns are much more rigid than the portal bracing it will be assumed that the column is hinged at the top of the portal and continuous over the portal struts.

(c) From the above assumptions it follows that for all loads applied within the depth of the portal the shearing force H and the moments $M_1$ and $M_2$ are the same for each column.

The above describes the arrangement and loading for which equations for the safe working stress $f_w$ will be calculated, 1 by the approximate method as described, and 2 by the more precise method which takes into account the effect of the deflection due to the displacement of the line of action of the axial compressive force P.

The case of a column fixed at both ends will be first considered: then the slope of the column at the bottom of the portal and the effect of the axial compressive force P on this slope will be calculated; and finally the two cases described above will be combined to cover the general case shown in Fig. 1.

## The Column Below the Portal

In Fig. 2(a) is shown a simply supported beam having a length L with a lateral load 2H acting at midspan and an axial compressive force P applied at each end.

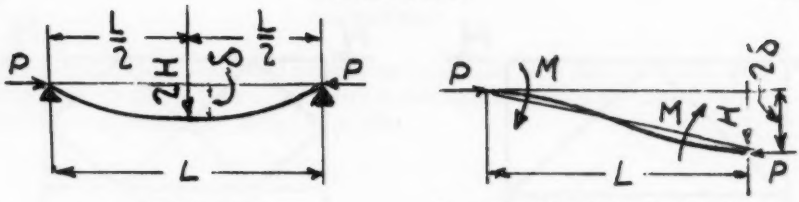


a. Simple Beam b. Laterally Deflected Column

Fig. 2. Showing Elastic Curves.

In Fig. 2(b) is shown a laterally deflected column fixed at both ends with a lateral shearing force H and an axial compressive force P applied at each end.

The beam in Fig. 2(b) is the semi inverted form of the beam in Fig. 2(a) and has the following similarity;

(a) The moment at a distance x from the ends of the laterally deflected column is numerically equal to the moment at a distance x from the midspan of the simple beam, therefore, the moments acting at the ends of the laterally deflected column are numerically equal to the moment at midspan of the simple beam.
(b) The curvature at any point of the laterally deflected column is numerically equal to the curvature at the same point in the simple beam.
(c) From the above it follows that the deflection of the point of contraflexure of the laterally deflected column is equal to the deflection at midspan of the simple beam.

The solution for the moment at midspan of the simple beam is known,(2) from which it follows that the moments at the ends of the laterally deflected column are

$$M = \frac{HL}{2}\,\frac{\tan u}{u} \tag{3}$$

in which

$$u = \frac{L}{2r}\sqrt{\frac{f}{E}} \tag{3a}$$

In Eq. (3a) r is the radius of gyration in the plane of bending, f is the average compressive stress due to P, and E is the modulus of Elasticity in tension and compression.

Eq. (3a) can be written

$$u = \frac{L}{2}\sqrt{\frac{P}{EI}} \tag{3b}$$

from which

$$P = 4u^2\frac{EI}{L^2} \tag{3c}$$

Substituting $\frac{\pi}{2}$ for u in Eq. (3c) the value of the critical load $P_c$ is

$$P_c = \pi^2\frac{EI}{L^2} \tag{4}$$

This is the smallest load that can keep the column in the deflected shape shown in Fig. 2(b). The load $P_c$ is the Euler load for the column, the deflection due to this load is apparently indeterminate. This is because the approximate expression for curvature $\frac{d^2y}{dx^2}$ has been used in deriving Eq. (3).

The value of the average compressive stress obtained from Eq. (3a) is

$$f = 4u^2r^2\frac{E}{L^2} \tag{5}$$

which when u is taken as $\frac{\pi}{2}$ becomes the buckling stress $f_b$, where

$$f_b = \pi^2r^2\frac{E}{L^2} \tag{6}$$

When the deflection due to P is ignored the deflection of the point of contraflexure of the laterally deflected column is

$$\delta = \frac{HL^3}{24EI} \tag{7}$$

Substituting Eqs. (3c) and (7) in Eq. (2) gives the following approximation for the moments at the ends of the column

$$M = \frac{HL}{2}\left\{1 + \frac{u^2}{3}\right\} \tag{8}$$

The difference between Eq. (2) and (8) is shown by the following infinite series

$$\frac{\tan u}{u} = 1 + \frac{u^2}{3} + \frac{2u^4}{3.5} + \frac{17u^6}{3^2.5.7} \cdots\cdots\cdots \tag{9}$$

in which it is seen that the first two terms appear in Eq. (8), the remaining terms representing the effect of P. When u is equal to $\frac{\pi}{4}$, taking the first two terms of the series the error is six and one half per cent. Therefore for smaller values of u Eqs. (2) and (8) are in good agreement.

Equating the yield point stress to the total stress in the column

$$f_y = f_w\left\{1 + \frac{Hc}{Pr}\frac{L}{2r}\frac{\tan u'}{u'}\right\}n \tag{10}$$

in which $f_w$ is the allowable average compressive stress based on using a safety factor n, c is the distance from the neutral axis of the column to the extreme fibre, and

$$u' = \frac{L}{2r}\sqrt{f_w\frac{n}{E}} \tag{11}$$

Solving Eq. (10) for $f_w$

$$f_w = \frac{\frac{f_y}{n}}{1 + \frac{Hc}{Pr}\frac{L}{2r}\frac{\tan u'}{u'}} \tag{12}$$

Values of $\frac{\tan u}{u}$ are given in the appendix.

The corresponding equation for $f_w$ based on the approximate method is

$$f_w = \frac{\frac{f_y}{n}}{1 + \frac{Hc}{Pr}\frac{L}{2r}\left\{1 + f_w \frac{n L^2}{12 E r^2}\right\}} \tag{13}$$

It has been stated that the secant formula is not applicable to lateral deflected columns unless modified. The following form of the secant formula is noted as Formula C in AASHO specifications.

$$S = \frac{\frac{f_y}{n} - \frac{Mc}{I}}{1 + \left\{.25 + (e_o + d)\frac{c}{r^2}\right\} \sec \frac{1}{2}\phi} \tag{14}$$

In the above formula, M is the bending moment due to loads applied transverse to the axis of the column, d is the deflection due to M, $e_o$ is the eccentricity of the axial compressive force P, which is taken to act on the same side of the column at each end, s corresponds to $f_w$, sec $1/2\,\phi$ corresponds to secu', and the factor .25 is taken to represent the inherent crookedness of the column; the remaining terms correspond to the notation used in this paper.

This formula is approximate to the same extent as Eq. (12) except for the secant term which is an additional approximation since it is correct only for the case of a continuous uniform load.

Taking the transverse load as 2H the column can be semi-inverted and can be taken to apply to the laterally deflected column by making the following substitutions; $M = \frac{HL}{2}$, $d = \frac{HL^3}{24EI}$, and using Eqs. (3c) and (8), from which the following equation is finally obtained.

$$f_w = \frac{\frac{f_y}{n}}{1 + \frac{Hc}{Pr}\frac{L}{2r}\left\{1 + \frac{u'^2 \sec u'}{3}\right\}} \tag{15}$$

The term $(1 + u'^2 \sec u')$ is closely equal to $\frac{\tan u'}{u'}$ for values of u' not larger than one.

The factor of safety is taken as 1.76 in AASHO specifications, using this value for n the Euler stress becomes equal to $\frac{f}{n}y$ when

$$\frac{L}{r} = \pi \sqrt{\frac{1.76\,E}{33{,}000}} \tag{16}$$

Therefore, the yield point stress 33,000 p.s.i. can be used for $f_y$ in Eqs. (11),(12) and (15) when applied to primary members.

Eqs. (11) and (15) must be solved by trial and error, Eq. (15) giving results which compare favorably with the results obtained by Eq. (11) but is more

troublesome to solve. Eq. (13) is quadratic in respect to $f_w$ and can be used to obtain a trial value of $f_w$ to use in the solution of Eq. (11) or (15).

### The Column Within the Portal

In the following a general equation, which takes into account the effect of the axial compressive force P, will be developed for slope of the elastic curve of the column at the bottom of the portal.

The situation of the column within a two panel portal is shown in Fig. 3; an axial compressive force is applied at each end, and a moment $M_2$ is applied at support 2 which represents the bottom of the portal. $M_2$ can be due to any loads on the column below the portal or at the portal panel points.

The slope $\theta_2$, at support 2, can be determined when the relation between $M_2$ and $M_3$ is found.

In span aL the moment $M_x$ at distance x from support 2 is

$$M_x = + M_2 - (M_2 - M_3)\frac{x}{aL} + Py \tag{17}$$

Substituting Eq. (17) in the differential equation of the elastic curve the following differential equation of the second order is obtained;

$$EI\frac{d^2y}{dx^2} = - M_2 + (M_2 - M_3)\frac{x}{aL} - Py \tag{17a}$$

The complete solution of Eq. (17a) is

$$y = A\cos kx + B\sin kx - \frac{M_2}{P} + (M_2 - M_3)\frac{x}{PaL} \tag{17b}$$

in which

$$k = \sqrt{\frac{P}{EI}} \tag{17c}$$

The constants of integration, A and B, are determined from the condition that y is zero at each end of span aL. It is, therefore, concluded that

$$A = + \frac{M_2}{P} \tag{17d}$$

and

$$B = - \frac{M_2}{P\tan kaL} + \frac{M_3}{P\sin kaL} \tag{17e}$$

Substituting the above values of A and B in Eq. (17b) gives the following equation for y

$$y = + M_2\cos kx - \frac{M_2\sin kx}{P\tan kaL} + \frac{M_3\sin kx}{P\sin kaL} - \frac{M_2}{P} + (M_2 - M_3)\frac{x}{PaL} \tag{18}$$

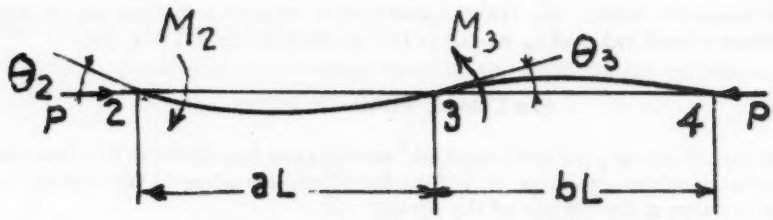


Fig. 3. Showing Elastic Curve of Column Within Portal.

The first derivative of Eq. (18) is

$$\frac{dy}{dx} = -\frac{M_2}{P}k\sin kx - \frac{M_2}{P}\frac{k\cos k}{\tan kaL} + \frac{M_3}{P}\frac{k\cos kx}{\sin kaL} + \frac{(M_2 - M_3)}{PaL} \tag{19}$$

Substituting x = 0 and x = aL in Eq. (19) gives the following equations for the slopes at supports 2 and 3

$$\theta_2 = +\frac{M_2}{P}k\left\{\frac{1}{kaL} - \frac{1}{\tan kaL}\right\} + \frac{M_3}{P}k\left\{\frac{1}{\sin kaL} - \frac{1}{kaL}\right\} \tag{19a}$$

$$\theta_3 = +\frac{M_2}{P}k\left\{\frac{1}{kaL} - \frac{1}{\sin kaL}\right\} + \frac{M_3}{P}k\left\{\frac{1}{\tan kaL} - \frac{1}{kaL}\right\} \tag{19b}$$

Introducing the notations

$$p_{u_a} = \frac{3}{2u_a}\left\{\frac{1}{2u_a} - \frac{1}{\tan 2u_a}\right\} \tag{20}$$

$$q_{u_a} = \frac{3}{u_a}\left\{\frac{1}{\sin 2u_a} - \frac{1}{2u_a}\right\} \tag{20a}$$

in which

$$u_a = \frac{kaL}{2} \tag{20b}$$

Using the notations $p_{u_a}$ and $q_{u_a}$ Eqs. (19a) and (19b) take the following abbreviated forms,

$$\theta_2 = +\frac{M_2}{3P}k^2aL\,p_{u_a} + \frac{M_3}{6P}k^2aL\,q_{u_a} \tag{21}$$

$$\theta_3 = -\frac{M_2}{6P}k^2aL\,q_{u_a} - \frac{M_3}{3P}k^2aL\,p_{u_a} \tag{21a}$$

The factors $p_{u_a}$ and $q_{u_a}$ are found tabulated in existing works[3] as an argument of 2u, and represent the effect of the axial compressive force P on the moments $M_2$ and $M_3$ and, therefore, the effect on the slope of the elastic curve

of the column at the bottom of the portal. For any given value of the load P as a is increased the values of $p_{u_a}$ and $q_{u_a}$ increase very rapidly. For example when u is increased from .50 to 1.00 $p_{u_a}$ and $q_{u_a}$ increase 35% and 60% respectively.

From the condition that support 4 is assumed to be hinged the slope of the elastic curve at the left end of span bL is found to be

$$\theta_3 = + \frac{M_3 k^2 bL}{3P} p_{u_b} \tag{22}$$

where

$$u_b = \frac{kbL}{2} \tag{22a}$$

Substituting Eq. (22) in Eq. (21b), the following relation between $M_2$ and $M_3$ is obtained

$$M_3 = -\frac{M_2}{2}\left\{\frac{a q_{u_a}^2}{a p_{u_a} + b p_{u_b}}\right\} \tag{23}$$

which when substituted in Eq. (21) gives the following equation for the slope of the elastic curve of the column at the bottom of the portal.

$$\theta_2 = + M_2 k^2 aL\left\{4 p_{u_a} - \frac{a q_{u_a}^2}{a p_{u_a} + b p_{u_b}}\right\} \tag{24}$$

Denoting the bracketed term on the right side of Eq. (24) by $X_r$, where subscript r denotes the number of panels in the portal, Eq. (24) becomes

$$\theta_2 = \frac{M_2 k^2 L}{3P} X_r \tag{24a}$$

in which for a one panel portal

$$X_1 = a p_{u_a} \tag{24b}$$

and for a two panel portal

$$X_2 = a\left\{p_{u_a} - \frac{a q_{u_a}^2}{4(a p_{u_a} + q p_{u_b})}\right\} \tag{24c}$$

When the effect of P is ignored, then

$$X_1 = a \tag{24d}$$

$$X_2 = a\left\{1 - \frac{a}{4(a+b)}\right\} \tag{24e}$$

For a portal having any number of equal panels and the effect of the axial load is not included, the moment at the second panel point can not be larger than $.268M_2$,[4] or smaller than $.250M_2$. The value of $X_2$ when a = b in Eq. (24e) is .875a. For an infinite number panels the value of $X_{inf}$ is .867. From which it is seen no additional stiffness is gained by using more than two panels

in a portal. However, as a is diminished the column tends to be fixed at the bottom of the portal, providing the portal has sufficient depth to resist rotation.

From the above it is seen that proper design can keep the effect of lateral deflection of the column at a minimum.

## Combined Action of the Column and Portal

Fig. 5 shows the situation of the column below the portal; the column is fixed at the base and rotates through an angle $\theta_2$ at the bottom of the portal, which deflects a distance $\delta$ in reference to the tangent of the elastic curve at the column base.

An axial compressive force P is applied to each end of the column and a lateral load Q is applied at a distance cL from the base of the column, which are resisted by a lateral shearing force H applied at the bottom of the portal and the moments $M_1$ and $M_2$ applied as shown.

The equations for the bending moment to the left and right of the load and at the bottom of the portal are

$$M_x = -M_1 - (Q-H)x + Py \tag{25}$$

$$M_x = -M_1 - QcL + Hx + Py \tag{25a}$$

$$M_2 = -M_1 - QcL + HL + P\delta \tag{25b}$$

Substituting Eqs. (25) and (25a) in the differential equation of the elastic curve then for x less than cL

$$y = A\cos kx + B\sin kx + \frac{M_1}{P} + (Q-H)\frac{x}{P} \tag{26}$$

and for x larger than cL

$$y = C\cos kx + D\sin kx + \frac{M_1}{P} + \frac{QcL}{P} - \frac{Hx}{P} \tag{26a}$$

When x = 0 Eq. (26) and its first derivative are zero, from which it is concluded that

$$A = -\frac{M_1}{P} \tag{26b}$$

$$B = -\frac{(Q-H)}{Pk} \tag{26c}$$

At the point of application of the load the two portions of the elastic curve as given by Eqs. (26) and (26a) have the same deflection and a common tangent, then

$$y_{(x=cL)} = -\frac{M_1}{P}\cos kcL - \frac{(Q-H)}{Pk}\sin kcL = \tag{27}$$

$$C\cos kcL + D\sin kcL$$

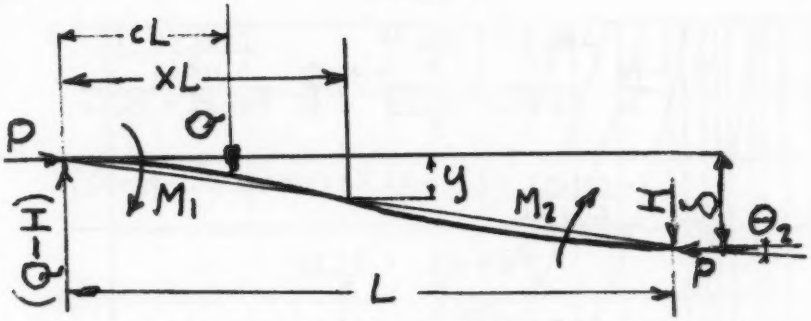


Fig. 5. Showing Elastic Curve of Column below Portal.

$$\frac{dy}{dx}_{(x=cL)} = +\frac{M_1}{P}k\sin kcL - \frac{(Q-H)}{P}\cos kcL + \frac{Q}{P} = \tag{27a}$$

$$- Ck\sin kcL + Dk\cos kcL$$

from which

$$C = -\frac{M_1}{P} - \frac{Q}{Pk}\sin kcL \tag{27b}$$

$$D = -\frac{(Q-H)}{Pk} + \frac{Q}{Pk}\cos kcL \tag{27c}$$

Substituting the above values of C and D in Eq. (26a), then when x = L

$$\delta = \frac{M_1}{P}(1-\cos kL) - \frac{HL}{P} + \frac{H}{Pk}\sin kL + \frac{Q}{Pk}\sin k(L-cL) \tag{28}$$

$$+ \frac{Q}{Pk}\sin kL - \frac{Q}{P}cL$$

Substituting the above value of $\delta$ in Eq. (25b) the following relation between $M_1$ and $M_2$ is obtained

$$M_2 = -M_1\cos kL + \frac{H}{k}\sin kL + \frac{Q}{k}\sin k(L-cL) - \frac{Q}{k}\sin kL \tag{29}$$

When x = L the first derivative of Eq. (26a) is equal to $\theta_2$ which is given by Eq. (24a), then

$$\frac{M_1}{P}k\sin kL + \frac{Q}{P}\cos k(L-cL) - \frac{(Q-H)}{P}\cos kL - \frac{H}{P} \tag{30}$$

$$= \frac{M_2}{3P}k^2LX_r$$

Substituting the right hand side of Eq. (29) in Eq. (30) gives the following equation for $M_1$

$$M_1 = \frac{H}{k}\,\frac{\sec kL - 1 + \frac{kL}{3}X_r}{\tan kL + \frac{kLX_r}{3}} + \frac{Q}{k}\,\frac{\frac{\cos k(L-cL)}{\sin kL}}{\tan kL + \frac{kLX_r}{3}} \tag{31}$$

$$+\frac{Q}{k}\,\frac{1 - \frac{\cos k(L-cL)}{\cos kL} + \frac{kL}{3}X_r\left(\sin k(L-cL) - \tan kL\right)}{\tan kL + \frac{kLX_r}{3}}$$

Substituting wdcL for QcL in Eq. (31) and integrating between the limits zero and L gives the following equation which if added to the first term on the right hand side of Eq. (31) will give the value of $M_1$ due to a continuous uniformly distributed load having an intensity w, extending from the base of the column to the bottom of the portal

$$\frac{wL^2}{2v}\,\frac{1 - \frac{\tan kL}{kL} + \frac{X_r}{3}(\sec kL - 1 + \tan kL)}{\tan kL + \frac{kLX_r}{3}} \tag{31a}$$

When H is the only lateral load applied to the column Eq. (31) becomes

$$M_1 = \frac{HL}{2}\,\frac{\tan u}{u}\,\frac{1 + \frac{2uX_r}{3\tan u}}{1 + \frac{2uX_r}{3\tan 2u}} \tag{31b}$$

Denoting the trignometric multiplier of $\frac{HL}{2}\,\frac{\tan u}{u}$ by $K_1$ then

$$M_1 = \frac{HL}{2}K_1\,\frac{\tan u}{u} \tag{31c}$$

In the denominator of $K_1$ 2u is the second quadrant, and negative when u is larger than $\frac{\pi}{2}$, and the value of 2u is negative when $K_1$ is infinite. A table containing values of $\frac{\tan u}{u}$ for the second quadrant is in the appendix.

When $X_r$ is zero the column is fixed at the bottom of the portal and Eq. (31b) reduces to Eq. (3).

Values of $K_1$ are shown in Fig. 6 as an argument of u for several stated values of $X_r$.

The heavy vertical lines in Fig. 6 are the asymptotic values of u, $u_c$ at which $K_1$ becomes infinite for $X_r$ equal to 1.00, .80, .60, .40 and .20 respectively.

The buckling stress occurs in the elastic range for values of $\frac{L}{r}$ larger than given by the following equation,

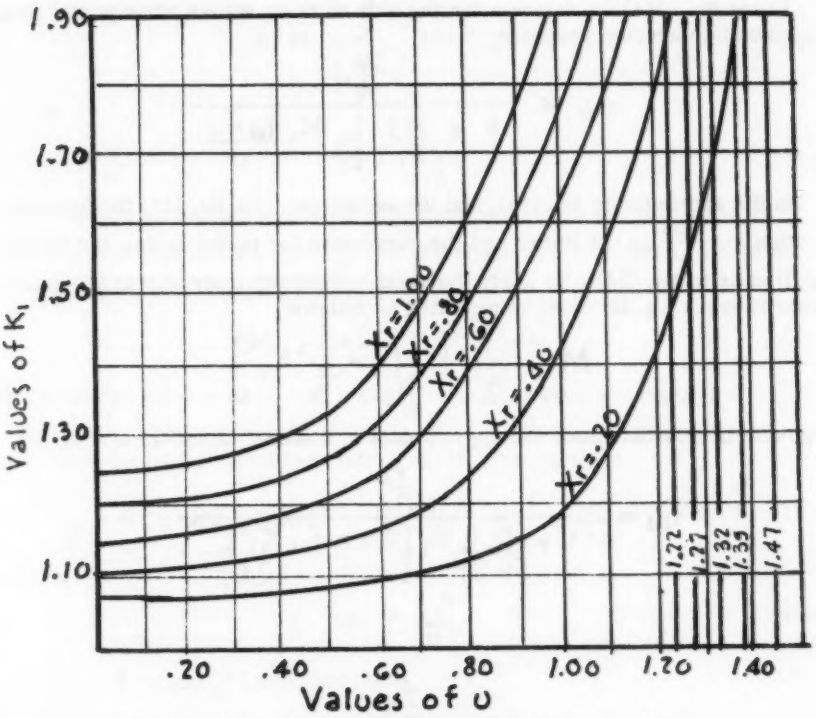


Fig. 6. Showing Variation of $K_1$ in Respect to u and $X_r$.

$$\frac{L}{r} = 2u_c\sqrt{\frac{En}{f_y}} \tag{32}$$

Tabulated below are the values of $\frac{L}{r}$ beyond which buckling occurs in the elastic range.

| $X_r$ | 1.00 | .80 | .60 | .40 | .20 |
|---|---|---|---|---|---|
| $f_y$ = 33,000 p.s.i. | 93 | 99 | 103 | 107 | 115 |
| $f_y$ = 50,000 p.s.i. | 81 | 84 | 87 | 91 | 96 |

It is noted from Fig. 6 that as u is increased the column approaches a hinged condition at the bottom of the portal, from which it is concluded that if mL is the distance to the point of contraflexure of the column then

$$mL = K_1\frac{L}{2} \tag{33}$$

As u is decreased $\frac{\tan u}{u}$ approaches unity, therefore, when u is small or the effect of the axial compressive force P is ignored, then mL can be approximated by $K_2\frac{L}{2}$ where

$$K_2 = \frac{3+2X_r}{3+X_r} \tag{33a}$$

Using Eq. (31c) the formula for the safe working stress when portal action is taken into account becomes

$$f_\omega = \frac{\frac{f_y}{n}}{1 + \frac{Hc}{Pr}\frac{L}{2r} K_1 \frac{\tan u'}{u'}} \tag{34}$$

In the approximate Eq. (12), and the secant formula Eq. (15) the approximation for $\frac{\tan u}{u}$ is not linear and the correction for portal action can not be applied as in Eq. (34). To apply the axial compressive force P at the point of contraflexure Eq. (8) must be modified as follows

$$M = \frac{HL}{2} K_2 \left\{1 + \frac{u^2 K_2^2}{3}\right\} \tag{35}$$

and with this modification the approximate and secant formula become

$$f_\omega = \frac{\frac{f_y}{n}}{1 + \frac{Hc}{Pr}\frac{L}{2r} K_2 \left\{1 + n f_\omega \frac{K_2^2 L^2}{12 E r^2}\right\}} \tag{36}$$

$$f_\omega = \frac{\frac{f_y}{n}}{1 + \frac{Hc}{Pr}\frac{L}{2r} K_2 \left\{1 + \frac{(K_2 u')^2 \sec u'}{3}\right\}} \tag{37}$$

In modifying the secant formula to cover the case of lateral deflection the factors $e_o$ and .25 were omitted, for the reasons that follow.

Since $e_o$ is a known or calculated eccentricity the stresses calculated from the moment $Pe_o$ are secondary. The stresses calculated from the moments in a portal are also secondary, and since these moments are calculated there is no need for the factor $e_o$ in the equations for the working stress.

The following statements can be found in Steel Column Research Final Report of the Special Committee.(5)

(a) The factor .25 is assumed to contain an allowance of 0.15 for secondary stress and 0.10 for crookedness.
(b) For members bent to reverse curvature the effect of crookedness is small and need scarcely be considered.

In AASHO Specifications the secondary stress is represented by $e_o$ and .25 is taken to represent the effect of inherent crookedness regardless of the nature of the curvature.

In the following a comparison will be made of the effect of inherent crookedness on a pin end column and a laterally deflected column.

Assuming the shape of a pin end column when the loading is removed to be a sine curve with a mid-ordinate $a_o$, it has been shown(6) that when a load P is applied to the ends of the column the equation of the elastic curve is

$$y = \frac{a_o}{(1-\alpha)} \sin \frac{\pi x}{L} \tag{38}$$

in which

$$\alpha = \frac{4v^2}{\pi^2} \tag{38a}$$

For a laterally deflected column with fixed ends when the loading is removed the mid ordinate would be $\frac{a}{4}$o and the shape of the crooked column could be described by the following equation

$$y_o = \frac{a_o}{8}\left(1 - \cos \frac{2\pi x}{L}\right) \tag{39}$$

which satisfies the condition that y and $\frac{dy}{dx}$ are zero when x = 0 and x = L.

Placing Eq. (39) in the differential equation of the elastic curve for a laterally deflected column with fixed ends, and integrating, then

$$y_1 = A\cos kx + B\sin kx + \frac{M}{P} - \frac{Hx}{P} - \frac{a_o}{8}\left\{1 + \frac{\alpha'}{1+\alpha'} \cos \frac{2\pi x}{L}\right\} \tag{40}$$

in which

$$\alpha' = \frac{v^2}{\pi^2} \tag{40a}$$

When x = 0 $y_1$ and $\frac{dy}{dx}1$ are zero, then

$$A = -\frac{M}{P} + \frac{a_o}{8(1-\alpha')} \tag{40b}$$

and

$$B = \frac{H}{Pk} \tag{40c}$$

Substituting Eqs. (40b) and (40c) in Eq. (40), and adding Eq. (39) gives the following equation for y

$$y = -\frac{M}{P}\cos kx + \frac{a_o \cos kx}{8(1-\alpha')} + \frac{H}{Pk}\sin kx + \frac{M}{P} - \frac{Hx}{P} - \frac{a_o}{8}\left\{1 + \frac{\cos 2\pi x}{(1-\alpha')L}\right\} \tag{41}$$

Differentiating Eq. (41) and letting x = L it is found that the moment $\frac{HL}{2}\frac{\tan u}{u}$ is increased by

$$\frac{Pa_o}{(1-\alpha)} \tag{42}$$

From Eq. (38) the maximum moment at mid-span of the pin end column is

$$\frac{Pa_o}{8(1-\alpha')} \tag{43}$$

A comparison of the effect of inherent crookedness for the pin end column and the laterally deflected column is given below.

| u | $\frac{\pi}{8}$ | $\frac{\pi}{4}$ | $\frac{3\pi}{8}$ |
|---|---|---|---|
| Equation 43 | 1.22 | 1.33 | 2.22 |
| Equation 42 | .004 | .017 | .041 |

From the above it is seen that the effect of inherent crookedness need not be considered for laterally deflected columns.

In the equations of this paper a length L has been used which has not been qualified. The recommendations for reduced length in AASHO specifications do not apply. A laterally deflected column has reverse curvature and in Steel Column Research Final Report of The Special Committee it is stated that little or no consideration be given to the length of columns with reverse curvature as the maximum moment occurs at the ends.

However, in a portal column the column becomes reinforced as it enters the gusset and it would be conservative to measure the length of the column at a point midway between the top of the floor beam and the upper edge of the gussets.

Denoting the three formulae for the working stress in a laterally loaded column as the Tangent Formula, the modified Secant Formula and the Approximate Formula, a comparison of the stresses calculated by these three formulae will be given for a silicon steel column. $\frac{L}{r}$ will be taken as 90 and 120, $X_r$ as 1.00, .50 and zero, and $\frac{He}{Pr}$ as .02, .06 and .10.

For $\frac{L}{r} = 90$ and $\frac{L}{r} = 120$ buckling occurs in the elastic range for $X_r = 1.00$, and $X_r = 1.00$, .50 and zero, respectively, and the unit stress to use in the denominator of the equations for the working stress is obtained from Eq. (32).

In the tabulation below the safe working stresses are given in kips per square inch.

| | | Tangent Formula | | Modified Secant Formula | | Approximate Formula | |
|---|---|---|---|---|---|---|---|
| | | $\frac{L}{r} = 90$ | $\frac{L}{r} = 120$ | $\frac{L}{r} = 90$ | $\frac{L}{r} = 120$ | $\frac{L}{r} = 90$ | $\frac{L}{r} = 120$ |
| $X_r$ | $\frac{He}{Pr}$ | | | | | | |
| 1.0 | .02 | 7.4 | 4.2 | 7.2 | 3.9 | 8.0 | 4.7 |
| | .06 | 4.1 | 2.4 | 3.9 | 2.3 | 4.2 | 2.5 |
| | .10 | 2.9 | 1.9 | 2.8 | 1.8 | 2.8 | 1.9 |
| .5 | .02 | 9.3 | 4.5 | 9.0 | 4.4 | 10.3 | 5.6 |
| | .06 | 5.5 | 2.6 | 5.0 | 2.6 | 5.7 | 3.1 |
| | .10 | 3.7 | 2.0 | 3.7 | 2.0 | 3.8 | 2.3 |
| 0 | .02 | 10.2 | 5.0 | 10.0 | 4.8 | 11.8 | 6.9 |
| | .06 | 5.9 | 2.9 | 5.8 | 2.9 | 6.0 | 3.4 |
| | .10 | 4.4 | 2.3 | 4.2 | 2.3 | 4.3 | 2.8 |

## CONCLUSIONS

It has been shown that the modified secant formula gives results which compare favorably with the results obtained by the tangent formula.

Therefore, AASHO Specifications contains a formula which if properly handled is applicable to laterally deflected columns.

A formula of the type which can be modified to cover the case of lateral deflection is not contained in A.R.E.A. specifications, however portals in railway bridges are invariably so stiff that lateral deflection need scarcely be considered.

In building construction long columns with shallow portals often occur the minimum depth of which can be determined by calculating the lateral deflection. There is no column formula in A.I.S.C. specifications which can be modified to cover the case of lateral deflections.

Truss members having reverse curvature have their ends displaced and belong to the class of laterally deflected columns. The formulae in this paper can be applied to such truss members after H is determined from the end moments.

For the proportions of portals, and the ratio $\frac{Hc}{Pr}$, used in computing the comparative stresses in this paper, it is seen that the modified secant formula is sufficiently precise. This formula and the approximate formula are based on applying the axial compressive force P at the point of contraflexure calculated from H. Therefore, the consideration of buckling is limited to determining the stress to replace $f_y$ in the denominator of these formulae.

The approximate formula is not as precise as the modified secant formula, particularly when the stresses are small. Since the conditions at the ends of the column are not definitely known this formula should be satisfactory for use in design. In fact this is the only practical method to use when the moment of inertia of the column is variable. Furthermore, since the bending stresses are secondary in nature refined calculations should not be required.

When the column is very slender and the portal deep, a condition frequently occurring in erection of cantilever bridges, the precise method should be applied to obtain the safe working stresses.

The precise method, from which the tangent formula was derived, makes the usual approximation for curvature. Therefore as the angle u approaches its critical value the method becomes less precise and should not be used.

## APPENDIX

### Notation

| | |
|---|---|
| E | = Modulus of elasticity in tension and compression. |
| H | = Horizontal shearing force. |
| I | = Moment of inertia in the plane of bending. |
| $K_1$ | = Precise magnification factor for portal action. |
| $K_2$ | = Approximate magnification factor for portal action. |
| L | = Length. |
| M | = Bending moment. |
| P | = Axial compressive force |
| Q | = Concentrated load. |

| | |
|---|---|
| $X_r$ | = A factor of the slope of the elastic curve of the column at the bottom of the portal. |
| $a_o$ | = Mid-ordinate of a crooked column. |
| aL, bL and cL | = Lengths. |
| c | = Distance from the neutral axis to the extreme fibre in compression. |
| f | = Average unit stress due to P. |
| $f_b$ | = Buckling stress. |
| $f_c$ | = Critical stress. |
| $f_w$ | = Safe working stress. |
| $f_y$ | = Yield point stress. |
| k | $= \sqrt{\frac{P}{EI}}$ |
| mL | = Distance from base of column to the point of contraflexure. |
| n | = Factor of safety. |
| r | = Radius of gyration in the plane of bending. |
| u | $= \frac{kL}{2}$ |
| u' | = nu. |
| w | = Intensity of uniform loading. |
| x and y | = Coordinates of the elastic curve. |
| $\alpha$ | $= \frac{4u^2}{\pi^2}$ |
| $\alpha'$ | $= \frac{u^2}{\pi^2}$ |
| $\delta$ | = Deflection. |
| $\theta$ | = Slope of elastic curve. |

## REFERENCES


1. American Railway Eng. Association, American Association of State Highway Officials, and American Inst. of Steel Construction.
2. Timoshenko's Theory of Elastic Stability, first edition page 5, Eq. (12).
3. Timoshenko's Theory of Elastic Stability, first edition pages 499 through 505.
4. Mathematics in Engineering, Kármán and Biot, first edition page 443, Eq. (3.3).
5. Transactions ASCE, Vol. 98, pages 1449 and 1458.
6. Timoshenko's Theory of Elastic Stability, First Edition page 32, Eq. (47).

TABLE 1

$\frac{\tan u}{u}$ First Quadrant

| u | .00 | .01 | .02 | .03 | .04 | .05 | .06 | .07 | .08 | .09 |
|---|---|---|---|---|---|---|---|---|---|---|
| .0 | 1.000 | 1.000 | 1.001 | 1.001 | 1.001 | 1.001 | 1.001 | 1.002 | 1.003 | 1.003 |
| .1 | 1.003 | 1.004 | 1.005 | 1.006 | 1.007 | 1.008 | 1.009 | 1.010 | 1.011 | 1.012 |
| .2 | 1.014 | 1.015 | 1.017 | 1.018 | 1.020 | 1.021 | 1.023 | 1.025 | 1.027 | 1.029 |
| .3 | 1.031 | 1.033 | 1.035 | 1.038 | 1.040 | 1.043 | 1.046 | 1.048 | 1.051 | 1.054 |
| .4 | 1.057 | 1.060 | 1.063 | 1.067 | 1.070 | 1.073 | 1.077 | 1.081 | 1.085 | 1.089 |
| .5 | 1.093 | 1.097 | 1.101 | 1.106 | 1.110 | 1.115 | 1.120 | 1.125 | 1.130 | 1.135 |
| .6 | 1.140 | 1.146 | 1.151 | 1.157 | 1.163 | 1.169 | 1.176 | 1.183 | 1.190 | 1.197 |
| .7 | 1.204 | 1.211 | 1.218 | 1.226 | 1.234 | 1.242 | 1.251 | 1.259 | 1.268 | 1.278 |
| .8 | 1.287 | 1.297 | 1.307 | 1.317 | 1.328 | 1.339 | 1.351 | 1.362 | 1.375 | 1.387 |
| .9 | 1.400 | 1.414 | 1.428 | 1.442 | 1.456 | 1.472 | 1.489 | 1.504 | 1.521 | 1.539 |
| 1.0 | 1.557 | 1.577 | 1.596 | 1.617 | 1.638 | 1.660 | 1.683 | 1.708 | 1.733 | 1.759 |
| 1.1 | 1.786 | 1.815 | 1.845 | 1.876 | 1.909 | 1.943 | 1.979 | 2.017 | 2.056 | 2.099 |
| 1.2 | 2.144 | 2.193 | 2.224 | 2.292 | 2.348 | 2.408 | 2.468 | 2.538 | 2.611 | 2.688 |
| 1.3 | 2.771 | 2.860 | 2.975 | 3.062 | 3.177 | 3.302 | 3.436 | 3.584 | 3.753 | 3.937 |
| 1.4 | 4.141 | 4.369 | 4.633 | 4.933 | 5.275 | 5.675 | 6.171 | 6.803 | 7.423 | 8.280 |
| 1.5 | 9.400 | 10.87 | 12.94 | 16.00 | 21.13 | 39.31 | 961.9 | | | |

TABLE 2

$\frac{\tan u}{u}$ Second Quadrant

All values are negative

| u | .00 | .01 | .02 | .03 | .04 | .05 | .06 | .07 | .08 | .09 |
|---|---|---|---|---|---|---|---|---|---|---|
| 1.6 | 21.400 | 15.860 | 12.540 | 10.350 | 8.800 | 7.646 | 6.732 | 6.022 | 5.432 | 4.943 |
| 1.7 | 4.529 | 4.175 | 3.868 | 3.601 | 3.364 | 3.155 | 2.968 | 2.799 | 2.647 | 2.508 |
| 1.8 | 2.386 | 2.261 | 2.156 | 2.056 | 1.967 | 1.883 | 1.805 | 1.737 | 1.660 | 1.596 |
| 1.9 | 1.542 | 1.483 | 1.430 | 1.380 | 1.332 | 1.287 | 1.244 | 1.203 | 1.169 | 1.137 |
| 2.0 | 1.097 | 1.051 | 1.024 | 0.994 | 0.965 | 0.936 | 0.910 | 0.885 | 0.861 | 0.837 |
| 2.1 | 0.814 | 0.791 | 0.770 | 0.750 | 0.730 | 0.712 | 0.694 | 0.686 | 0.658 | 0.641 |
| 2.2 | 0.625 | 0.609 | 0.594 | 0.579 | 0.565 | 0.551 | 0.538 | 0.525 | 0.512 | 0.500 |
| 2.3 | 0.488 | 0.477 | 0.464 | 0.453 | 0.442 | 0.432 | 0.422 | 0.411 | 0.401 | 0.391 |
| 2.4 | 0.381 | 0.373 | 0.363 | 0.355 | 0.347 | 0.338 | 0.330 | 0.322 | 0.314 | 0.306 |
| 2.5 | 0.298 | 0.292 | 0.285 | 0.278 | 0.270 | 0.263 | 0.257 | 0.250 | 0.244 | 0.238 |
| 2.6 | 0.233 | 0.225 | 0.219 | 0.214 | 0.208 | 0.201 | 0.197 | 0.192 | 0.185 | 0.180 |
| 2.7 | 0.175 | 0.170 | 0.165 | 0.160 | 0.155 | 0.150 | 0.145 | 0.140 | 0.136 | 0.132 |
| 2.8 | 0.127 | 0.123 | 0.119 | 0.115 | 0.110 | 0.105 | 0.101 | 0.097 | 0.093 | 0.089 |
| 2.9 | 0.085 | 0.081 | 0.077 | 0.073 | 0.070 | 0.066 | 0.063 | 0.060 | 0.056 | 0.052 |
| 3.0 | 0.048 | 0.044 | 0.040 | 0.036 | 0.033 | 0.030 | 0.027 | 0.024 | 0.020 | 0.017 |
| 3.1 | 0.014 | 0.010 | 0.007 | 0.004 | 0.000 | | | | | |

Journal of the
STRUCTURAL DIVISION
Proceedings of the American Society of Civil Engineers

# THEORY AND TEST RESULTS ON THE FATIGUE OF METALS

F. Stuessi[1]

This paper was the basis for an oral presentation at the Joint ASCE-IABSE Meeting at the New York Convention, October 1958. All Joint Meeting papers published in Proceedings or in Civil Engineering will be reprinted in one volume.

## SUMMARY

This paper presents an empirical fatigue relationship between the mean stress and the alternating stress of a cycle; five material characteristics; and the resulting number of cycles to failure. The influence of rate of cycling, of strain-hardening, and of stress concentration is considered separately.

## List of Symbols

$\sigma_{max}$ = upper limit of stress range that leads to failure after n cycles—with no stress concentration present.

$\sigma_{k\,max}$ = upper limit of range of nominal stress that leads to failure after n cycles—with stress concentration present.

$\sigma_{min}$ = lower limit of stress range that leads to failure after n cycles.

$\sigma_m = (\sigma_{max} + \sigma_{min})/2$ = mean stress of range.

$\Delta\sigma = (\sigma_{max} - \sigma_{min})/2$ = single amplitude of stress range.

= alternating stress.

$\sigma_w$ = fatigue strength for complete stress reversal and n cycles—with no stress concentration present.

Note: Discussion open until March 1, 1960. Separate Discussions should be submitted for the individual papers in this symposium. To extend the closing date one month, a written request must be filed with the Executive Secretary, ASCE. Paper 2222 is part of the copyrighted Journal of the Structural Division, Proceedings of the American Society of Civil Engineers, Vol. 85, No. ST 8, October, 1959.

1. Pres., IABSE; Swiss Federal Inst. of Technology, Zurich, Switzerland.

$\sigma_{kw}$ = nominal fatigue for complete stress reversal and n cycles—with stress concentration present.

$\sigma_{aw}$ = asymptotic value of fatigue strength for complete stress reversal and $n = \infty$ cycles.

$\sigma_z$ = creep-rupture strength as a function of time—or of the number of stress cycles as $\Delta\sigma$ approaches 0.

$\sigma_{oz}$ = short-time tensile strength as obtained by conventional test.

$\sigma_{az}$ = asymptotic value of creep-rupture strength for an infinitely long time.

$\sigma_D$ = compressive strength (Fig. 16).

$\sigma_r$ = relaxation stress for constant strain; for instance, stress in wire held at constant length.

$\sigma_{or}$ = initial stress in material held at constant strain.

$\sigma_{ar}$ = asymptotic value of relaxation stress after an infinitely long time during which material is held at constant strain.

$k^2$ = invariant of creep, characterizing the creep behavior of a material at a given temperature.

n = number of identical stress cycles to failure. Note from Fig. 1 that n = 0 at the moment maximum stress has been applied just prior to beginning of cycling.

i = $\log_{10} n$

p = exponent for n

t = time

i' = $\log_{10} t$

p' = exponent for t

f = "balance factors" as defined in text.

$\lambda$ = $\log_{10} f$

$\alpha$ = stress ratio = $\sigma_{min}/\sigma_{max}$

$\beta$ = $(1-\alpha)/(1+\alpha)$, Eq. (11)

$\phi$ = $\sigma_{k\,max}/\sigma_{max}$

$\phi_w$ = $\sigma_{kw}/\sigma_w$

Subscripts:

a refers to asymptotic value for an infinite number of stress cycles or for an infinitely long time.
k refers to nominal stress (based on net area) for conditions with stress raiser.
m refers to mean stress.
r refers to stress relaxation.
w refers to complete stress reversal.
z refers to static tensile stress.

## 1. INTRODUCTION

The importance of fatigue is steadily increasing in structural engineering as well as in mechanical and aeronautical engineering. Fatigue failures cause heavy losses every year, but only a small portion of these losses becomes generally known. A great deal of human effort and expenditure for tests are currently being devoted to fatigue studies; however, the study of an individual problem represents an isolated case, without general significance, unless it can be fitted into the framework of a comprehensive relationship. Such a comprehensive relationship must be furnished by a Theory of Fatigue, which thus serves several important purposes:

(a) To provide insight into the various aspects governing fatigue behavior and their relationships;
(b) To permit prediction of material behavior under any particular set of cyclic stresses from the least possible number of material characteristics, and thus to permit the engineer to evaluate a specific problem without the need for special tests;
(c) To make best use of available test data;
(d) To guide the researcher in setting up his test programs to obtain the most significant data with a minimum of effort and cost.

There are two possible avenues of approach in setting up a theory of fatigue: the theoretical approach based on the mechanism of crack formation and crack propagation, and the empirical approach which attempts to set up a generally valid analytical relationship between test data obtained for a wide variety of conditions and material properties. At the present state of the art, the empirical approach appears more promising. Hence, it is the object of this paper to present an analytical relationship arrived at empirically, to illustrate it by examples from a broad selection of conditions and to show that it fits test data very closely.

### 2. Statement of Problem and Method of Attack

As used in this paper, the expression "fatigue failure" means failure under repeated applications of a stress that is below the short-time tensile strength of the material.(1) Generally, the stress cycle, as defined by the mean stress and the alternating stress (Fig. 1), as well as the rate of cycling and the temperature, are imposed by external conditions; then, the properties of the material govern the number of cycles to failure.

The comprehensive theory presented here covers all ratios of mean stress to alternating stress, from the static stress-rupture case to the case of complete stress reversal. Furthermore, it covers any number of cycles to failure, from single loading (see Fig. 1) to infinity.

Material properties change with temperature; the theory offered here applies for any given set of material properties, i.e., for any given temperature. Hence, temperature will be considered as constant for any particular case.

In order to keep the relationships reasonably simple, the rate of cycling will be dealt with separately. For the same reason, the basic theory is confined to metals without strain-hardening effects and without stress concentration in the area of failure. These influences will also be considered separately.

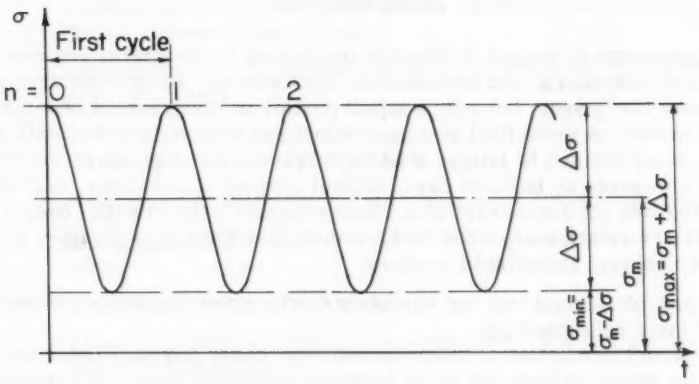


Fig. 1. Definition of stress-cycles and stress nomenclature.

For the conditions stipulated above, a theory of fatigue failure is established to provide a relationship between the material properties on one hand and the mean stress, the alternating stress, and the resulting number of cycles to failure on the other hand. The relationship is reasonably simple, expresses the material properties by a minimum number of readily established, conventional material characteristics, and fits well into test data covering a wide variety of conditions and materials.

Fig. 2 represents the case of a smooth bar of steel at room temperature, i.e., a case without creep effect. The failure criteria, as governed by material properties, are depicted by a surface in a system of coordinates:

$\sigma_m$ = mean stress

$\Delta\sigma$ = alternating stress

i = log n = log (cycles to failure) .

The surface divides space into a region where failure should be expected and a region where failure should not be expected. The empirical relationship to be established is the analytical expression of this surface.

It would appear best to consider first a number of special, simpler cases representing partial problems and then to develop a governing, over-all relationship by a combination of special cases.(2)

## 3. Partial Problems

### a. Complete Stress Reversal

In the case of complete stress reversal (i.e., $\sigma_m = 0$), the alternating stress amplitude $\Delta\sigma$ that leads to fatigue failure after n cycles is called the "alternating fatigue strength", $\sigma_w$. The relationship between $\sigma_w$ and n is the so-called Woehler curve for fatigue strength. Careful study of many test results indicates that this relationship follows very closely the expression

$$\sigma_w = \frac{\sigma_{oz} + C_w n^p \sigma_{aw}}{1 + C_w n^p} \qquad (1)$$

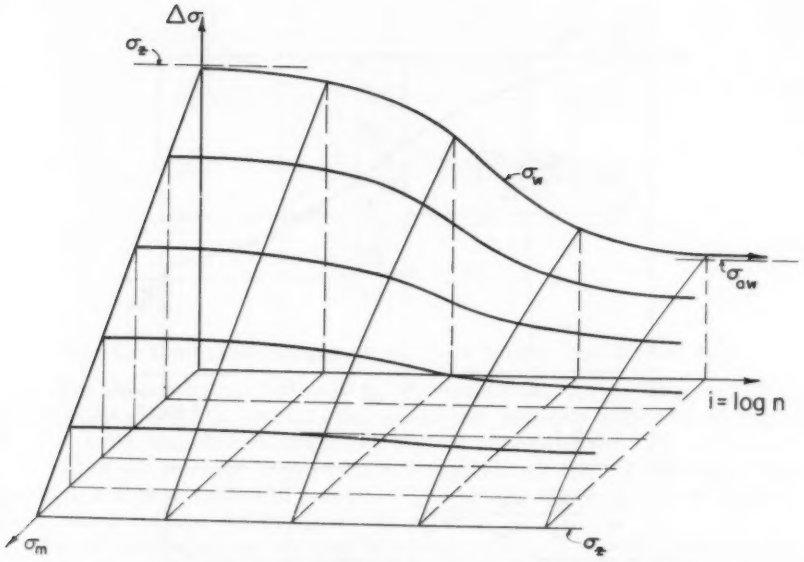


Fig. 2. Surface depicting the failure criteria for a material without creep effect. $\sigma_m$ and $\Delta\sigma$ are imposed by external conditions and the material properties govern the number of cycles to failure.

where $\sigma_{oz}$ = static tensile strength

$\sigma_{aw}$ = asymptotic value of $\sigma_w$ for an infinite number of complete stress reversals

$C_w$ = Woehler coefficient, a characteristic of the material

p = exponent for n, a characteristic of the material

By setting

$$f_w = C_w n^p$$

Eq. (1) becomes

$$\sigma_w = \frac{\sigma_{oz} + f_w \sigma_{aw}}{1 + f_w} \tag{1a}$$

or

$$\sigma_{oz} - \sigma_w = f_w(\sigma_w - \sigma_{aw}) \tag{1b}$$

Eq. (1b) permits a clear interpretation, as illustrated in the upper part of Fig. 3: $(\sigma_{oz} - \sigma_w)$ represents the difference between the static tensile strength and the alternating fatigue strength for n cycles, whereas $(\sigma_w - \sigma_{aw})$ represents the difference between the alternating fatigue strengths for n cycles and for an infinite number of cycles. The sum of these differences is $\sigma_{oz} - \sigma_{aw}$, i.e., constant; the relative magnitudes are governed by a "balance factor" that depends on the number of cycles.

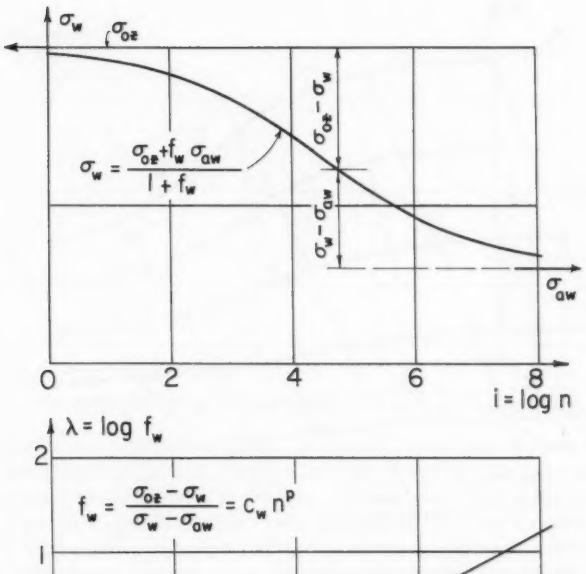


Fig. 3. Empirical relationship between completely reversing stress $\sigma_w$ and number of cycles to failure, n.

On the other hand, if Eq. (1) is written in the form

$$f_w = \frac{\sigma_{oz} - \sigma_w}{\sigma_w - \sigma_{aw}} = C_w n^p \tag{1c}$$

it can be linearlized by taking logarithms:

$$\lambda = \log f_w = \log \frac{\sigma_{oz} - \sigma_w}{\sigma_w - \sigma_{aw}} = pi + \log C_w \tag{1d}$$

This expression is particularly useful for the evaluation of test results. The relationship between $\sigma_w$ and n involves four material characteristics; hence, at least four test results are required to establish it.

For $f_w = 1$, the alternating fatigue strength is equal to the average between short-time tensile strength and the alternating fatigue strength for an infinite number of cycles. Since $\lambda = 0$ for this point and $\lambda$ varies linearly with i, the plot of $\sigma_w$ vs. i is point-symmetrical with respect to this point; hence, this point is also the point of inflection.

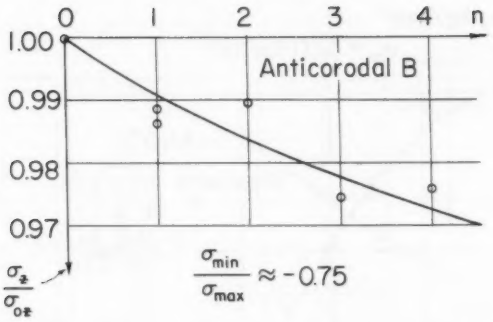


Fig. 4. Low-cycle fatigue strength of Anticorodal B (Ref. 13).

Eq. (1a) shows that any value of $f_w > 0$ leads to $\sigma_w < \sigma_{oz}$. However, $f_w = 0$ requires that n = 0, i.e., initial load application prior to beginning of cycling (see Fig. 1 for definition of beginning of first stress cycle). For n = 1, i.e., at the end of the first cycle, $f_w = C_w > 0$, hence $\sigma_w < \sigma_{oz}$. This means that a bar which has been loaded to just below the tensile strength can no longer withstand a complete stress cycle with $\sigma_w = \sigma_{oz}$.

This conclusion can be verified by a simple test; this test, however, requires a careful observer and a "feel" for the behavior of metals just prior to fracture. If we load a bar to just below the tensile strength, i.e., to the point of incipient necking, then relieve the load and apply the maximum compressive stress the bar can withstand without buckling, and finally apply tensile stress once more, the bar will break at a stress lower than that of the first tensile loading. Fig. 4 shows the results of a series of such tests[12] on bars of Anticorodal B. In these tests the ratio $\sigma_{min}/\sigma_{max}$ was -0.75 and although there was considerable scatter, the tensile stress at failure was distinctly lower than the bar had previously withstood one or several times.

b. Static Stress-Rupture

The static tensile rupture strength ($\Delta\sigma = 0$) of smooth steel bars at room temperature is essentially unaffected by time; the $\sigma_z$ vs. time curve is essentially a straight line (Fig. 2). On the other hand, steel at elevated temperature (Fig. 5) and non-ferrous metals even at room temperature (Fig. 6) show a decrease in static tensile strength with increasing time. It is of interest to note from Figs. 3, 5 and 6 that the shape of the static stress-rupture curve ($\sigma_z$ vs. log time) is very similar to that of the Woehler curve ($\sigma_w$ vs. log n). Indeed, an exactly analogous algebraic expression can be set up:[4]

$$\sigma_z = \frac{\sigma_{oz} + C_z t^{p'} \sigma_{az}}{1 + C_z t^{p'}} \qquad (2)$$

where $\sigma_{az}$ = the asymptotic value of the static rupture strength $\sigma_z$ for an infinitely long time

$t$ = time

$p'$ = exponent for t, a characteristic of the material

$C_z$ = stress rupture coefficient, a characteristic of the material

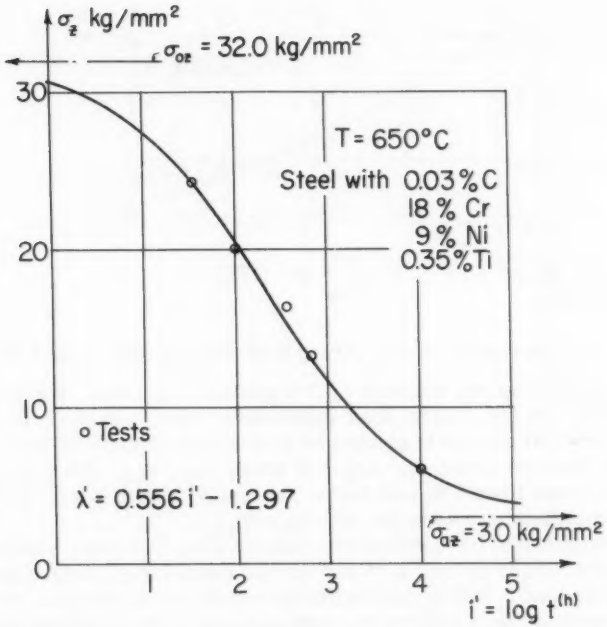


Fig. 5. Creep-rupture strength of steel at 650° C (W. Stauffer and A. Keller, Ref. 3) and curve to fit test data calculated by empirical formula.

Again, by setting

$$f_z = C_z t^{p'}$$

Eq. (2) becomes

$$\sigma_z = \frac{\sigma_{oz} + f_z \sigma_{az}}{1 + f_z} \tag{2a}$$

or

$$\sigma_{oz} - \sigma_z = f_z(\sigma_z - \sigma_{az}) \tag{2b}$$

which permits interpretation similar to Eq. (1b).

Eq. (2) can also be written in the form

$$f_z = \frac{\sigma_{oz} - \sigma_z}{\sigma_z - \sigma_{az}} = C_z t^{p'} \tag{2c}$$

so that it can be linearized by taking logarithms:

$$\lambda' = \log f_z = \log \frac{\sigma_{oz} - \sigma_z}{\sigma_z - \sigma_{az}} = p' i' + \log C_z \tag{2d}$$

where $i' = \log t$.

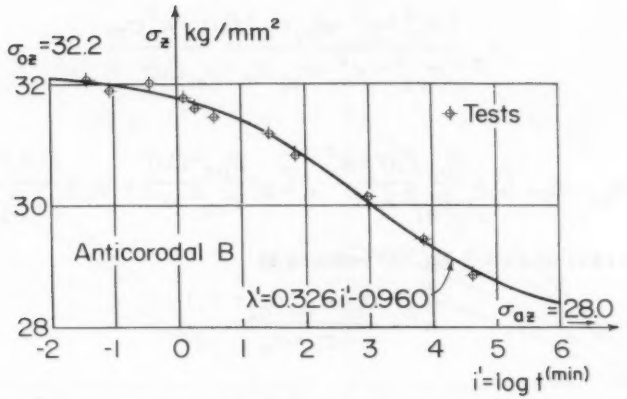


Fig. 6. Creep-rupture strength of Anticorodal B (Ref. 13) and curve to fit test data calculated by empirical formula.

Fig. 5 shows λ' calculated from test data and the corresponding curve of $\sigma_z$ vs. i'.

c. Constant Number of Stress Cycles

For a constant number of stress cycles to failure, the variables are $\sigma_m$ and $\Delta\sigma$. An empirical relationship between them has been proposed[2] for the case of materials with no creep effect. Additional study of many sets of test data has led to an empirical relationship for the criterion of failure that also applies to metals having creep effects:

$$\kappa^2 = \frac{\sigma_{oz}(\sigma_{oz}-\sigma_m)(\sigma_w-\Delta\sigma)-\sigma_m\sigma_w\Delta\sigma}{\sigma_m-\sigma_w+\Delta\sigma} \tag{3}$$

$k^2$ is the invariant characterizing the creep effect of the material at the temperature under study; it has the dimension of stress squared. For a given temperature, $k^2$ is constant, irrespective of the number of stress cycles to failure. For materials with no creep effect, $k^2 = 0$.

By introducing the coefficients

$$C_1 = \frac{\sigma_{oz}\sigma_w+\kappa^2}{\sigma_{oz}^2+\kappa^2} \tag{4a}$$

and

$$C_2 = \frac{\sigma_{oz}-\sigma_w}{\sigma_{oz}^2+\kappa^2} \tag{4b}$$

the equation for the $\Delta\sigma$ vs. $\sigma_m$ curve can be derived from Eq. (3) for any given value of $\sigma_w$:

$$\Delta\sigma = \frac{\sigma_w - C_1\sigma_m}{1-C_2\sigma_m} \tag{5}$$

In particular, for $\sigma_m = 0$, the expected relationship $\Delta\sigma = \sigma_w$ is found.

Furthermore, Eq. (3) can be solved for $\sigma_w$ for any given set of values of $\sigma_m$ and $\Delta\sigma$ that lead to failure for the same number of cycles:

$$\sigma_w = \frac{(\sigma_{oz}^2 + \kappa^2 - \sigma_{oz}\sigma_m)\Delta\sigma + \kappa^2\sigma_m}{\sigma_{oz}^2 + \kappa^2 - \sigma_{oz}\sigma_m - \sigma_m\Delta\sigma} \tag{6}$$

or with

$$\overline{\sigma}_{oz} = \sigma_{oz} - \sigma_m,\quad \overline{C}_1 = \frac{\overline{\sigma}_{oz}\Delta\sigma + \kappa^2}{\overline{\sigma}_{oz}^2 + \kappa^2},\quad \overline{C}_2 = \frac{\overline{\sigma}_{oz} - \Delta\sigma}{\overline{\sigma}_{oz}^2 + \kappa^2},\quad \sigma_w = \frac{\Delta\sigma + \overline{C}_1\sigma_m}{1 + \overline{C}_2\sigma_m} \tag{6a}$$

For the case of $\Delta\sigma \approx 0$ Eq. (3) reduces to

$$\kappa^2 = \frac{\sigma_{oz}\sigma_w(\sigma_{oz} - \sigma_z)}{\sigma_z - \sigma_w}$$

from which

$$\sigma_m \approx \sigma_z = \frac{\sigma_w(\sigma_{oz}^2 + \kappa^2)}{\sigma_{oz}\sigma_w + \kappa^2} = \frac{\sigma_w}{C_1} \tag{7}$$

By setting $k^2 = 0$ in Eq. (7), the expected relationship is obtained for a material without creep effect subjected to a static stress $\sigma_m \approx \sigma_z = \sigma_{oz}$.

The two expressions for $\sigma_z$ of Eqs. (2a) and (7) are linked by Eq. (1a) and the relationship

$$f_z = f_w(1 - \sigma_{oz}C_{a2}) = f_w C_{a1} \tag{8}$$

where $C_{a1}$ and $C_{a2}$ are the asymptotic values of $C_1$ and $C_2$, respectively, for an infinite number of cycles and are obtained by substituting $\sigma_{aw}$ for $\sigma_w$ in Eqs. (4a) and (4b).

Eq. (7) yields the stress-rupture strength for an infinitely long time as

$$\sigma_{az} = \frac{\sigma_{aw}}{C_{a1}} \tag{7a}$$

Fig. 7a shows some $\Delta\sigma$ vs. $\sigma_m$ curves for a material without creep effect ($k^2 = 0$), and Fig. 7b shows the analogous curves for a material with creep effect ($k^2 > 0$). Both families of curves are hyperbolas with a common axis of symmetry passing through the point ($\sigma_m = \sigma_{oz}$, $\Delta\sigma = 0$) and forming an angle of 45° with the $\sigma_m$ axis. All hyperbolas intersect the $\Delta\sigma$-axis ($\sigma_m = 0$) at $\Delta\sigma = \sigma_w$ for the respective number of cycles.

For materials without creep effect ($k^2 = 0$), all hyperbolas have a common tangent at the point ($\sigma_m \approx \sigma_z = \sigma_{oz}$, $\Delta\sigma = 0$). This common tangent makes an angle of -45° with the $\sigma_m$-axis, which is entirely in agreement with the fact already established by August Woehler that "stress cycles, for which the difference between maximum and minimum stress does not exceed certain values to be determined by experiment, even in the case of stresses which approach the ultimate tensile strength, can take place continuously, without rupture occurring".(5)

For materials with creep effect ($k^2 > 0$), the hyperbolas intersect the $\sigma_m$-axis at points characterized by $\sigma_m \approx \sigma_z < \sigma_{oz}$. The angle of intersection between the hyperbolas and the $\sigma_m$-axis is the more acute, the greater the number of cycles; it approaches -45° asymptotically for n = 0 (or i = - ∞).

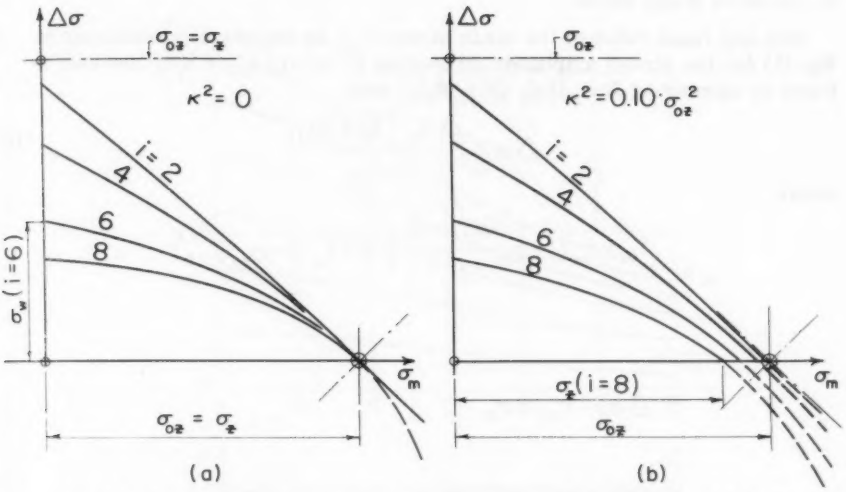


Fig. 7. Empirical relationship between mean stress $\sigma_m$ and alternating stress $\Delta\sigma$ for several numbers of stress cycles $n = 10^i$,
(a) for a material without creep effects,
(b) for a material with creep effects.

Incidentally, for n = 0, i.e., the condition where the initial load has just been applied prior to cycling (Fig. 1), the hyperbola becomes a straight line that passes through the points ($\sigma_m = \sigma_{oz}$, $\Delta\sigma = 0$) and ($\sigma_m = 0$, $\Delta\sigma = \sigma_{oz}$). This is as expected, since for a single loading to failure it is immaterial what is considered to be the mean stress and the alternating stress. In this connection it is also of interest to note that introduction of the conditions of initial loading to the static tensile strength, $\sigma_m + \Delta\sigma = \sigma_{max} = \sigma_{oz}$ and $\sigma_w = \sigma_{oz}$, in Eq. (3), leads to $k^2 = 0/0$. This simply means that the invariant stress characterizing the creep effect cannot be obtained from an ordinary tensile test.

It can be shown that for the empirical law of Eq. (3) the invariant $k^2$ is independent of the origin of coordinates. This means that if $k^2$ is evaluated from test results, it does not matter from where the stresses $\sigma_{oz}$ and $\sigma_m$ were measured, providing the corresponding value of $\sigma_w$ is introduced ($\Delta\sigma$ is not affected). Thus, if two pairs of experimental values $\sigma_{m1}$, $\Delta\sigma_1$ and $\sigma_{m2}$, $\Delta\sigma_2$ are available, it is possible to set

$$\left.\begin{aligned} \overline{\sigma}_w &= \Delta\sigma_1 \\ \overline{\Delta\sigma} &= \Delta\sigma_2 \\ \overline{\sigma}_m &= \sigma_{m2} - \sigma_{m1} \\ \overline{\sigma}_{oz} &= \sigma_{oz} - \sigma_{m1} \end{aligned}\right\} \qquad (9)$$

Then, Eqs. (3), (4), (5), (6) and (7) hold for $\overline{\sigma}_w$, $\overline{\Delta\sigma}$, $\overline{\sigma}_m$ and $\overline{\sigma}_{oz}$ substituted, respectively, for $\sigma_w$, $\Delta\sigma$, $\sigma_m$ and $\sigma_{oz}$. This substitution is particularly convenient in the evaluation of experimental data.

d. Constant Mean Stress

For any fixed value of the mean stress $\sigma_m$, an expression analogous to Eq. (1) for the stress amplitude $\Delta\sigma$ leading to failure after n cycles can be found by combining Eqs. (1a), (3) and (4) into

$$\Delta\sigma = \frac{\Delta\sigma_o + f_m \Delta\sigma_a}{1 + f_m} \tag{10}$$

where

$$f_m = f_w\left(1 - \sigma_m \frac{\sigma_{oz} - \sigma_{aw}}{\sigma_{oz}^2 + \kappa^2}\right) = f_w(1 - \sigma_m C_{a2})$$

$$\Delta\sigma_o = \sigma_{oz} - \sigma_m$$

$$\Delta\sigma_a = \frac{\sigma_{aw} - C_{a1}\sigma_m}{1 - C_{a2}\sigma_m}$$

= asymptotic stress amplitude for failure after an infinite number of cycles with mean stress $\sigma_m$.

This remarkably simple relationship between the curves $\Delta\sigma$ vs. i for $\sigma_m$ = constant is illustrated in Fig. 8 for the case of Fig. 7b.

e. Constant Ratio $\sigma_{min}/\sigma_{max}$

For any given ratio $\alpha = \sigma_{min}/\sigma_{max}$, the alternating stress and the mean stress can be expressed as

$$\Delta\sigma = \frac{1 - \alpha}{2}\sigma_{max} \quad \text{and} \quad \sigma_m = \frac{1 + \alpha}{2}\sigma_{max}$$

or

$$\Delta\sigma = \frac{1 - \alpha}{1 + \alpha}\sigma_m = \beta\sigma_m$$

With this value for $\Delta\sigma$ substituted, Eq. (5) becomes

$$\beta\sigma_m = \frac{\sigma_w - C_1\sigma_m}{1 - C_2\sigma_m}$$

which leads to a quadratic equation for $\sigma_m$:

$$\sigma_m^2 - \frac{C_1 + \beta}{C_2\beta}\sigma_m + \frac{\sigma_w}{C_2\beta} = 0 \tag{11}$$

Once $\sigma_m$ is determined, $\sigma_{max}$ is obtained as

$$\sigma_{max} = (1 + \beta)\sigma_m$$

The relationship between $\sigma_{max}$ and the number of cycles, n, or i = log n, for a fixed value of $\alpha$ is ordinarily also referred to as Woehler curves. It should

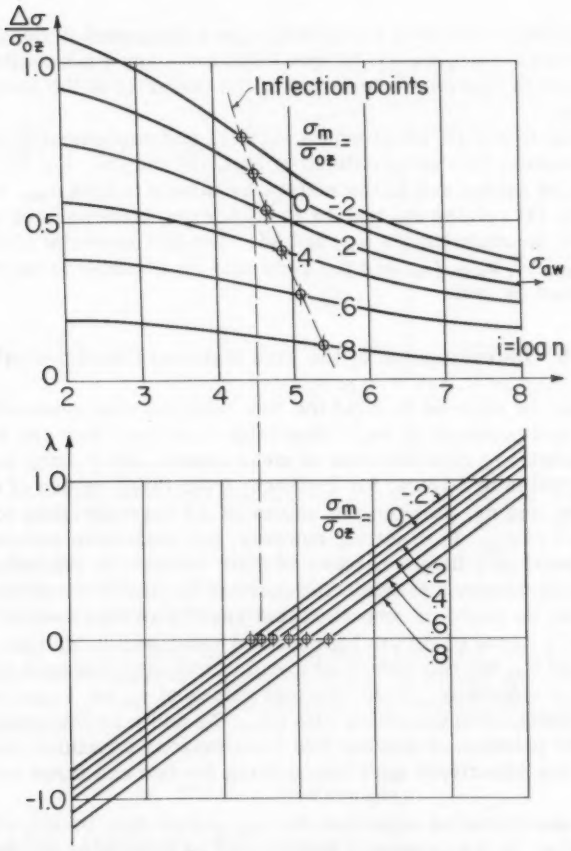


Fig. 8. Curves of $\Delta\sigma$ vs. i for constant mean stress $\sigma_m$.

be noted, however, that for this type of curve the relationship of Eq. (1), with constant exponent p, does not hold.

On the other hand, if the value of $\sigma_{min}$ or of $\sigma_{max}$ is prescribed, the alternating stress becomes

$$\Delta\sigma = \sigma_m - \sigma_{min} \text{ or } \Delta\sigma = \sigma_{max} - \sigma_m$$

Then, Eq. (5) leads to

$$\sigma_m^2 - \sigma_m\left(\frac{1+C_1}{C_2} - \sigma_{min}\right) + \frac{\sigma_{min}+\sigma_w}{C_2} = 0 \tag{11a}$$

or

$$\sigma_m^2 - \sigma_m\left(\frac{1-C_1}{C_2} + \sigma_{max}\right) + \frac{\sigma_{max}-\sigma_w}{C_2} = 0 \tag{11b}$$

## 4. The Over-All Problem

Several combinations of the special cases discussed in Section 3 may be used to describe the over-all fatigue behavior. Any such combination comprises a total of five characteristics of the material at the temperature under consideration.

In general it will be found most practical and convenient[2] to split up the over-all problem into the problems of Eqs. (1) and (3). Eq. (1) relates $\sigma_w$ to the number of cycles and to the material characteristics $\sigma_{oz}$, $\sigma_{aw}$, $C_w$ and p, whereas Eq. (3) relates $\sigma_m$ and $\Delta\sigma$ to $\sigma_w$ for the same number of cycles and the material characteristics $\sigma_{oz}$ and $k^2$. The five material characteristics thus are $\sigma_{oz}$, $k^2$, $\sigma_{aw}$, $C_w$ and p. They may be considered as the unknowns to be determined by test.

## 5. Determination of the Five Material Characteristics

Tests may be planned to yield the five material characteristics in the most convenient and economical way. Basically, however, they can be determined from five arbitrary combinations of mean stress, alternating stress, and number of cycles to failure; for instance, from three values of $\sigma_w$ corresponding to $n_1$, $n_2$, and $n_3$, plus the two values of $\Delta\sigma$ corresponding to $n_1$ and $n_3$ and a fixed value of $\sigma_m$. In practice, however, the evaluation should be carried out on the basis of a larger number of tests in order to minimize the effect of unavoidable scatter. Notably, the solution for the five material characteristics may be based on smoothed test results as represented by a curve of $\sigma_w$ vs. i and a curve of $\Delta\sigma$ vs. i for a fixed value of $\sigma_m$. In this case, values of $\sigma_w$, $\Delta\sigma$ and $\sigma_m$ for two values of i lead to two simultaneous equations with $\sigma_{oz}$ and $k^2$ as unknowns. Then, the test values of $\sigma_w$ vs. i can be used to set up three simultaneous equations with $\sigma_{aw}$, $C_w$ and p as the remaining unknowns. The problem of solving five simultaneous equations for five unknowns is thus effectively split into solving for two and three unknowns at a time.

The two simultaneous equations for $\sigma_{oz}$ and $k^2$ may be solved analytically or graphically. In the graphical solution, $k^2$ is calculated for several values of $\sigma_{oz}$ or of $\sigma_{oz} = \sigma_{oz} - \sigma_{m1}$. Then, the calculated values of $k^2$ are plotted vs. $\sigma_{oz}$ for each equation and the intersection of the two curves yields the values of $\sigma_{oz}$ and $k^2$.

Certain data (such as in the following example) lends itself quite well to analytical solution; in some cases, however, the graphical solution has decided advantages: When more than two pairs of data (for more than two values of i) are available for determining $\sigma_{oz}$ and $k^2$, the graphical solution provides means for distributing errors, and thus for reducing them (triangle of errors instead of point of triple intersection). Furthermore, when the available values for $\sigma_{m1}$ and $\sigma_{m2}$ are different for the several values of i and Eq. (9) thus is not applicable, two equations of the type of Eq. (6) may be set up to eliminate $\sigma_w$ for each value of i. The result is an equation between $\sigma_{oz}$ and $k^2$ for each value of i. Here, the graphical method is more convenient because of the somewhat involved nature of these simultaneous equations.

Reliability in the determination of the five characteristics of the material increases with the range of the experimental investigation, both as to the number of cycles and to the spread in the mean stress. This fact should be

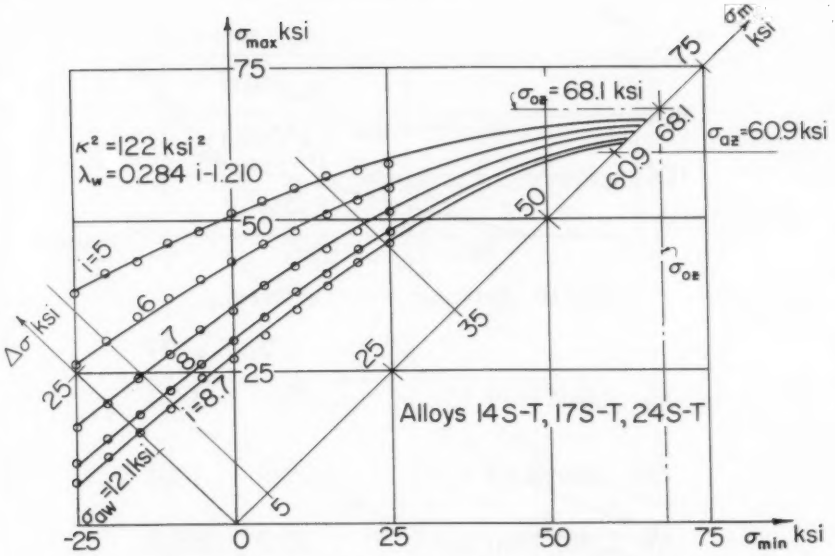


Fig. 9. Fatigue-test data for aluminum alloys 14S-T, 17S-T and 24S-T (Alcoa Handbook, Ref. 14) and material characteristics calculated by empirical formula.

taken into account when setting up test programs and when judging the reliability of the calculated material characteristics. It should also be noted that for best results more than slide rule accuracy is required for many of the analytical calculations.

### 6. Illustrative Examples

a. Aluminum Alloys 14S-T, 17S-T and 24S-T

Table 6 of the Alcoa Structural Handbook, 1945,[14] lists fatigue strength values for aluminum alloys that may be regarded as carefully smoothed, average values. These data are plotted in Fig. 9. From the smooth curves drawn to fit the plotted points the following test data—covering the widest possible range for greatest reliability—were selected for the evaluation of the five material characteristics:

| | | i=5 | i=7 | i=8.7 |
|---|---|---|---|---|
| For | $\sigma_{m1}$ = 5 ksi; $\Delta\sigma_1$ (ksi) = | 32.1 | 19.5 | 14.6 |
| For | $\sigma_{m2}$ = 35 ksi; $\Delta\sigma_2$ (ksi) = | 21.2 | | 10.8 |

To establish $\sigma_{oz}$ and $k^2$ from the two pairs of $\sigma_m$ and $\Delta\sigma$ values for i = 5 and i = 8.7, first revert to Eq. (9):

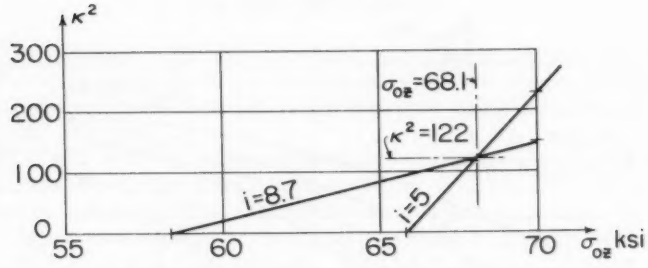


Fig. 10. Determination of $k^2$ and $\sigma_{oz}$.

| | i=5 | i=8.7 |
|---|---|---|
| $\overline{\sigma_w} = \Delta\sigma_1$ (ksi) = | 32.1 | 14.6 |
| $\overline{\Delta\sigma} = \Delta\sigma_2$ (ksi) = | 21.2 | 10.8 |
| $\overline{\sigma_m} = \sigma_{m2} - \sigma_{m1}$ = | 30.0 | 30.0 |

$$\overline{\sigma_{oz}} = \sigma_{oz} - \sigma_{m1} = \sigma_{oz} - 5.0$$

These values now lead to two simultaneous equations of the type of Eq. (3) with $\overline{\sigma}_{oz}$ and $k^2$ as unknowns:

For i = 5:

$$\kappa^2 = \overline{\sigma}_{oz}(\overline{\sigma}_{oz} - 30)\,0.5707 - 1{,}068.9$$

For i = 8.7:

$$\kappa^2 = \overline{\sigma}_{oz}(\overline{\sigma}_{oz} - 30)\,0.1450 - 180.5$$

Analytical solution of the simultaneous equations leads to $k^2 = 122.2$ $(ksi)^2$ and $\overline{\sigma}_{oz} = 63.1$ ksi, from which $\sigma_{oz} = 68.1$ ksi. The graphical solution is shown in Fig. 10.

With $k^2$ determined, Eq. (6) can be solved for $\sigma_w$ corresponding to three values of i, since the respective values of $\Delta\sigma_1$ are known for $\sigma_{m1} = 5$ ksi:

$$\sigma_w = \frac{4419.3\,\Delta\sigma_1 + 611}{4419 - 5\Delta\sigma_1}$$

| | i=5 | i=7 | i=8.7 |
|---|---|---|---|
| $\sigma_w$ (ksi) = | 33.5 | 20.1 | 15.0 |

From $\sigma_{oz}$ and the three sets of values of i and $\sigma_w$, the values of $\sigma_{aw}$, p and $C_w$ can be calculated from Eq. (1d). Since this is a transcendental equation, it must be solved by trial and error. It is most convenient to make an estimate for $\sigma_{aw}$, calculate the corresponding three values of $\lambda$ and finally, two values of p. The process is then repeated until the two values of p are sufficiently

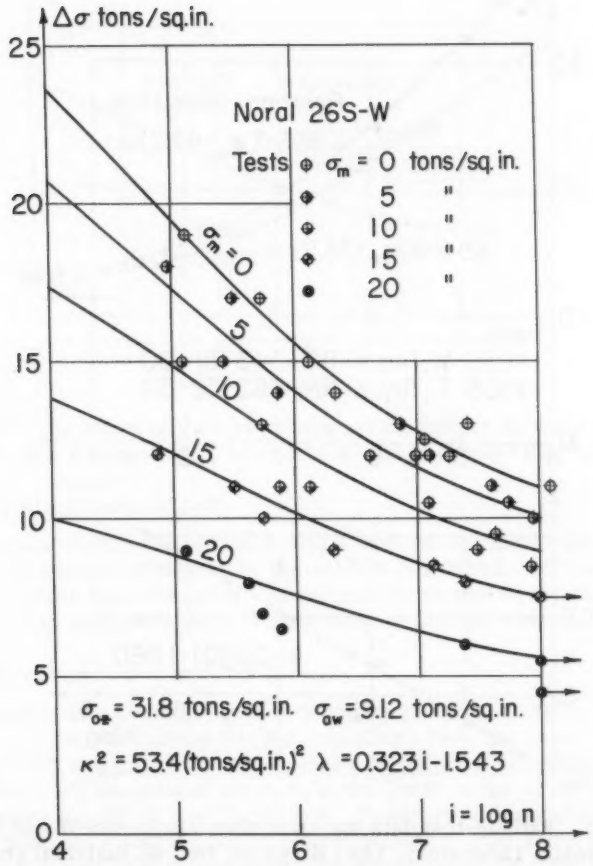


**Fig. 11. Fatigue-test data for aluminium alloy Noral 26S-W (Aluminium Laboratory, Ltd., Banbury, Ref. 6), material characteristics calculated by empirical formula and the corresponding calculated curves.**

close to each other, or, in other words, until the three (or more) values of $\lambda$, plotted against i, fall on a straight line.

Final estimate $-\sigma_{aw} = 12.09$ ksi

$$\lambda = 0.284\,i - 1.210$$

$$f_w = 0.0757\,n^{0.284}$$

Then, Eq. (4a) with $\sigma_{aw}$ substituted for $\sigma_w$, leads to

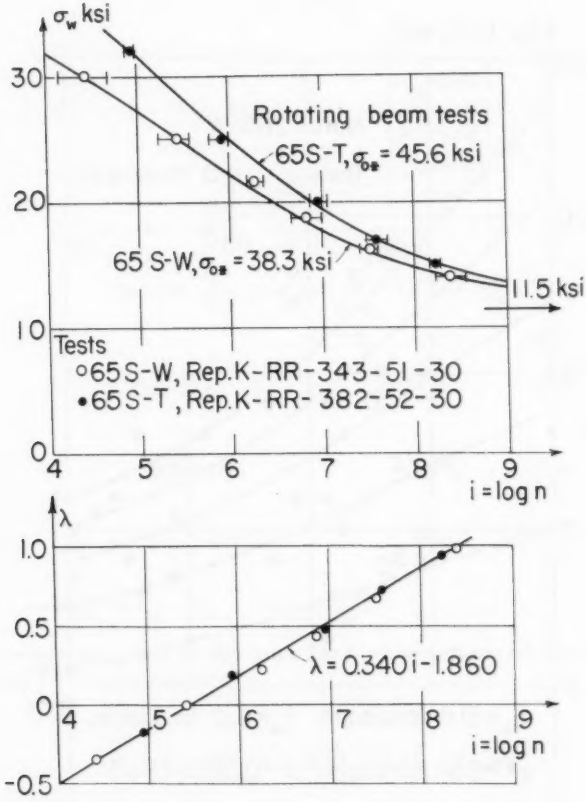


Fig. 12. Fatigue-test data for aluminium alloys 65S-W and 65S-T (Aluminium Laboratory, Ltd., Kingston, Ref. 8), material characteristics calculated by empirical formula and the corresponding calculated curves.

$$C_{a1} = \frac{68.1 \times 12.1 + 122.2}{68.1^2 + 122.2} = 0.1988$$

from which $\sigma_{az}$ is calculated by means of Eq. (7a),

$$\sigma_{az} = \frac{12.1}{0.1988} = 60.9 \text{ ksi}$$

Hence, the fatigue tests permit prediction of the asymptotic stress-rupture strength. No data are available for direct comparison; however, the reduction from $\sigma_{oz}$ = 68.1 ksi in short-time tensile tests to a predicted 60.9 ksi for infinite time is generally in line with the data of Fig. 6. These data were obtained by loading suspended bars with various weights and observing the time to fracture.(13)

The curves shown in Fig. 9 come very close to the hyperbolas calculated from the material characteristics established above, as can readily be verified.

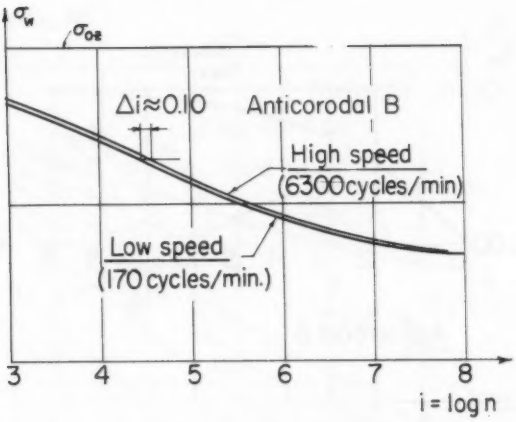


Fig. 13. The effect of rate of cycling on the fatigue strength of Anticorodal B subjected to complete stress reversal (Ref. 13).

b. Aluminum Alloy Noral 26S-W

Fig. 11 shows the results obtained with a wrought aluminum alloy,(6) together with the curves calculated by the method described. Although the test data reveal a great deal of scatter, the calculated curves fit the data quite well; indeed, they represent natural smoothing of the test results.

c. Aluminum Alloys 65S-T and 65S-W

Fig. 12 shows data obtained from rotating beam tests (complete stress reversal) in two aluminum alloys.(8) The two alloys have the same composition, but different heat treatment. It is of interest to note that the short-time tensile strength and the fatigue strength in the lower range of cycles is considerably better for 65S-T than for 65S-W. However, in the higher range of cycles, the difference decreases and nearly vanishes. $\sigma_{aw}$ and $\lambda$ were calculated for the two sets of data and within the accuracy of the data, were found to be identical for the two alloys. Hence, full heat treatment does not increase the fatigue strength for an infinite number of complete stress reversals over that available from partial heat treatment. Furthermore, the function of $f_w = C_w n^p$ is the same for the two alloys.

## 7. The Influence of Rate of Cycling

For metals which show a creep effect, i.e., a decrease in rupture strength with time, the rate of stress-cycling must obviously have an influence on the alternating fatigue strength. Fig. 13 shows this effect for Anticorodal B.(13) Cycling rates were 170 cycles per minute for the slow pulsator and 6300 cycles per minute for the high-speed pulsator. In the plots of $\sigma_w$ vs. i = log n, the rate of cycling appears to cause merely a parallel displacement of the curve in the direction of the i-axis. The lower cycling rate corresponds to a somewhat smaller i, or a smaller number of cycles to failure for the same alternating fatigue strength.

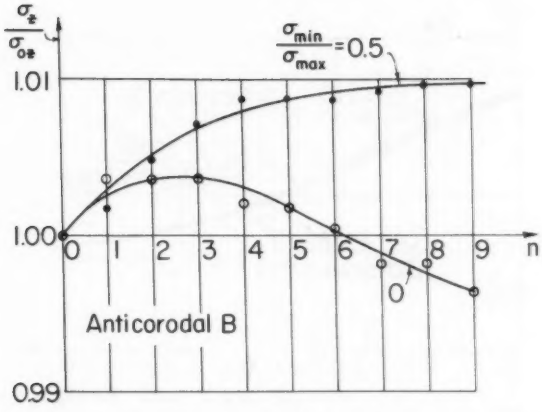


Fig. 14. The effect of strain-hardening on the low-cycle fatigue strength of Anticorodal B (Ref. 13).

### 8. The Influence of Strain-Hardening Effects

Fig. 14 shows the results of tests on Anticorodal B[13] when subjected to stress cycles with ratios $\sigma_{min}/\sigma_{max}$ of 0 and 0.5. An increase in strength is observed for each cycle of the first few cycles; the increase is more pronounced for the higher value of $\sigma_{min}/\sigma_{max}$. Undoubtedly, in this instance the fatigue behavior is masked by the progressive effect of cold-working, i.e., strain-hardening.

It is of interest to note that in the case of similar tests with $\sigma_{min}/\sigma_{max}$ = -0.75 (Fig. 4), the effect of strain-hardening was masked by the fatigue behavior. Hence, the influence of strain-hardening becomes more pronounced as the ratio of $\sigma_{min}/\sigma_{max}$ increases—at least to a certain point.

Fig. 15 shows the results of fatigue tests on an extruded bar of Aluminum Alloy 75S-T6.[7] It is seen that the effect of strain-hardening is felt to about 25,000 cycles for a ratio of $\sigma_{min}/\sigma_{max}$ = -0.33, and to about 250,000 cycles for a ratio of $\sigma_{min}/\sigma_{max}$ = 0.5. This would indicate that strain-hardening produces only a temporary, or unstable increase in strength, rather than a permanent and stable effect.

The material characteristics were calculated from fatigue-test results in the range of cycles beyond the influence of strain-hardening. The curves calculated from the material characteristics fit the test points as well as can be expected for the very considerable scatter in the test data. Of particular interest is the calculated curve for $\sigma_{min}/\sigma_{max}$ = 1.0, which corresponds to the creep-rupture strength. The marked decrease in the creep-rupture strength as compared with the short-time static tensile strength is most striking. Evaluation of numerous other tests has led to the belief that this pronounced creep effect is caused mainly by the zinc component of the alloy.

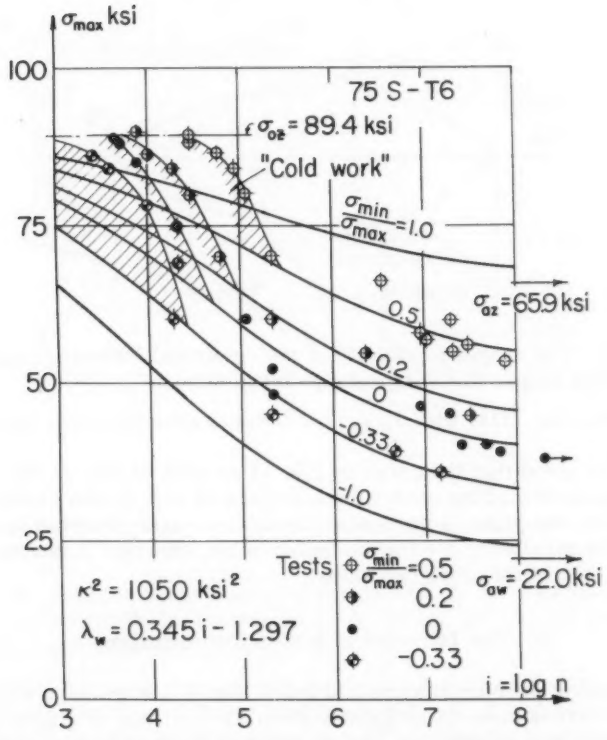


Fig. 15. The effect of strain-hardening on the fatigue strength of aluminum alloy 75S-T6 (E. C. Hartmann, M. Holt and I. D. Eaton, Ref. 7).

### 9. Range of Validity for Mean Stresses

The theory of fatigue presented in Sections 3 and 4, and particularly in Section 3c, generally applies to cases where the mean stress is zero or tensile. To a certain extent it also holds for a compressive mean stress. However, it is obvious that there must be a limit to the validity of the hyperbolas of Fig. 7 (or of Eq. (5)) as $\sigma_m$ assumes greater and greater negative values.

An exactly analogous theory may be worked out based on compressive mean stresses. In the compression theory the alternating stress increases as the mean stress increases algebraically, whereas for the tension theory the alternating stress increases as the mean stress decreases algebraically (Fig. 16). The two cases reach the limit of their respective validity at the point where the alternating stress is of the same magnitude; $\sigma_m$ is generally negative for this point.

The validity of this approach is very nicely confirmed by results of fatigue tests under axial compression conducted at the University of Illinois.(9) These results are plotted in Fig. 17; for the portion governed by tension, the curve

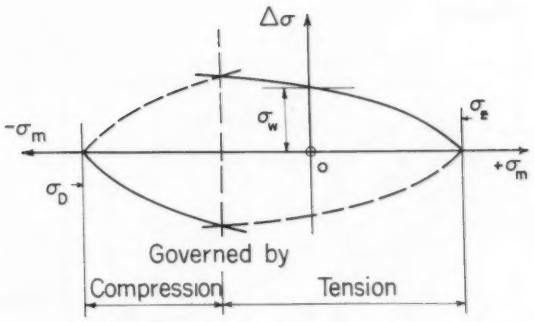


Fig. 16. The ranges of validity of the empirical formulas based on tests with tensile and compressive mean stress.

calculated from Eq. (11b) with $\sigma_{max} = -1.0$ ksi is seen to match the test points very closely.

It should be noted that the curve of Fig. 16 as well as that of Fig. 17 represents an intersection of the generalized surface of Fig. 2 with planes. In the case of Fig. 16, the plane is perpendicular to the i-axis, whereas in the case of Fig. 17 it is parallel to the i-axis, but does not intersect it and is not parallel to either of the other two axes.

## 10. The Influence of Stress Concentration

Stress raisers, such as notches and holes, cause a non-linear distribution of the elastic stress over the critical section. In the case of single loading of ductile materials, plastic flow occurs before failure, causing almost perfect equalization of stress. Hence, the tensile strength over the net area of a bar with a stress raiser is almost equal to the tensile strength of a smooth bar. In the case of fatigue failure, on the other hand, where $\sigma_{max} < \sigma_z$, the non-linear stress distribution plays a decisive role; the nominal fatigue strength $\sigma_{k\,max}$ (based on the net area) is less than the corresponding fatigue strength $\sigma_{max}$ of a plain bar.

For any given material and number of cycles, the fatigue strength with stress raiser may be compared with the fatigue strength without stress raiser by plotting the maximum stresses $\sigma_{k\,max}$ and $\sigma_{max}$, respectively, as ordinates vs. the mean stress $\sigma_m$ as abscissa (Fig. 18).

Then, a plot of $\phi$

$$\varphi = \frac{\sigma_{k\,max}}{\sigma_{max}} \tag{12}$$

vs. $\sigma_m$ is found to be very nearly a straight line.[2] In the case of short-time tensile strength, i.e., for $\sigma_m \approx \sigma_{k\,max} \approx \sigma_{max} = \sigma_z$, the ratio approaches the value $\phi = 1$. In the case of complete stress reversal,

$$\varphi_w = \frac{\sigma_{kw}}{\sigma_w} \tag{13}$$

The straight-line relationship may thus be expressed as

$$\varphi = \varphi_w + (1 - \varphi_w)\,\frac{\sigma_m}{\sigma_z} \tag{14}$$

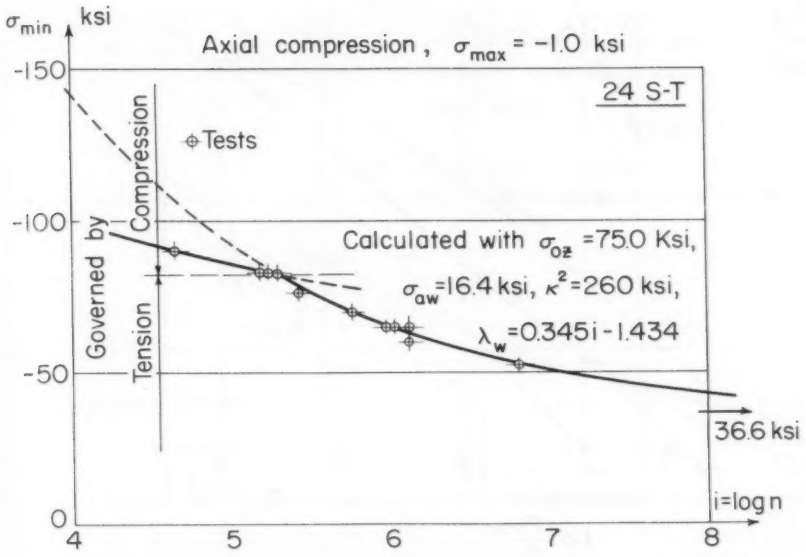


Fig. 17. Fatigue tests in axial compression (N. M. Newmark, R. J. Mosborg, W. H. Munse and R. E. Elling, Ref. 9) and curve calculated by Eq. (11b).

The ratio of $\phi_w$ obviously depends on the number of cycles, n; as n increases, $\phi_w$ decreases. It starts from $\phi_w = 1$ for $n = 0$ and reaches its final value at $n \approx 10^5$ cycles for steel and at $n \approx 10^6$ cycles for aluminum alloys.

In addition to showing the relationships between the fatigue strength of a bar with a hole and a smooth bar, Fig. 18 shows the influence of compressive mean stress and the ranges governed by tensile and compressive mean stress.

It should be noted that the fatigue strength of welded joints follows the same relationship as the one shown above for elements with stress raisers.(11)

## 11. Relaxation of Pre-Stressed Wires

Relaxation means a decrease of the stress $\sigma_r$ in a wire that is being kept at constant length. The initial stress, or "pre-stress" is $\sigma_{or}$; the final stress cannot exceed an asymptotic value $\sigma_{ar}$, irrespective of the magnitude of $\sigma_{or}$.

Study of a considerable amount of test data has led to the conclusion that the relaxation process follows a law analogous to Eq. (1):

$$\sigma_r = \frac{\sigma_{or} + f_r \sigma_{ar}}{1 + f_r} \tag{15}$$

where

$$f_r = C_r t^{p'}$$

or, with

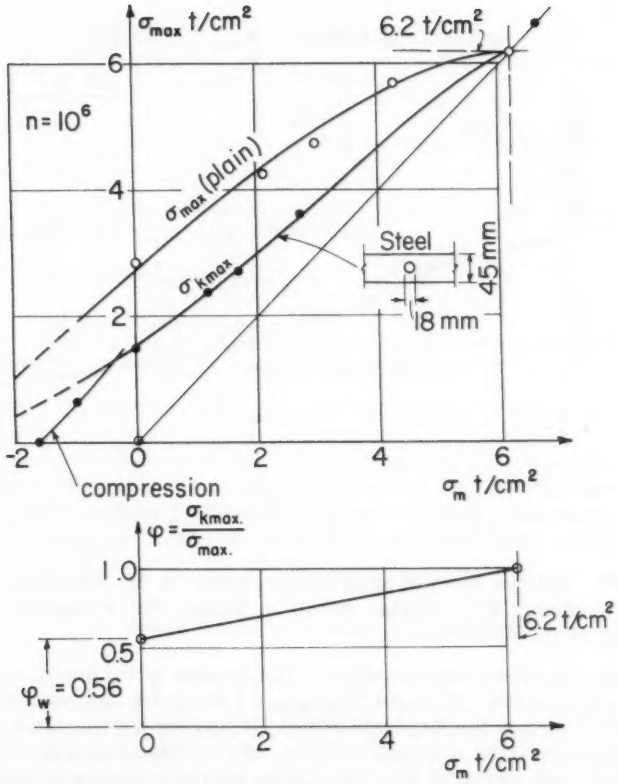


Fig. 18. The influence of stress concentration on the fatigue strength of steel bars subjected to longitudinal force (M. Rŏs and A. Eichinger, Ref. 10).

$$i' = \log t$$

$$\lambda' = \log f_r = p' i' + \log C_r$$

Fig. 19 shows the results of relaxation tests on steel wires,(12) together with the curve representing the above relationship.

Relaxation of pre-stressed wires is of particular importance in the design of pre-stressed concrete members. At present the effect of relaxation is often greatly underestimated. In the future, greater allowance should be made in the design of pre-stressed concrete members for the loss in force in the steel due to relaxation.

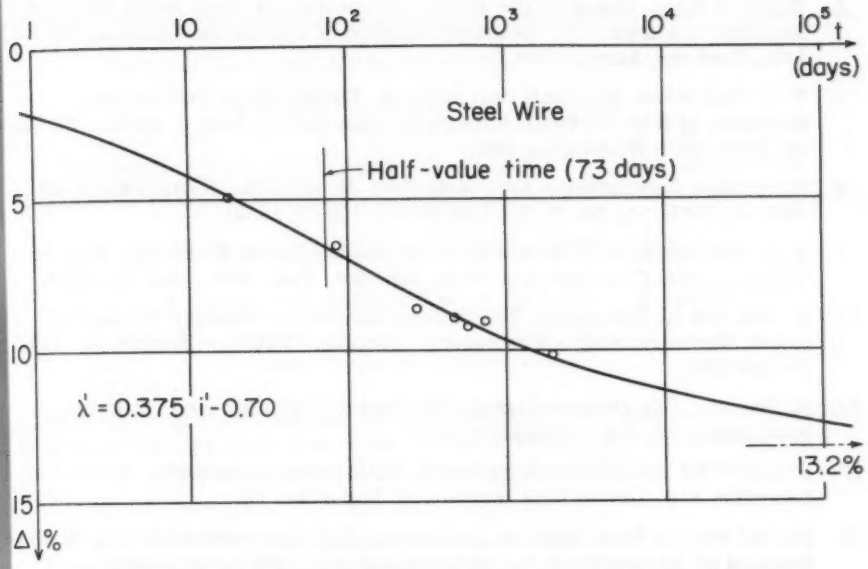


Fig. 19. Test data on relaxation of stress in a steel wire held at constant length (F. Levi, Ref. 12; Wire No. 13) and curve to fit test data calculated by empirical formula.

## ACKNOWLEDGMENT

The author wishes to acknowledge with thanks the cooperation of Mr. J. H. Meier (General Engineering Laboratory, General Electric Company) in editing this paper.

## REFERENCES

1. A. Woehler: Ueber die Festigkeitsversuche mit Eisen und Stahl. Zeitschrift fuer Bauwesen, Jahrgang XX, Berlin 1870.
2. F. Stuessi: Die Theorie der Dauerfestigkeit und die Versuche von August Woehler. Mitteilungen der T.K.V.S.B., (Schweizer Stahlbauverband), Nr. 13, Zurich 1955.
3. W. Stauffer und A. Keller: Durchfuehrung von Zeitstandsversuchen im Vielstabofen mit kleiner Stabform. Schweizer Archiv, 22. Jg., Heft 10, 1956.
4. F. Stuessi: Theorie und Praxis im Stahlbau, Mitteilungen der T.K.V.S.B., Nr. 16, 1956.
5. A. Woehler: Resultate der in der Central-Werkstatt der Niederschlesisch-Maerkischen Eisenbahn zu Frankfurt a.d.O. angestellten Versuche ueber die relative Festigkeit von Eisen, Stahl und Kupfer. Zeitschrift fuer Bauwesen, Jg. XVI, Berlin 1866, S. 72.

6. Effect of Mean Stress on the Fatigue Properties of Some Noral Wrought Aluminium Alloys. The Research Bulletin of Aluminium Laboratories, Ltd., Banbury, March 1956.

7. E. C. Hartmann, Marshall Holt and I. D. Eaton: Static and Fatigue Strengths of High-Strength Aluminum-Alloy Bolted Joints. NACA, Technical Note 2276, Washington 1951.

8. Aluminium Laboratories Ltd., Kingston: Reports No. K-RR-343-51-30 (65S-W, 1951) and No. K-RR-382-52-30 (65S-T, 1952).

9. N. M. Newmark, R. J. Mosborg, W. H. Munse and R. E. Elling: Fatigue Tests in Axial Compression, Proc. Am. Soc. Test. Mat., Vol. 51, 1951.

10. M. Rŏs and A. Eichinger: Die Bruchgefahr fester Koerper bei wiederholter Beanspruchung - Ermuedung - Metalle. EMPA - Bericht No. 173, Zurich 1950.

11. F. Stuessi: Zur Dauerfestigkeit von Schweissverbingungen. Schweiz. Bauzeitung, 75. Jg., Dezember 1957.

12. F. Levi: Le Problème des Aciers de Précontrainte en Italie. 3. Congress FIP, Berlin 1958, Session II, Paper No. 16.

13. Partial results from tests on Anticorodal B (a heat-treated Al-Mg-Si alloy supplied by Aluminium A.G., Switzerland) currently being conducted in cooperation with Mr. E. Peters at the author's section of the Structures Laboratory, Swiss Federal Institute of Technology, Zurich. It will take considerable time to complete this series and to report the results.

14. Alcoa Structural Handbook, Aluminum Company of America, Gulf Building, Pittsburgh, Pennsylvania, 1945.

Journal of the
STRUCTURAL DIVISION
Proceedings of the American Society of Civil Engineers

# BENDING MOMENTS ON SHELL BOUNDARIES

H. H. Bleich,[1] F. ASCE and M. G. Salvadori,[2] F. ASCE

This paper was the basis for an oral presentation at the Joint ASCE-IABSE Meeting at the New York Convention, October 1958. All Joint Meeting papers published in Proceedings or in Civil Engineering will be reprinted in one volume.

## ABSTRACT

As introduction, the penetration of bending stresses due to edge effects is considered for the cases of flat plates, cylindrical and rotational shells. The essential part of the paper is an estimate of edge effects and their penetration for the case of hyperbolic parabolids supported on straight generatrices.

## SYNOPSIS

The structural analysis of thin shells is usually performed by determining the state of membrane stress due to the loads and by introducing bending corrections in the neighborhood of the shell boundaries. The corrections are required to satisfy the boundary conditions which cannot be satisfied by membrane stresses alone. The penetration of the bending stresses into the shell depends on the thickness and the dimensions of the shell, and also on the characteristics of the middle surface of the shell.

A comparison is made of bending stresses due to an applied boundary moment in flat plates, cylindrical shells, rotational shells, and saddle shells.

Note: Discussion open until March 1, 1960. Separate discussions should be submitted for the individual papers in this symposium. To extend the closing date one month, a written request must be filed with the Executive Secretary, ASCE. Paper 2223 is part of the copyrighted Journal of the Structural Division, Proceedings of the American Society of Civil Engineers, Vol. 85, No. ST 8, October, 1959.

1. Prof. of Civ. Eng., Director, Inst. of Flight Structures, Columbia Univ., New York, N. Y.
2. Prof. of Civ. Eng., Columbia Univ., New York, N. Y.

The comparison illustrates the mechanism of bending stress penetration in the most commonly used types of thin shells.

The behavior of the shallow hyperbolic paraboloid supported along four straight generatrices is studied by means of Vlasov-type equations. The boundary disturbances to be added to the membrane stresses are known quantitatively in a rather special case, and qualitatively only in the general case. Their determination remains an open problem.

## 1. Flat Plates

Consider a simply supported, rectangular plate of sides a and b which is acted upon by a bending moment $M_B = M_0 \sin(\pi x/a)$ on its boundary $y = b/2$ (Fig. 1). The bending moment $M_y$ along the axis $x = a/2$ of the plate, when b is so much larger than a that

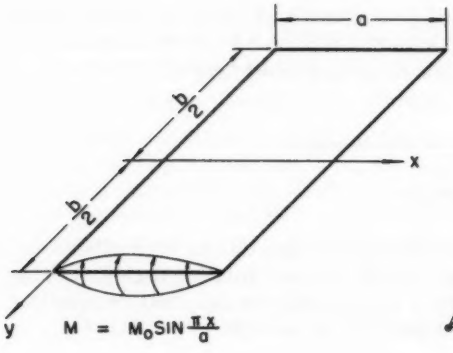


FIG.1 FLAT PLATE

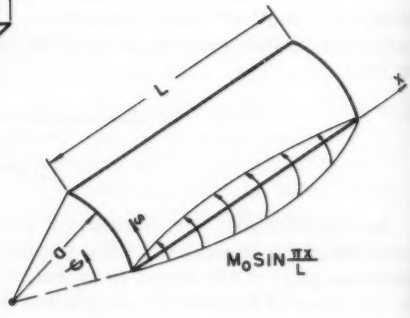


FIG.3 CYLINDRICAL SHELL

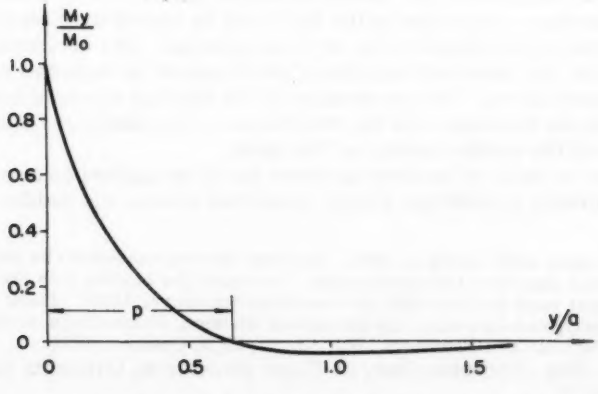


FIG.2 $M_y/M_B$ FOR PLATE $b/a = 8/\pi$

$$\sinh\left(\frac{\pi a}{2b}\right)=\cosh\left(\frac{\pi a}{2b}\right)=\frac{e^{\pi a/2b}}{2},$$

can be derived by means of a solution given by Timoshenko.(1) Assuming Poisson's ratio equal to zero, the ratio of $M_y$ to $M_B$ is given by:

$$\frac{M_y}{M_B}=\left[\frac{1}{2}-\frac{\alpha}{4}(1-\eta)\right]\frac{e^{\alpha\eta}}{\sinh\alpha} \tag{1}$$

where

$$\eta=\frac{2y}{b}\ ;\ \alpha=\frac{\pi b}{2a} \tag{2}$$

Fig. 2 gives $M_y/M_B$ versus y/a for $\alpha = 4$. It should be observed that $M_y$ becomes zero at $\eta = 1-2/\alpha$. As b/a approaches infinity, $M_y$ becomes first zero at the center of the plate and the penetration, defined by the equation:

$$p=\frac{1}{a}\left[\frac{b}{2}-y\Big|_{M_y=0}\right] \tag{3}$$

becomes infinite.(2)

The boundary rotation $\theta$ due to the sinusoidally distributed boundary moment is also sinusoidal, and for $\alpha=\infty$ has an amplitude

$$\frac{(h/a)\theta_m}{M_o/Eh^2}=\frac{6}{\pi}=1.91 \tag{4}$$

## 2. Circular Cylindrical Shells

### a) Moment Applied to Longitudinal Boundary

Consider a thin cylindrical shell of radius a, length L, and thickness h as shown in Fig. 3. The values of the bending moments $M_\phi$ due to a sinusoidal moment of intensity $M_o$ applied to a longitudinal boundary of the thin cylindrical shell have been computed by A. L. Parme, M. ASCE.(3) The values are given in terms of the parameter $ah/L^2$ and are plotted versus s/L in Fig. 4 for $ah/L^2 = 0.002$ and 0.100.(4)

It is seen that the penetration

$$p=\frac{s\big]_{M_\phi=0}}{L} \tag{5}$$

equals 0.40 and 0.90 for the two cases considered. It increases with increasing values of $ah/L^2$, and is of the order of 2/5 for the thinnest shells considered in practice.

The boundary rotation $\theta_m$ was also computed by Parme(5) and has an amplitude of

$$\left.\begin{aligned}&\frac{(h/L)\theta_m}{M_o/Eh^2}=2.05 \quad \text{for} \quad \frac{ah}{L^2}=0.002\\ \text{and}\quad &\frac{(h/L)\theta_m}{M_o/Eh^2}=2.54 \quad \text{for} \quad \frac{ah}{L^2}=0.100\end{aligned}\right\} \tag{6}$$

These values are of the same order of magnitude as that of the rotation of a flat plate.

b) Moment Applied to Curved Boundary

In this case, consider a semi-infinite cylindrical shell of radius a which has a moment of constant intensity $M_o$ applied to a free curved boundary of the shell (Fig. 5). The value of the bending moments $M_x$ in the shell is given by:(6)

$$\frac{M_x}{M_o} = \sqrt{2}\, e^{-\xi/\gamma} \sin\left(\frac{\xi}{\gamma} + \frac{\pi}{4}\right) \tag{7}$$

where

$$\xi = \frac{x}{a} \; ; \; \gamma = \frac{1}{\sqrt[4]{3}} \sqrt{\frac{h}{a}} = 0.76 \sqrt{\frac{h}{a}} \tag{8}$$

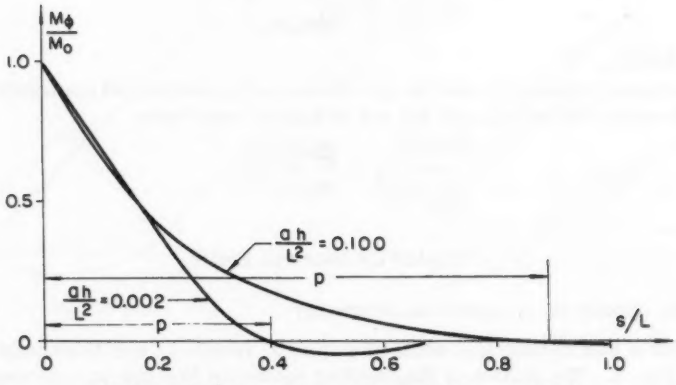


FIG.4 $M_\phi/M_o$ FOR CYLINDRICAL SHELL
(MOMENT APPLIED ON STRAIGHT BOUNDARY)

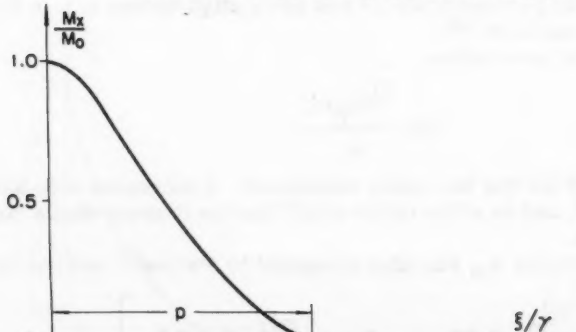


FIG.6 $M_x/M_o$ FOR CYLINDRICAL SHELL
(MOMENT APPLIED TO CURVED BOUNDARY)

Fig. 6 gives the values of $M_x$ versus $\zeta/\gamma$. For the boundary conditions considered, the penetration is given by $\zeta/\gamma = 3\pi/4$ or:

$$p = \xi]_{M_x=0} = \frac{3\pi}{4\sqrt[4]{3}}\sqrt{\frac{h}{a}} = 1.79\sqrt{\frac{h}{a}} \tag{9}$$

and the boundary rotation equals

$$\frac{\sqrt{h/a}\ \theta_m}{M_o/Eh^2} = 4(\sqrt[4]{3})^3 = 9.1 \tag{10}$$

When the boundary is simply supported, i.e., prevented from displacing radially, the rotation is $\frac{1}{2}\theta_m$.

It is noted that as the ratio h/a becomes smaller, the penetration and rotation are smaller of a different order with respect to those valid for plates and for longitudinal cylinder boundaries.

The maximum boundary moment and transverse shear due to a uniform outside pressure on the cylinder with a built-in edge have the values

$$M = (\gamma^2/2)\,pa^2 \quad ; \quad Q = \gamma pa \tag{11}$$

The formulas of this section can be applied with sufficient accuracy to sinusoidal boundary moments $M_o \sin n\varphi$ provided the wave length $\lambda = \frac{2\pi}{n}$ a is not too small compared to a.

### 3. Rotational Shells

It can be proved[7] that the formulas for the moment penetration and boundary rotation due to end moments obtained for the case of cylinders can be applied with satisfactory accuracy to rotational shells (Fig. 7), provided:

a) The opening angle $\varphi_o$ is not more than 20°.
b) The shell thickness is small enough for the penetration to be less than 1/3 (or 20°).
c) The shell hugs the tangent sphere in the boundary region limited by the penetration. This condition, for example, is not satisfied in the elliptical shell of Fig. 8a but is satisfied in the toroidal shell of Fig. 8b.

For rotational shells the formulas of Sec. 2b must be applied with:

$$\xi = \frac{s}{R_1} \quad ; \quad \gamma = 0.76\sqrt{\frac{h}{R_2}} \tag{12}$$

where $R_1$ is the meridional radius at the boundary and $R_2$ the radius at right angles to the meridional section (Fig. 7).

In order to gauge the accuracy of these approximate formulas it may be mentioned that[8] for a hemispherical dome ($\varphi_o = 90°$) of h/a = 1/15 the error in the rotation is 0.50%, while for a conical shell with $\varphi_o = 30°$ and h/a = 1/160 the error is 1.23%.

The formulas of Eq. (11) for built-in edges of cylindrical shells give safe limits for the boundary moments and shears of any shell supported on a curved boundary, provided the penetration p be evaluated with a radius equal to the radius of the shell in the boundary plane.

4. Hyperbolic Paraboloid Supported on Four Straight Generatrices

The shells of the preceding section had moments applied at curved boundaries. Hyperbolic paraboloids are often supported, instead, along straight generatrices. In this case cylindrical bending theory becomes unavailable for the simplified solution of the complete stress problem in the shell and the problem must be tackled from a different viewpoint.

Let the equation of the middle surface of the shell be defined by the equation:

$$z = c\frac{xy}{ab} \tag{13}$$

Where the z axis is vertical, the x and y axes are parallel to the sides a and b of the shell, and c is the shell rise ($c \ll a, b$) (Fig. 9).

Let $\bar{u}$, $\bar{v}$, $\bar{w}$ be the displacements in the x, y, z directions and, indicating partial derivatives by subscripts, let:

$$w = \overline{w} \;;\; u = \bar{u} + z_x \overline{w} \;;\; v = \bar{v} + z_y \overline{w} \tag{14}$$

be the displacements in the direction of z and of the straight generatrices of the paraboloid. The rise c is assumed small enough for the angle between the generatrices to be considered a right angle. Within the same degree of approximation, the cosine of the angle between the normal to the shell and the z-axis is unity, the $\bar{w}$ displacement may be considered normal to the shell and

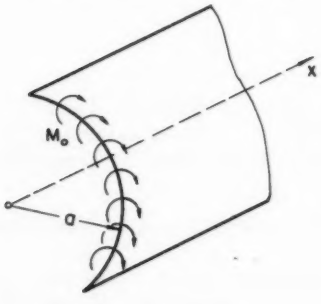


FIG. 5 CYLINDRICAL SHELL

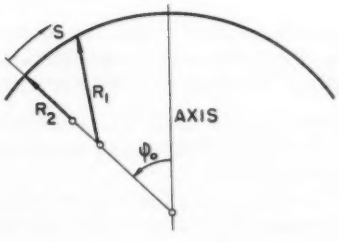


FIG. 7 RADII OF CURVATURE

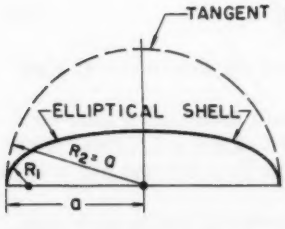


FIG. 8a

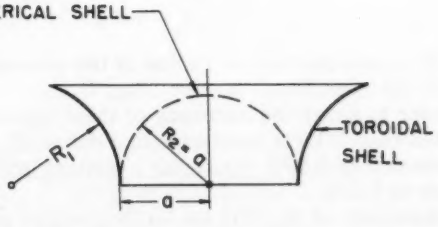


FIG. 8b

the projection of a shell element on the x, y-plane has the same area as the element itself.

The strains in the x and y directions due to $\bar{u}$, $\bar{v}$ and $\bar{w}$ are:

$$\epsilon_x = \bar{u}_x + z_x \bar{w}_x = u_x \quad ; \quad \epsilon_y = \bar{v}_y + z_y \bar{w}_y = v_y \tag{15}$$

The shear strain if w = 0 (Fig. 10a) is $u_y + v_x$; the shear strain if u = v = 0 (Fig. 10b) is -(2c/ab)w; hence the total shear strain $\gamma$ is given by:

$$\gamma = u_y + v_x - (2c/ab)w \tag{16}$$

The membrane energy due to these strains is expressed by:(9)

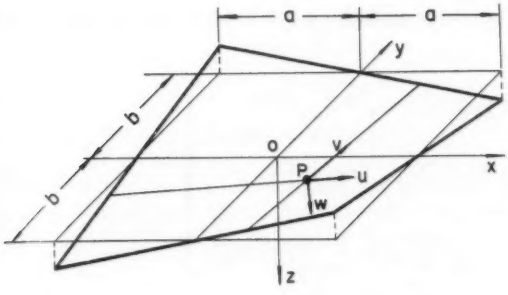


FIG. 9 HYPERBOLIC PARABOLOID

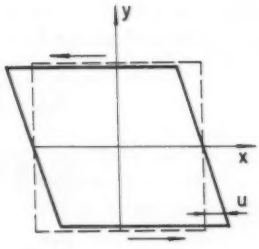


FIG. 11

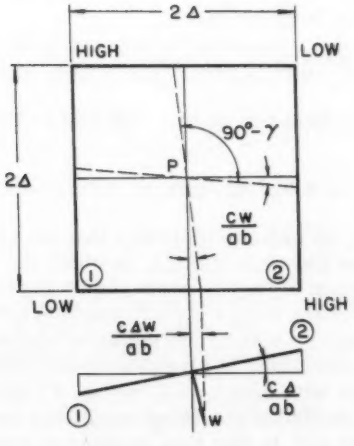


FIG. 10b

SHEAR STRAIN IF u=v=0

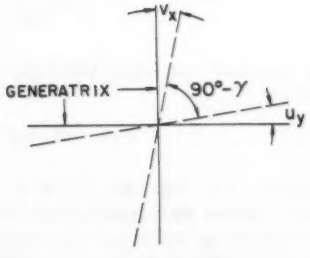


FIG. 10a

SHEAR STRAIN IF W=0

$$U_M = \frac{Eh}{2(1-\mu^2)} \iint \left[\epsilon_x^2 + \epsilon_y^2 + \frac{1-\mu^2}{2}\gamma + 2\mu\epsilon_x\epsilon_y\right] dx\,dy \tag{17}$$

The bending energy of the shallow shell may be taken equal to the energy of a plate:[10]

$$U_B = \frac{Eh^3}{24(1-\mu^2)} \left[(\nabla^2 w)^2 - 2(1-\mu)(w_{xx}w_{yy} - w_{xy}^2)\right] dx\,dy \tag{18}$$

Indicating by $q_u$, $q_v$, $q_w$ the components of the load per unit area of plate surface in the u, v, w directions the potential energy of the load is:

$$U_q = -\iint (q_u u + q_v v + q_w w)\,dx\,dy \tag{19}$$

Variating the total energy of the system with respect to u, v, w and letting Poisson's ratio $\mu = 0$, the displacement equations for the hyperbolic paraboloid are obtained in the form:

$$\left.\begin{aligned} u_{xx} + \tfrac{1}{2}(u_{yy} + v_{xy} - 2\alpha w_y) &= q_u/Eh \\ v_{yy} + \tfrac{1}{2}(u_{xy} + v_{xx} - 2\alpha w_x) &= q_v/Eh \\ \nabla^4 w - \frac{12\alpha}{h^2}(u_y + v_x - 2\alpha w) &= q_w/(Eh^3/12) \end{aligned}\right\} \tag{20}$$

where:

$$\alpha = \frac{c}{ab} \tag{21}$$

Equivalent equations in terms of w and of a stress function F have been obtained by E. Reissner.[11] A particular solution of Eqs. (20) for the case of vertical loads only $q_u = q_v = 0$; $q_w = q$ is given by:

$$u = u_o y \quad ; \quad v = v_o x \quad ; \quad w = w_o \tag{22}$$

This solution satisfies identically the first two of Eqs. (20) and reduces the third to:

$$-\alpha(u_o + v_o - 2\alpha w_o) = q/Eh \tag{23}$$

If $v_o = w_o = 0$, Eq. (23) gives $u_o = -q\,ab/cEh$ and indicates that the shell exhibits a shear deformation of the type shown in Fig. 11, in which the external load q does no work and the deformation energy is produced by the boundary shears. An analogous deformation occurs if $u_o = w_o = 0$, but it is obvious that these solutions do not lead to suitable membrane states of stress which can be modified by local boundary corrections to give practically significant solutions. A third membrane solution with $u_o = v_o = 0$, but $w_o \neq 0$ is much more significant, because the only unsatisfied boundary conditions involve the displacement w and the slopes $w_x$ and $w_y$. In fact this solution is correct everywhere except near the boundaries. Unfortunately it is not possible to obtain the boundary disturbances for this case by elementary means. The shell behavior is clarified by the following considerations.

Let us try to find complete solutions with

$$q_u = q_v = 0 \; ; \; q_w = q \; ; \; u = v = 0 \tag{24}$$

and $w \neq 0$. In this case the third of Eqs. (20) becomes:

$$\nabla^4 w + \frac{24a^2}{h^2} w = \frac{q}{(Eh^3/12)} \tag{25}$$

and shows that the shallow shell behaves like a plate on elastic foundation with a foundation modulus:

$$K = \frac{24c^2}{a^2 b^2 h^2} \tag{26}$$

This equation has a particular (membrane) solution:

$$w_o = \frac{qa^2b^2}{2Ec^2h} \tag{27}$$

identical with the solution mentioned above.

In order to have $w = 0$ on the shell boundaries bending disturbances $w(x, y)$ must be added to $w_o$. Assuming, for example, b so much larger than a that w is almost everywhere a function of x only, the equation for w reduces to the equation for a beam on an elastic foundation:

$$\frac{d^4w}{dx^4} + 4\beta^4 w = \frac{q}{Eh^3/12} \tag{28}$$

with:

$$\beta = \sqrt{\frac{4c}{b}} \frac{\sqrt[4]{3}}{\sqrt{ah}} = 1.56 \sqrt{\frac{c}{bah}} \tag{29}$$

The bending moment at the boundary due to the displacement $w_o$ of Eq. (27) for a shell built in at the boundary is given by:(12)

$$M_o = \frac{1}{2\sqrt{6}} \left(\frac{b}{c}\right) qah = 0.204 \left(\frac{b}{c}\right) qah \tag{30}$$

while the penetration is given by:

$$p = \frac{3\pi}{4\sqrt[4]{6}} \sqrt{\frac{b}{c} \frac{h}{a}} = 1.51 \sqrt{\frac{b}{c} \frac{h}{a}} \tag{31}$$

For a ratio $b/c = 4$, the penetration is 70% higher than for a cylindrical surface with end moment (Eq. (9)).

The maximum bending stress due to the moment $M_o$ of Eq. (30) is:

$$\sigma_B = \pm \frac{\sqrt{6}}{2} q \frac{ab}{ch} = \pm 1.23 q \frac{ab}{ch} \tag{32}$$

The corresponding membrane shear stress is:(13)

$$\tau_m = \pm \frac{1}{2} q \frac{ab}{ch} \tag{33}$$

These results confirm quantitatively the qualitative statements of E. Reissner in Reference 11 to the effect that: a) the penetration is small compared to $\frac{1}{2}\sqrt{b/a}$ as long as h/c is much less than 1; b) the bending stresses $\sigma_B$ which occur in the edge zone are of the same order of magnitude as the membrane shear stresses.

If the solution just obtained for a shell of large length b loaded by $q_w = q$,

$$u = v = 0 \quad , \quad w(x,y) = w(x) \tag{34}$$

is substituted in the three original Eqs. (20), the first and third are satisfied while the second is violated. However, this violation can be removed by providing an appropriate load $q_v$, i.e.,

$$\frac{q_v}{Eh} = -\alpha w_x \tag{35}$$

As the derivative $w_x$ is inherently small except near the boundaries it follows that the necessary loads $q_v$ are of importance only near the boundaries $x = \pm a$. It is important to notice, however, that these shears are not small. By integrating $q_v$ over the width pa of the disturbed zone one finds that, because

$$\int_0^{pa} w_x dx \doteq w_o \tag{36}$$

the resultant of the corrective forces $q_v$ is qab/2c. This value is exactly the membrane shear used in conventional design. The difference between the above solution including the forces $q_v$ and the actual conditions lies in the fact that the membrane shear is not applied at the edge of the plate as it should but acts in a distributed manner within a narrow region near the edge.

The complete solution of the stress problem of the hyperbolic paraboloid with commensurate sides a, b can only be achieved by integrating Eqs. (20) without the assumption that u = v = 0 everywhere, and with physically significant boundary conditions. These equations seem more suitable for the problem than formulations involving a stress function for the membrane stresses because some of the boundary conditions involve displacements.

## REFERENCES

1. Theory of Plates and Shells, by S. Timoshenko, McGraw-Hill Book Co., New York, 1940, p. 204.

2. The moment $M_y$ is so small beyond its first line of contraflexure that only the zone between the edge and this line may be considered as affected by the edge moment.

3. Design of Cylindrical Concrete Shell Roofs, ASCE Manual of Engineering Practice No. 31, 1952, pp. 36-39.

4. The radius, thickness and length are indicated by r, t and l in ASCE Manual No. 31. Letting:

$$\frac{rt}{l^2} = k^4 \quad ; \quad \frac{s}{L} = \frac{ks}{\sqrt[4]{rtl^4}}$$

5. Design of Cylindrical Concrete Shell Roofs, ASCE Manual of Engineering Practice No. 31, 1952, p. 44.

6. Theory of Plates and Shells, by S. Timoshenko, McGraw-Hill Book Co., New York, 1940, p. 389.

7. Theory of Plates and Shells, by S. Timoshenko, McGraw-Hill Book Co., New York, 1940, p. 467.

8. Scienza della Costruzioni, Vol. Terzo, by O. Belluzzi, Nicola Zanichelli, Editore, Bologna, 1953, pp. 390 and 393.

9. A Strain Energy Expression for Thin Cylindrical Shells, by H. H. Bleich and F. DiMaggio, Journ-Appl. Mech., Sept. 1953.

10. Theory of Plates and Shells, by S. Timoshenko, McGraw-Hill Book Co., New York, 1940, p. 50.

11. On Some Aspects of the Theory of Thin Elastic Shells, by E. Reissner, Journal, Boston Soc. of Civ. Engr., Vol. 42, No. 2, 1955.

12. Theory of Plates and Shells, by S. Timoshenko, McGraw-Hill Book Co., New York, 1940, Sec. 81.

13. Statik und Dynamik der Schalen, by W. Flügge, Springer, Berlin, 1957, p. 118.

Pr

Var
The ac
stress
by a n

Fol
range
which
action
light
work.
It
made
and a
sever
in fol
the ac
which
stres

Th
homo

Note:
wr
pa
Ar
1. Se

Journal of the
STRUCTURAL DIVISION
Proceedings of the American Society of Civil Engineers

# THE DESIGN OF FOLDED PLATES

Eliahu Traum[1]

## SYNOPSIS

Various design theories of folded plate structures are critically reviewed. The advantages and generality of the Method of Particular Loadings are stressed and an outline of its application is given. The method is illustrated by a numerical example.

## 1. INTRODUCTION

Folded plates have become in recent years increasingly popular; their use ranges from roofs, silos, staircases through such a variety of structures to which the engineer's imagination sets the only limits. The three-dimensional action of folded plates made it possible to roof considerable spans with a light and economical concrete structure, erected on relatively simple formwork.

It is therefore quite natural that the design theories of folded plates have made during the past few decades considerable strides towards both simplicity and accuracy. In the present paper an attempt is made to review critically several theories that have been used to determine the moments and stresses in folded plates. In conclusion of such a review the author tries to point out the advantages and generality of Yitzhaki's Method of Particular Loadings,(1) which appears to have become so far the simplest and most general way of stress analysis for folded plates.

## 2. The Membrane Theory

The first design theory published(2,3) was based on the assumption of an homogeneous, elastic structure in which the lines of intersection between the

Note: Discussion open until March 1, 1960. To extend the closing date one month, a written request must be filed with the Executive Secretary, ASCE. Paper 2229 is part of the copyrighted Journal of the Structural Division, Proceedings of the American Society of Civil Engineers, Vol. 85, No. ST 8, October, 1959.

1. Senior Lecturer, Technion, Israel Inst. of Technology, Haifa, Israel.

individual plates, the ridges, do not undergo any displacement. Some authors refer to the theory based on last assumption as to the membrane theory of folded plates. The moments and stresses in the structure are accordingly found by the following procedure:

a) A strip of unit width cut from the structure by two parallel transverse sections is subjected to its own dead and superimposed load. With the ridges assumed as unyielding supports, moments and reactions in the continuous one-way slab thus formed are then determined. This is generally referred to as the "slab-action" of the folded plate.
b) Forces equal and opposite to the reactions of the slab-structure at the ridges are then applied to the "plate-structure". These forces are resolved into their components in the direction of the plates meeting at the common ridge. The sum of these components in the plane of each plate is causing in it a bending moment in the longitudinal direction; the span of the plate is the distance between two traverses.
c) The bending stresses caused in the extreme fiber of each plate are then computed. In general, the longitudinal stresses in the fibers of two adjacent plates meeting at a common edge will not be equal to each other. This, of course, is impossible in a continuous homogeneous structure. Longitudinal shearing stresses must therefore act along every ridge tending to equalize the stresses in both fibers meeting at it. It follows from equilibrium conditions that these shearing stresses are internally balanced by axial forces loading each plate at its edge.
d) The next step is to determine these longitudinal forces. With it each plate can be designed for the combined moment and axial load acting on it.

The first design theories derived the magnitude of the longitudinal axial forces from the condition that stresses in adjacent fibers on both sides of any ridge must be equal. Thus a series of simultaneous linear equations was established, their number being equal to the amount of ridges in the folded plates structure. Consequently the solution of the simultaneous equations was quite wearisome, especially for a great number of plates in the structure.

A very substantial simplification and reduction of the amount of work involved in finding the longitudinal forces was introduced by Winter and Pei.[4] Recognizing the form of the simultaneous equations for the determination of the stresses as analogous to those of the Three Moment Theorem, Winter and Pei applied the Cross' Distribution Method, by which all longitudinal forces at the ridges were directly obtained in one single operation.

Later on, this method was further simplified by the introduction of a similar distribution which yields directly the longitudinal stress at the ridge.[5,13] This shortcut not only obviates the need to compute the stresses from the moments and eccentric axial loads but also gives clear physical meaning to the distribution, which becomes easy to follow and control. An additional advantage in distributing stresses rather than some imaginary forces $(\frac{Mo}{h})$ becomes obvious when certain longitudinal stresses are known at the outset as is the case when applying a prestressing force along any plate. Illustrations of stress distributions under such loadings are given in Yitzhaki's book.[1]

## 3. The Bending Theory

Experiments[5] as well as theoretical considerations prior to them,[6,7] have shown that the assumption of unyielding ridges was unjustified in most cases. Moreover, considering the settlement of the ridges and the consequent rotation of the plates, bending moments are caused in the transverse direction that may radically change all stresses computed by the membrane theory. A more exact theory, taking into account the settlement of the ridges, was therefore developed. This is generally referred to as the bending theory of folded plates.

In the following the basic philosophy of different approaches for consideration of ridge settlements will be examined.

### 3.1 The Iterative Procedure

A given settlement at any ridge changes the slab moments and consequently their reactions at the ridges. But the new reactions applied at the ridge will in turn give a different settlement than was originally found, i.e. a further change in these reactions. One could suggest the use of an iterative procedure by which the reactions are first computed assuming unyielding supports and then corrected for settlements. The revised reactions applied to the plate structure would then cause further change of ridge settlements which in turn requires further revision of moments and reactions.

This iterative procedure, though relatively simple to use, requires not only a substantial amount of numerical work but—what is more important—is in many cases convergent very slowly or not at all. Moreover, it can be shown that in certain cases, as for small angles between adjacent plates, the iterative procedure is actually divergent.

An iterative procedure for the determination of stresses due to ridge settlements was therefore discarded in favour of other approaches that treated directly the final ridge moment as the unknown. The basic difference between various theories thus concentrated in the conditions and methods from which the final ridge moments could be derived.

### 3.2 Exact Bending Theories

It would be far beyond the scope of the present paper to dwell on the detailed differences between various bending theories. This also is not necessary here since this subject was treated quite extensively in a book by Born.[8] The only thing that might be stated here is that the first bending theories[9,10] developed simultaneous differential equations of the fourth order for the determination of the ridge moments or settlements. The equations, though giving an exact solution, became so complex that their actual use in office practice was extremely time consuming.

The conditions for the determination of final ridge moments were derived from considerations of slope deflection at the ridges. In the folded plate structure with stiff connections at all ridges no angle change between two adjacent plates is possible. In other words, the sum of angle changes at any ridge—resulting from the external loads on the slabs, from the ridge moments and the differential settlements between adjacent ridges—must vanish. Most authors chose the settlement of any ridge as independent variable, expressed the transverse moment as proportional to its second derivative and the external load as a function of its fourth derivative. They thus obtained for each

ridge a differential equation of the fourth order involving as many unknowns as ridges in the folded plates structure.

This bending theory was considerably simplified by Vlassow.[7] He was the first to express the ridge deflection in terms of stresses and thus was able to obtain a set of linear equations which yielded directly the longitudinal stresses as well as the ridge moments. Since this method is relatively little known in this country, yet was the first to contain the reasoning which formed later the basis for more recent and simpler methods, it will be shortly outlined in the next section.

### 3.3 Vlassow's Bending Solution

This solution aimed at determining directly by one set of simultaneous linear equations the longitudinal stresses and the ridge moments. Two conditions serve as basis for the determination of the unknown moments and stresses, namely: i) equilibrium and ii) zero angle change at any ridge. For the purpose of the analysis stresses due to external loads are treated first and then unit moments are applied consecutively at each ridge that is capable of resisting a bending moment.

The detailed solution is carried out by the following steps:

a) Resolve the external load into concentrated loads at the ridges (Fig. 1), i.e.:

$$R_n = \frac{1}{2}(p_n b_n + p_{n-1} b_{n-1}) \qquad (1)$$

b) Resolve these ridge loads into their components acting in the planes of the plates meeting at the respective ridge.

c) Obtain the total load acting in the plane of each plate, $P_n$:

$$P_n = S_{n,n+1} - S_{n+1,n} \qquad (2)$$

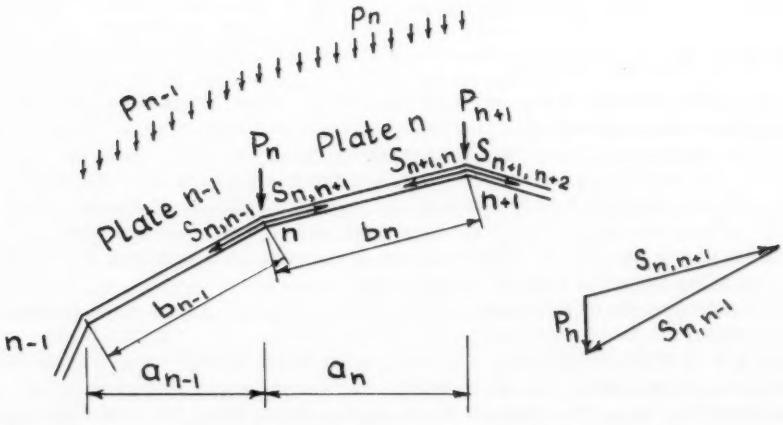


FIG. 1

RESOLUTION OF RIDGE LOADS

d) Compute the plate moments, considering each plate as a beam resting on two traverses:

$$M_n = \frac{P_n L^2}{8} \tag{3}$$

e) Assume the moment $M_n$ to be in equilibrium with a couple of internal longitudinal forces $F_n^o$ which act along the ridges, i.e.:

$$F_n^o = \frac{M_{n-1}}{b_{n-1}} + \frac{M_n}{b_n}$$

$$F_{n+1}^o = \frac{M_n}{b_n} + \frac{M_{n+1}}{b_{n+1}} \tag{4}$$

The moments are added algebraically, considering their sign. The index $^o$ denotes these ridge forces as the primary ones, assuming the ridge moments to be zero.

f) Based on Navier's assumption of linear stress distribution from ridge to ridge (Fig. 2), the longitudinal stresses are related to the forces $F^o$ by the equilibrium condition of Eq. (5):

$$\frac{1}{6}\sigma_{n-1} A_{n-1} + \frac{1}{3}\sigma_n (A_{n-1} + A_n) + \frac{1}{6}\sigma_{n+1} A_n = F_n^o \tag{5}$$

where $A_n$ denotes the cross-sectional area of plate n:

$$A_n = b_n \delta_n \tag{6}$$

g) Eqs. (5) can be established for each ridge and solving them simultaneously would yield all longitudinal stresses in the structure under the assumption of hinged ridges with zero deflection at them.

However, such an assumption would not conform with the actual behaviour of a continuous reinforced concrete structure. It becomes therefore necessary to take also into account the ridge moments and deflections. This is done by the following additional steps:

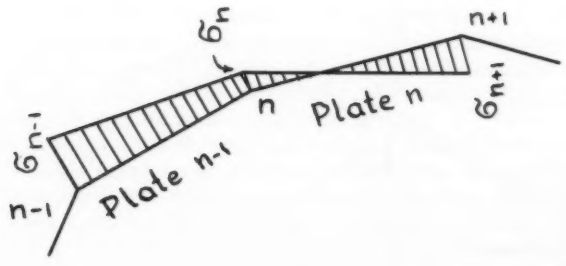


FIG. 2

EQUILIBRIUM OF LONGITUDINAL FORCES

h) The unknown moment $\mu_n$ acts at ridge n and causes in it and in the ridges adjacent to it additional reactions $\Delta R$ as shown in Fig. 3. Their magnitude is given by:

$$\Delta R^n_{n-1} = -\frac{\mu_n}{a_{n-1}}$$
$$\Delta R^n_n = \frac{\mu_n}{a_{n-1}} + \frac{\mu_n}{a_n} \qquad (7)$$
$$\Delta R^n_{n+1} = -\frac{\mu_n}{a_n}$$

Reactions $\Delta R$ cause additional plate loads $\Delta P$, moments $\Delta M$ and additional longitudinal forces $\Delta F$ which will change the magnitude of the stresses given in Eq. (5). If these stresses are considered to include already the influence due to $\mu_n$, the left side of Eq. (5) will remain unchanged and only $F^o_n$ will be affected. If a unit moment causes a change of $\Delta F$ in the longitudinal force, the total change in it due to $\mu_n$ will be $\mu_n \Delta F$. When other ridges are subsequently loaded by moments $\mu_{n-1}$, $\mu_{n+1}$ etc., Eq. (5) turns into:

$$\frac{1}{6}\sigma_{n-1}A_{n-1} + \frac{1}{3}\sigma_n(A_{n-1}+A_n) + \frac{1}{6}\sigma_{n+1}A_n + \qquad (8)$$
$$+\mu_{n-2}\Delta F^{n-2}_n + \mu_{n-1}\Delta F^{n-1}_n + \mu_n \Delta F^n_n + \mu_{n+1}\Delta F^{n+1}_n + \mu_{n+2}\Delta F^{n+2}_n = F^o_n$$

Here $\Delta F^{n-2}_n$ is the additional longitudinal force at ridge n due to a unit moment acting at ridge n-2.

Every equation of type (8) contains five unknown ridge moments $\mu$ and three unknown stresses $\delta$. If the total number of ridges, including the free edges, is m, the number of unknowns will be 2m-2, i.e. m stresses and m-2 moments. Yet the number of equations of type (8) is only m. It therefore becomes necessary to set up m-2 additional equations.

j) This is easily achieved by stipulating the condition that the total change of angle at any ridge, $\tau_n$, must vanish:

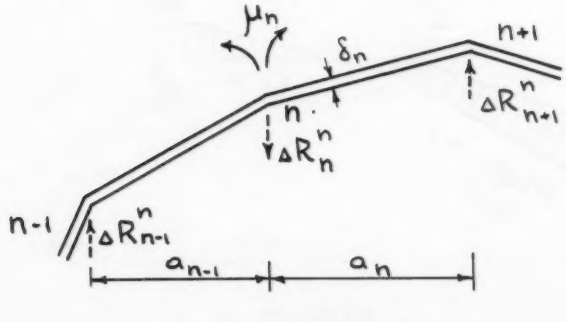


FIG. 3
MOMENT LOADING

$$\tau_n = \tau_n^{\mu} - \tau_n^{q} - \tau_n^{\sigma} = 0 \tag{9}$$

Here $\tau_n^{\mu}$ is the change of angle at n due to the moments $\mu$:

$$E\tau_n^{\mu} = \frac{\mu_{n-1} b_{n-1}}{6 I_{n-1}} + \frac{\mu_n}{3}\left(\frac{b_{n-1}}{I_{n-1}} + \frac{b_n}{I_n}\right) + \frac{\mu_{n+1} b_n}{6 I_n} \tag{10}$$

In - moment of inertia of plate n ($I_n = \frac{1}{12}\delta_n^3$). $\tau_n^{q}$ is the change of slope at n due to the external loading q:

$$E\tau_n^{q} = \frac{q_{n-1} b_{n-1}^2 a_{n-1}}{24 I_{n-1}} + \frac{q_n b_n^2 a_n}{24 I_n} \tag{11}$$

$\tau_n^{\delta}$ is the change of slope due to differential ridge settlements that result from the difference in longitudinal stresses between the top and bottom of the plate. The magnitude of $\tau_n^{\delta}$ is easily established by Maxwell's law of reciprocal deflections. The interrelation between longitudinal force and change of slope is such that the longitudinal force at n caused by a unit moment at that point is numerically equal to the rotation at n produced by a unit longitudinal force there. Now, since the coefficients of the moments $\mu$ in Eq. (8) express the change in longitudinal forces due to a unit moment, they must be numerically equal to the coefficients of the longitudinal stresses $\delta$ in the equation expressing the rotation of the plates meeting at ridge n (Eq. (12)):

$$E\tau_n^{\sigma} = \sigma_{n-2}\Delta F_n^{n-2} + \sigma_{n-1}\Delta F_n^{n-1} + \sigma_n \Delta F_n^{n} + \sigma_{n+1}\Delta F_n^{n+1} + \sigma_{n+2}\Delta F_n^{n+2} \tag{12}$$

k) We thus have m-2 equations of type (9) and m equations of type (8), which are sufficient for the determination of all unknown stresses $\delta$ and moments $\mu$. The solution can be tabulated and a relatively simple matrix form can be set up for the coefficients of all equations.

Vlassow's method and later on others that were based on the same principles[11,12] provided a very substantial simplification of the stress determination in folded plates compared with bending theories involving simultaneous differential equations. However, even a relatively simple structure as shown in Fig. 4, consisting of only five plates, still required the quite wearisome solution of ten simultaneous equations.

Another substantial disadvantage of this method lies in the fact that the ridge moments determined by the solution of the simultaneous equations comprise at once both the slab moments resulting from the external load and those due to ridge settlements. Since the first part varies along the structure in proportion to the distribution of the external load whereas the second part varies according to the elastic line, the distribution of the total ridge moments along the structure is not known. One possibility, though extremely time consuming, is to set up the same pattern of solution as described above at several sections along the span of the folded plate. Another possibility, normally preferred, is to assume the variation of load along the structure as similar to the elastic line, namely as a sine wave or to express it as a Fourier series. This, however, introduces a certain error in the results.

It might be pointed out, though, that the determination of moments and stresses by Vlassow's method can not only be easily tabulated, but the equations can also be directly set up in matrix form with geometric data only as coefficients. This form is very easily adaptable to a simple solution on an electronic computer, for which this method seems especially well suited.

### 3.4 The Simplified Bending Theory

With substantially the same approach as shown in the former section the determination of bending moments and stresses in folded plates was further considerably simplified.[5,13] The basic idea of this approach was to perform the stress analysis in several stages, for each one of which all moments and stresses are uniquely determined. In a form analogous to the determination of the redundants in a statically indeterminate structure or to the analysis of sidesway in a multistory frame, a primary system is chosen in which the ridges undergo no deflection. A unit rotation is then given to each plate separately and all stresses and deflections resulting from it are computed. By superposition, the final magnitude of each plate rotation is found and consequently all moments and stresses can be determined.

In this way the solution is reduced to the determination of the plate rotations only, which in the structure of Fig. 4, for example, would involve only three simple simultaneous equations.

Since a very clear and concise description of this method was given with a numerical example in a recent paper by Simpson,[13] there is no need to repeat here its detailed solution.

### 3.5 The Method of Particular Loadings

With the bending theory thus simplified it might appear as if no further treatment was necessary. This might have been the case were it not for a

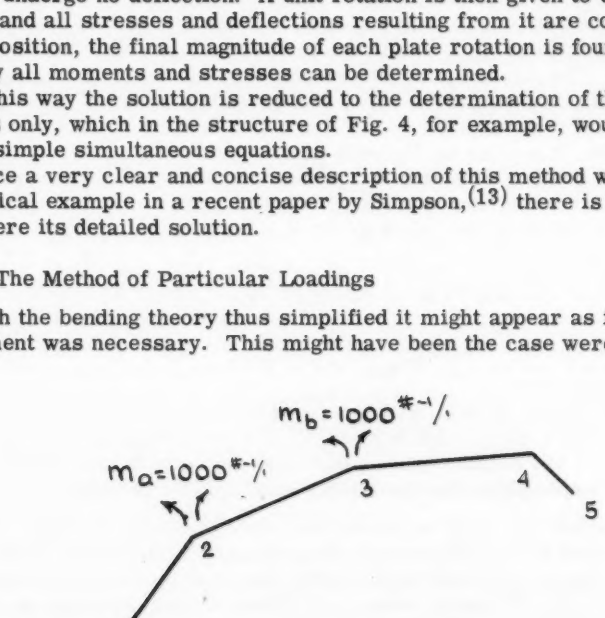


FIG. 4

A FOLDED PLATE ROOF
SHOWING ADDITIONAL PARTICULAR LOADING

certain lack in generality inherent in the methods described above which are not always directly applicable.

In the case, for instance, when more than two plates meet at a common ridge or when there are different support conditions for individual plates—as for edge members supported on intermediate columns—the above method dealing with plate rotations would not yield a straightforward solution. Moreover, since the moment causing the unit plate rotation is distributed along the ridge in a definite form, namely as a sine wave similar to the elastic line, continuous shells cannot be treated. In addition, to take into account torsional stiffness of edge beams or shear deflection of short plates and certain other cases would be impossible by the simplified theory of the former section.

Along similar lines of reasoning a method was developed instead by Yitzhaki[1] that dealt directly with deflections rather than with rotations. This not only made it possible to achieve a most general solution including all special cases, but also yielded directly the actual magnitude of the vertical deflection along any ridge of the structure. This, incidentally, is in many cases quite critical and always deserves careful checking.

In the Method of Particular Loadings the total moments and stresses are obtained by superimposing several stages of loading on the folded plates structure. The first stage deals with the external loads. In a clearly tabulated form the slab moments, ridge reactions and plate moments are computed, the stresses at all ridges are found and the plate deflections and slab moments due to them are determined. These moments cause additional reactions at the ridges, termed as superfluous loads ($R_o^n$).

Additional particular loadings are then required so as to deflect the slab to conform with the deformed plates structure. These loadings will consist of a group of vertical ridge loads that are externally in equilibrium or of a moment acting along a ridge, both being assumed initially as unity. The distribution of these loads along the structure is always according to functions, called normal functions, that will yield a plate deflection proportional to the load distribution. By applying the particular loading in a function similar to the plate deflection the superfluous loads caused by them can be added directly to the initial ridge loads, so that no correction for the plate settlement due to the additional loading is required. The variation of the particular loading along the structure can be taken as a function similar to the elastic line of a fixed beam if the support conditions of the folded plates are such or as any function similar to the elastic line of a given structure.

For each particular loading the procedure outlined above for the external load is repeated leading to the determination of the superfluous loads. The individual particular loadings are then superimposed so as to cancel the primary superfluous load at each ridge. This procedure is again analogous to the determination of the holding forces in the sidesway analysis of multistory frames by the Cross' Distribution Method.

The separation of the solution into the first stage dealing with the external load and the stages of additional particular loadings permits the exact determination of all stresses along any point of the structure. The variation of the stresses due to the first stage is proportional to the distribution of the external load along the span of the plates. Those due to the other stages vary by a different function that is practically fully expressed by the first term of a Fourier series but the accuracy can be increased, although entirely unnecessary, by taking an additional term. Superimposing each loading according to the function of its variation along the structure gives the exact values of moments and stresses at any point.

A step by step outline of this method is shown in the following in concise form and is further illustrated by a fully detailed numerical example given in the Appendix.

a) Determine the slab moments and reactions considering the structure as a one-way slab on unyielding supports.
b) Resolve the ridge reactions into plate loads and compute plate moments and primary stresses, assuming each plate to behave as an independent beam.
c) Distribute these primary stresses—in a method shown in the Appendix—so as to achieve the adjusted stress at every ridge, which will already be equal for the two extreme fibers of the plates meeting at the ridge.
d) Compute the ridge deflections and the fixed-end slab moments resulting from them.
e) Distribute these moments in the slab structure to obtain the ridge moments resulting from plate settlements caused by the external loads.
f) Determine the ridge reactions (called the superfluous loads) due to above moments.

Steps a) to f) are the typical procedure for each particular loading. The total number of additional particular loadings is equal to the amount of ridges at which the slab moments are unknown. (Such will be all edges except the free ones, at which the moments are zero, and those next to them, at which the moment must equal the cantilever moment of the marginal plate). In the folded plate shown in Fig. 4 two additional particular loadings will be required.

g) Apply on the slab-structure an additional particular loading "a" consisting of a moment acting along one ridge (ridge #2 in Fig. 4). The distribution of this moment along the structure will vary with conditions of support, but will be a sine-wave for a simply supported structure.
h) Repeat steps a) to f) for the influence of $m_a$ and determine the final particular loading $R_a$, which is the sum of the initial ridge load $(\frac{m_a}{a})$ and the superfluous load.
j) Repeat steps g) and h) for any further additional particular loading that is required ($m_b$ in the present example).
k) Superimpose the individual particular loadings, each multiplied by a proportionality factor a and b respectively, so as to cancel the primary superfluous loads $R''_o$ at each ridge. This is done according to Eq. (13).

$$a\,R_{2a} + b\,R_{2b} + R''_{2o} = 0$$
$$a\,R_{3a} + b\,R_{3b} + R''_{3o} = 0 \qquad (13)$$

R - denotes the particular ridge load; the first index gives the ridge and the second the case of particular loading.

$R''_{2o}$ - the superfluous load at ridge 2 under the primary loading (o).

l) After determining the factors a and b, the moments, stresses and deflections at any point are finally obtained by superposition according to Eq. (14) and the solution is completed.

$$\text{Stress:} \quad \sigma = \sigma_o + a\sigma_a + b\sigma_b$$
$$\text{Moment:} \quad m = m_o + am_a + bm_b \qquad (14)$$
$$\text{Deflection:} \quad \delta = \delta_o + a\delta_a + b\delta_b$$

For the determination of stresses at any point along the structure it should be remembered that the variation of $\delta_o$ is proportional to the external load (i.e. constant for uniformly distributed load) and that of $\delta_a$ and $\delta_b$ is proportional to the shape of the elastic line.

## 4. CONCLUSIONS

Within the framework of a single paper it is of course impossible to show all applications of the Method of Particular Loadings. It was tried though to point out the comprehensive form of the solution which can easily be checked at each stage and the advantage of dealing directly with the deflections. Thus there is no difficulty to analyze, for instance, the folded plates structure for more than two plates meeting at a common ridge; the condition of equal deflection of the plates meeting at the ridge will simply have to be satisfied. Or if the marginal plate rests on intermediate columns, the column reactions will have to be introduced as an additional particular loading of unknown forces. These will be such as to cause a zero deflection of the marginal plate at the columns.

The practicing designer will find it helpful not to have to worry about any sign conventions that are usually required when dealing with slope rotations, but to be able to reduce the work to the simplest algebraic form.

The solution of the folded plates structure by the Method of Particular Loadings is thus reduced to a problem of no further complexity than the design of a continuous beam.

## ACKNOWLEDGMENT

The author is indebted to Mr. Max Reiss, Senior Lecturer at Technion, Israel Institute of Technology, who was kind enough to read the manuscript and make some helpful suggestions.

## REFERENCES

1. Yitzhaki, D., "Prismatic and Cylindrical Shell Roofs", Haifa Science Publishers, Haifa, Israel, 1958.
2. Craemer, H., "Theorie der Faltwerke", Beton und Eisen, 1930, p. 276.
3. Ehlers, G., "Die Spannungsermittlung in Flaechentragwerken", Beton und Eisen, 1930, p. 281.
4. Winter, G. and Pei, M., "Hipped Plate Construction", Journ. ACI, 43, 1947, p. 505.
5. Gaafar, I., "Hipped Plate Analysis Considering Joint Displacements", Trans. ASCE, 119, 1954, p. 743.
6. Flügge, W., "Statik und Dynamik der Schalen", Springer Verlag, Berlin 1934.
7. Vlassow,,V. Z., "Structural Mechanics of Thin-Walled Shells" (in Russian), Mowcow 1936.
8. Born, J., "Faltwerke, Ihre Theorie und Anwendung", K. Wittwer Verlag, Stuttgart 1954.

9. Grüning, K., "Die Nebenspannungen in Prismatischen Faltwerken", Ing. Archiv, 1932, p. 44.

10. Gruber, E., "Berechnung Prismatischer Scheibenwerke", Proc. Int. Assoc. Bridge and Struct. Eng., 1932.

11. Girkmann, K., "Flächentragwerke", 2. Auflage, Springer Verlag, Wien 1948.

12. Ashdown, A. J., "The Design of Prismatic Structures", Concrete Publications Ltd., London 1951.

13. Simpson, H., "Design of Folded Plate Roofs", Proc. ASCE, Paper 1508, Jan. 1958.

## APPENDIX

### Illustrative Example: The Design of a Folded Plate Roof by the Method of Particular Loadings

a) General Data

The folded plate roof shown in Fig. A-1, that was given as an illustrative example in a paper by Simpson,(13) will here be redesigned by the Method of Particular Loadings.

The general geometric data of the individual plates that will be necessary in the course of computations are first summarized in Table I.

b) Moment Distribution

Assuming a strip of unit width of the cross section of the structure to act as a continuous one-way slab on unyielding supports, the ridge moments are determined by the moment distribution shown in Fig. A-2. Because of symmetry, the slab may be assumed as rigidly fixed at ridge 3.

The reactions at the ridges are now applied to the plate-structure as forces of equal magnitude and opposite direction. These ridge loads as well as their resolution in the direction of the plates meeting at the ridge are shown in

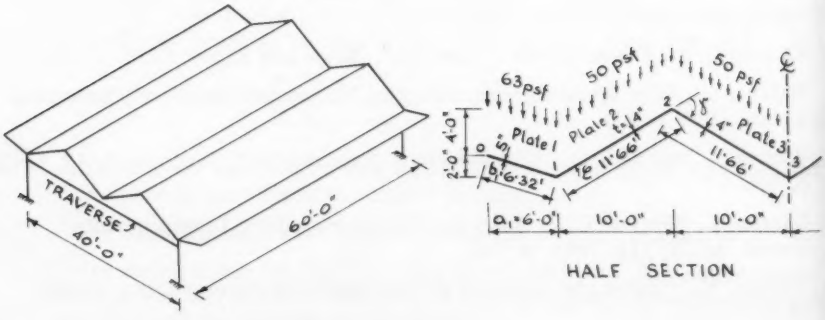


FIG. A-1

ILLUSTRATIVE EXAMPLE

## TABLE I : GENERAL DATA

| 1 | 2 | 3 | 4 | 5 | 6 | 7 | 8 | 9 | 10 | 11 | 12 | 13 |
|---|---|---|---|---|---|---|---|---|---|---|---|---|
| RIDGE | PLATE | b | t | A=bt | $S=\frac{tb^2}{6}$ | $\varphi$ | $\sin\varphi$ | $\cos\varphi$ | $\gamma$ | $\sin\gamma$ | $\alpha_n=\frac{\cos\varphi_n}{\sin\gamma_{n-1}}$ | $\beta_n=\frac{\cos\varphi_n}{\sin\gamma_n}$ |
| | | in | in | sq.in | $in^3$ | ° | | | ° | | | |
| 0 | | | | | | | | | | | | |
| | 1 | 75·9 | 5 | 379·5 | 4800 | -18·42 | -·316 | ·948 | | | | -1·25 |
| 1 | | | | | | | | | -49·37 | -·758 | | |
| | 2 | 140 | 4 | 560 | 13080 | 30·95 | ·515 | ·858 | | | -1·13 | ·974 |
| 2 | | | | | | | | | 61·90 | ·881 | | |
| | 3 | 140 | 4 | 560 | 13080 | -30·95 | -·515 | ·858 | | | ·974 | -·974 |
| 3 | | | | | | | | | -61·90 | -·881 | | |
| | 3' | | | | | | | | | | -·974 | |

Fig. A-3. From parts b) and C) of Fig. A-3 it is seen that the plate loads can be always expressed in general form by:

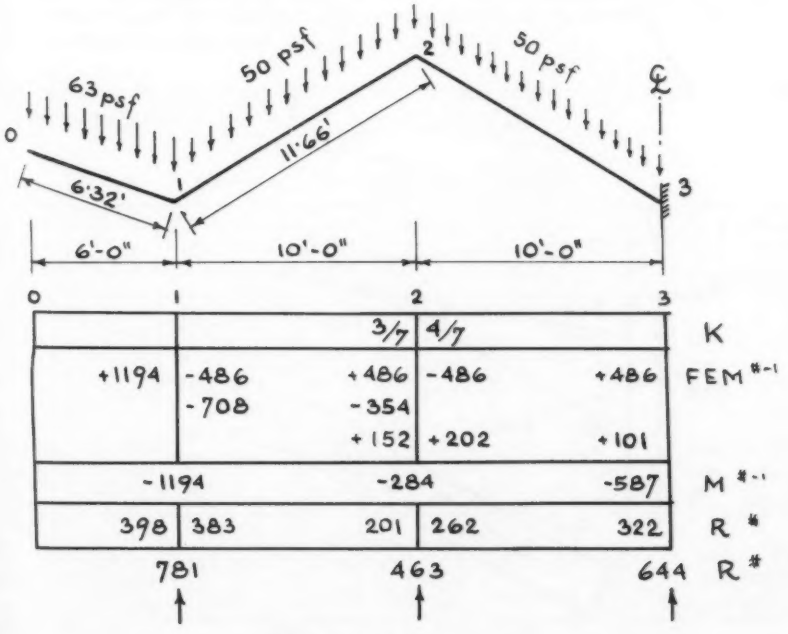


FIG. A-2

SLAB MOMENTS DUE TO EXTERNAL LOADS

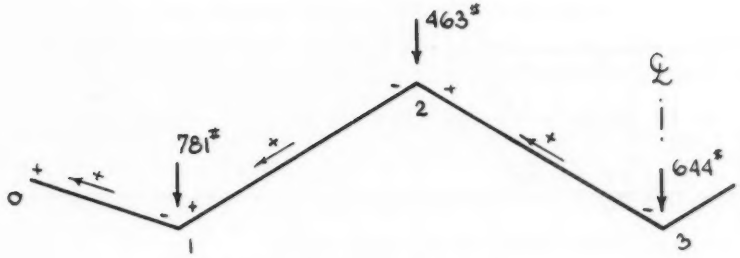


a) PLATE LOADING

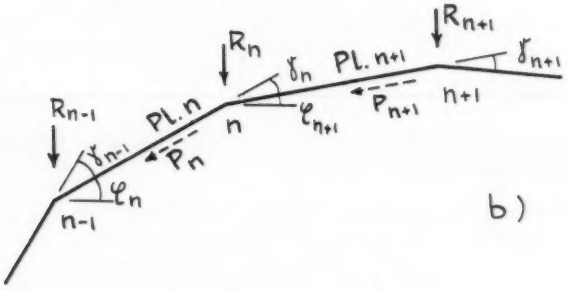


b)

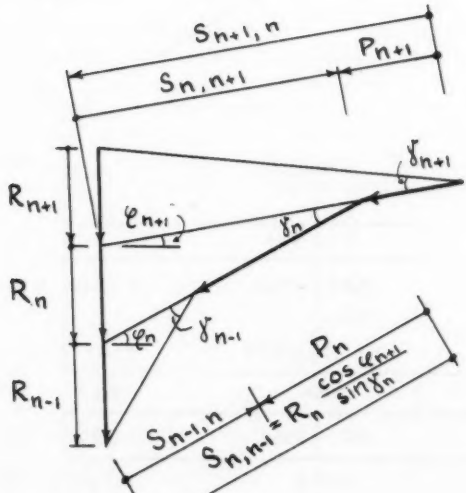


c)

FIG. A-3

RESOLUTION OF RIDGE LOADS

$$P_n = R_n \frac{\cos \varphi_{n+1}}{\sin \gamma_n} - R_{n-1} \frac{\cos \varphi_{n-1}}{\sin \gamma_{n-1}} =$$

$$= R_n \alpha_{n+1} - R_{n-1} \beta_{n-1}$$

where the values of $\alpha$ and $\beta$ are already given in Table I. The plate forces $P_n$ are tabulated in column 3 of Table II,* the Operation Table, which will contain all data necessary to complete the design.

With the values of P the moments are computed in each plate by:

$$M_o = \frac{Pl^2}{8} = \frac{P \cdot 60.0^2}{8} = 450 \text{ P \#-' or } 5400 \text{ P \#-"}$$

and with these the initial stresses $\delta_o$ are obtained by:

$$\sigma_o = \frac{M_o}{S}$$

S—the section modulus—is taken again from Table I. The values of $\delta_o$ are tabulated in column 4 of Table II.

c) Stress Distribution

The free edge stresses $\delta_o$ are now distributed in order to determine the final stresses $\delta_n$ at each ridge. The stress distribution is shown in Fig. A-4 and the results are tabulated in column 5 of Table II.

*This Table is the copyright of Prof. D. Yitzhaki and is reproduced here with his kind permission.

TABLE II: OPERATION TABLE

| | 0 | 1 | 2 | 3 | 4 | 5 | 6 | 7 | 8 | 9 | 10 | 11 | 12 | 13 | 14 |
|---|---|---|---|---|---|---|---|---|---|---|---|---|---|---|---|
| LOADING | RIDGE | PLATE | R | P | $\sigma_o$ | $\sigma_n$ | $\Delta\sigma = \sigma_{n-1} - \sigma_n$ | $Cv_n = \frac{\Delta\sigma}{b}$ | $C\delta$ | $\frac{C_a \delta}{\cos \varphi}$ | m' | m" | $\frac{\Delta m"}{a}$ | R" | R' |
| | | | #/. | #/. | psi | psi | psi | lbs/in³ | lbs/in³ | lbs/in³ | #-'/. | #-"/. | #/. | #/. | #/. |
| BASIC LOADS | 0 | 1 | | -883 | -992 | -855 | -1573 | -2078 | 34·92 | $C = \frac{96E}{l^2}$ | | | | 47·8 | |
| | 1 | 2 | 781 | 1426 | 591 | +718 | 1283 | 917 | 16·40 | 18·52 | -953 | 0 | 47·8 | -111·8 | |
| | 2 | 3 | 463 | -1077 | -446 | -565 | -1070 | -765 | 14·90 | 858 | -154 | -478 | -64·0 | 128·0 | |
| | 3 | | 644 | | | +505 | | | | 1·50 / 858 | | +162 | | | |
| ADDITIONAL PARTICULAR LOADING "a" (a=-463) | 0 | 1 | | -113 | -103 | - 69·3 | - 93·3 | - 1·23 | 1·65 | $C = \frac{\lambda^2 E}{l^2}$ | | | | 3·37 | 103·37 |
| | 1 | 2 | 100 | - 70 | - 23·4 | + 28·0 | + 29·2 | ·208 | ·215 | 1·673 | - 7·38 | 0 | 3·37 | - 7·45 | -207·45 |
| | 2 | 3 | -200 | 0 | 0 | - 1·2 | - 1·8 | - ·013 | ·025 | ·222 | - 19·5 | -33·7 | - 4·08 | 8·16 | 208·16 |
| | 3 | | 200 | | | + ·6 | | | | | | + 7·1 | | | |
| ADDITIONAL PARTICULAR LOADING "b" (b=·157) | 0 | 1 | | | | - 5·0 | - 15·2 | - ·20 | ·29 | $C = \frac{\lambda^2 E}{l^2}$ | | | | ·26 | ·26 |
| | 1 | 2 | | 97·4 | 32·5 | + 10·2 | 8·6 | ·057 | -·074 | ·425 | - 18·7 | 0 | ·26 | ·30 | 100·30 |
| | 2 | 3 | 100 | 97·4 | 32·5 | + 1·6 | 18·7 | ·133 | -·259 | ·216 | - 19·0 | -2·6 | ·56 | -1·12 | -201·12 |
| | 3 | | -200 | | | - 17·1 | | | | | | -8·2 | | | |
| FINAL VALUES | 0 | 1 | | | | -826 | | | 34·24 | $C = \frac{96E}{l^2}$ | | 0 | | | |
| | 1 | 2 | | | | +707 | | | 16·29 | | | -463 | | | |
| | 2 | 3 | | | | -565 | | | 14·85 | | | +158 | | | |
| | 3 | | | | | +502 | | | | | | | | | |

d) Determination of Ridge Settlements

The maximum displacement $v_n$ at midspan of any plate in its own plane is given by

$$v_n = \frac{5}{48} \frac{\sigma_{n-1} - \sigma_n}{bE} l^2 = \frac{\Delta\sigma_n l^2}{9.6\, bE}$$

Setting

$$C = \frac{9.6\, E}{l^2} \quad ; \quad \Delta\sigma = \sigma_{n-1} - \sigma_n$$

we get

$$C\, v_n = \frac{\Delta\sigma_n}{b}$$

These values are tabulated in column 7 of Table II.

The vertical displacement of any ridge can be seen from Fig. A-5 to be:

$$\delta_n = v_n \frac{\cos\varphi_{n+1}}{\sin\gamma_n} - v_{n+1} \frac{\cos\varphi_n}{\sin\gamma_n}$$

which becomes with the notation of Table I, after multiplying both sides of the equation by C

$$C\delta_n = Cv_n \alpha_{n+1} - Cv_{n+1} \beta_n$$

The values of $C\delta_n$ are given in column 8 of Table II.

e) Slab Moment due to Ridge Settlements

The fixed-end slab moments due to vertical ridge settlements are for a slab whose far end is simply supported, as slab 2,

| 0 | | 1 | | 2 | | 3 | |
|---|---|---|---|---|---|---|---|
| 379·5 | | 560 | | 560 | | | PLATE AREA $in^2$ |
| 0 | $\frac{560}{379·5+560}$ = ·596 | ·404 | ·50 | ·50 | 0 | | DISTRIB. FACTOR |
| ← -½ | | ← -½ → | | -½ → | | | CARRY OVER FACTOR |
| -992 | +992 | +591 | -591 | -446 | +446 | | FREE EDGE STRESS $\sigma_o$ - psi |
| +120 ← | -239 | +162 → | - 81 | | | | |
| | | - 56 ← | +113 | -113 → | + 56 | | |
| + 16 ← | - 33 | + 23 → | - 12 | | | | |
| | | - 3 ← | + 6 | - 6 → | + 3 | | |
| + 1 ← | - 2 | + 1 | | | | | |
| -855 | +718 | | -565 | | +505 | | $\sigma_n$ - psi |

FIG. A-4

STRESS DISTRIBUTION

$$m'_{2-1} = -\frac{3EI}{b^2}\,\frac{\Delta\delta}{\cos\varphi} = -\frac{3Il^2}{9{\cdot}6\,b^2}\,\frac{C\Delta\delta}{\cos\varphi}$$

For a slab fixed at both ends, as slab 3, the fixed-end moment due to vertical ridge settlement is given by:

$$m'_{3-2} = -m'_{2-3} = -\frac{6Il^2}{9{\cdot}6\,b^2}\,\frac{C\Delta\delta}{\cos\varphi}$$

The values of $\frac{C\Delta\delta}{\cos\varphi}$ are tabulated in column 9 of Table II; their coefficients are in the present example

$$\frac{3Il^2}{9{\cdot}6\,b^2} = \frac{3\times\frac{4^3}{12}\times 60{\cdot}0^2}{9{\cdot}6\times 11{\cdot}66^2} = 44{\cdot}1\ \text{in}^3$$

and

$$\frac{6Il^2}{9{\cdot}6\,b^2} = 88{\cdot}2\ \text{in}^3$$

respectively. The fixed-end moments are given in column 10 of Table II, as for instance

$$m_{2-1} = -44.1\,\frac{18.52}{0.858} = -953\ \#$$

These moments must be distributed to get the final slab moments at each ridge due to settlement of it. The distribution is shown in Fig. A-6. The values of m", the final slab moments, are given in column 11 of Table II.

The reactions R" due to the moments m", resulting from ridge settlements, are obtained by:

$$R''_n = -\frac{\Delta m''_n}{a} + \frac{\Delta m''_{n+1}}{a}$$

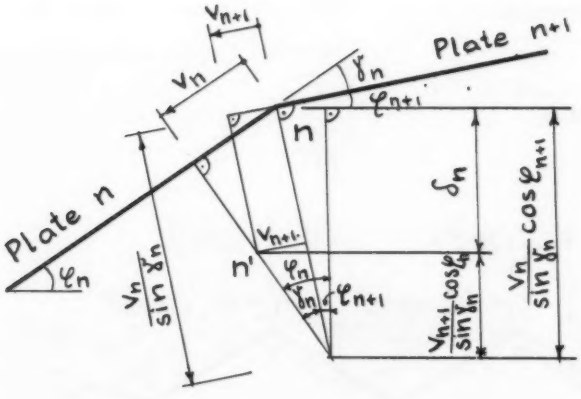


FIG. A-5

VERTICAL RIDGE DISPLACEMENT

| 0 | 1 | 2 | | 3 | |
|---|---|---|---|---|---|
| | | 3/7 | 4/7 | | K |
| | | -953 | +154 | -154 | FEM t-1/ |
| | | | -632 | +316 | |
| | | | -478 | +162 | m" - t-1/ |
| | -47·8 | +47·8 | +64·0 | -64·0 | -R" - t/ |

FIG. A-6

MOMENTS DUE TO RIDGE SETTLEMENTS

and are given in volumns 12 and 13 of Table II.

The values R" are the superfluous loads of the basic external loading; they will now have to be annulled by additional particular loadings.

f) Additional Particular Loading $m_a$ = 1000 #

This loading is shown in Fig. A-7; the variation of the load along the span of the folded plate is given by $m_a \sin \frac{nx}{l}$, which for all practical purposes may be considered as similar to the shape of the elastic line of the structure.

The procedure outlined above for the external loading is now repeated and all values are readily computed by aid of the Operation Table II and are tabulated there.

The moment for the sinusoidal loading is given by

$$M = \frac{P_n l^2}{\pi^2}$$

The deflection is given by

$$v_n = \frac{\Delta\sigma_n l^2}{\pi^2 b E}$$

so that for this loading

$$C = \frac{\pi^2 E}{l^2}$$

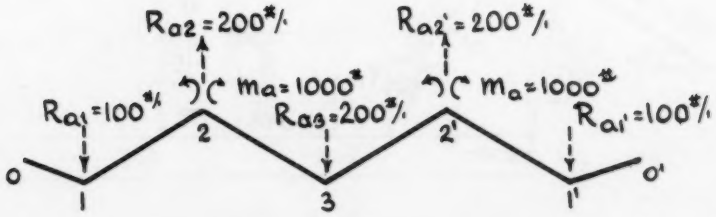


FIG. A-7

PARTICULAR LOADING "a"

The fixed-end moments due to ridge settlements are calculated as above and distributed; from their reactions the superfluous ridge loads $R''_a$ due to $m_a$ are obtained. This value of $R''_a$ added to the ridge load $R_a$ gives the total particular loading $R'_a$ due to the influence of $m_a$:

$$R'_{a1} = R_{a1} + R''_{a1} = 100.0 + 3.37 = 103.37 \ \#/'$$

The index 1 denotes the number of ridge at which this particular loading acts. The final values of the particular loading "a" are tabulated in the second section of Table II.

g) Additional Particular Loading $m_b = 1000$ #

The above outlined procedure is again repeated for the particular loading shown in Fig. A-8, and all values are tabulated in the third section of Table II.

h) Superposition of Particular Loadings

According to Eq. (13) we now get

$$\text{at ridge 2:} \quad -111.8 - 207.45a + 100.30b = 0$$

$$\text{at ridge 3:} \quad 128.0 + 208.16a - 201.12b = 0$$

The solution of these equations gives:

$$a = -0.463$$

$$b = +0.157$$

The final value of the stresses, moments and deflections are obtained by Eqs. (14) and are summarized in the bottom section of Table II. The ridge moment $m''$ at ridge 2, for instance, which is due to differential ridge settlements is thus obtained by:

$$m''_2 = m''_{2o} + a\, m''_{2a} + b\, m''_{2b}$$

$$m''_2 = -478 + (-0.463)(-33.7) + 0.157(-2.6) = -452 \ \#'/'$$

The settlement at ridge 1 becomes

$$c\delta_1 = 34.92 + \left[(-0.463)1.65 + 0.157 \times 0.29\right] \frac{9.6}{\pi^2} = 34.24 \ \#/\text{in}^3$$

where

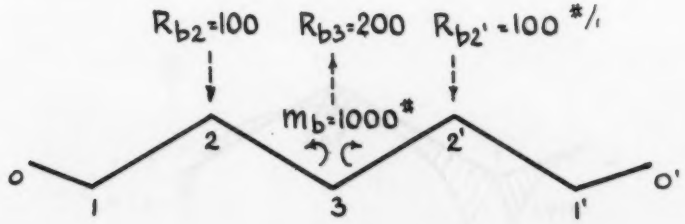


FIG. A-8

PARTICULAR LOADING "b"

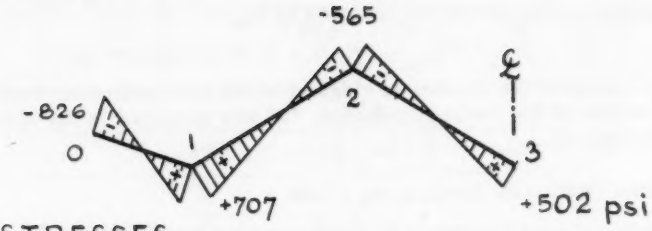


a. STRESSES

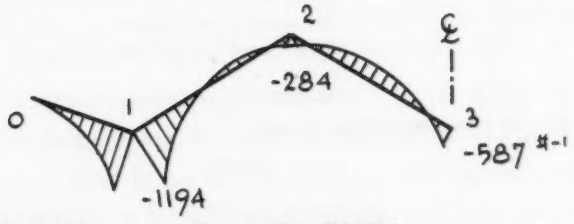


b. PRIMARY SLAB MOMENTS

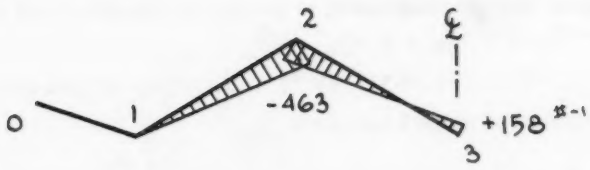


c. SLAB MOMENTS DUE TO SETTLEMENTS

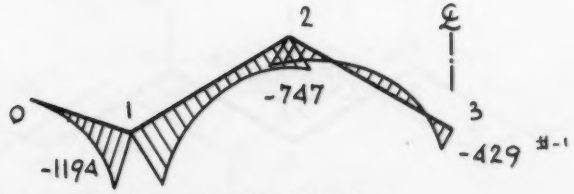


d. FINAL SLAB MOMENTS

FIG. A-9

$$C = \frac{9.6E}{l^2}$$

Assuming E = 1,000.000 psi, considering long time deflection due to sustained load, we get for the vertical deflection at ridge 1 $\delta$ = 1.85".

The final moments and stresses at the center of the folded plate structure are summarized in Fig. A-9. The results are, of course, identical to those obtained in Simpson's paper.(13)

Journal of the
STRUCTURAL DIVISION
Proceedings of the American Society of Civil Engineers

# ALPHA-GAMMA "HOT" CELLS FOR ENTRY BY PERSONNEL[a]

John M. Ruddy[1]

## ABSTRACT

The basic engineering definitions and the effect of the philosophy of maximum set-up and maintenance directly by people on design criteria is discussed for this type of "hot" cell. An example of this kind of cell is decribed in broad outline.

An Alpha-Gamma "Hot" Cell is a radiation shielded and contamination sealed enclosed space where large quantities of hazardous radioisotopes can be handled safely. The process or experimental manipulations within the cells are always done remotely but maintenance and equipment set-up is often partly done by men entering and working directly in the cells after most of the hazardous material has been remotely removed.

A reasonable definition of an Alpha-Gamma "Hot" Cell designed for a maximum of maintenance and equipment set-up directly (not remotely) by personnel might be as follows—although exact definitions in this field are difficult because of its newness and fluid state.

"An Alpha-Gamma Cell Complex designed for operation with a maximum of maintenance and set-up directly by people is one which uses only proven maintenance-free remote handling apparatus and which uses people in protective clothing for all other manipulation requirements".

Engineers responsible for the design of these integrated "Hot" Cell Complexes are interested in the fundamental factors affecting their safe operation for two main reasons. First, the degree of remote versus the planned direct maintenance in the cells affects their general arrangement and many appurtenant spaces; and second, the design creiteria for the main structure of the cells reflects these basically different methods of maintenance and set-up.

Note: Discussion open until March 1, 1960. To extend the closing date one month, a written request must be filed with the Executive Secretary, ASCE. Paper 2239 is part of the copyrighted Journal of the Structural Division, Proceedings of the American Society of Civil Engineers, Vol. 85, No. ST 8, October, 1959.

a. Presented at the May 1959 ASCE Convention in Cleveland, Ohio.

1. Chf. Engr., Architectural Planning Div., Brookhaven National Lab., Upton, Long Island, N.Y.

In present practice the primary design and layout responsibility for such a "Hot" Cell Complex will most likely fall to the lot of an engineer with either a civil-structural or with a mechanical background. In any event, both these branches of engineering will be substantially involved with each other as well as with electrical engineers and with nuclear specialists such as health-physicists. These circumstances emphasize the necessity for understanding and common technical language between the various branches of the professions.

The civil-structural engineer, because of his background and training in large and heavy construction in concrete and steel, is uniquely able to design, specify and build this type of facility. These "hot" cells, however, bear many resemblances to large machines and because of this there has to be a real and reasonably complete understanding between the mechanical and civil design engineers if a successful project is to result.

This means, among other things, that the structural design engineer must be able to understand and sensibly apply the usual mechanical commercial tolerances to any surfaces or access holes on to or into which mechanical items must mount. For example, in a 3 or 4 foot shielding wall, it is usually economically impossible to hold sleeves closer than 1/16" as to location or bore in standard construction practice and, in addition, the squareness of these holes to a mounting surface can deviate by several degrees. Therefore, if the mechanical alignment and fit tolerance requirements of the mechanisms to be mounted or inserted are more stringent than those obtainable in ordinary construction, it would seem advisable to use a rough sleeve into which a second more accurately aligned sleeve is set after the heavy work is done. The space between the rough and finished sleeve can be filled with lead wool or some other shielding material. On the other hand, the mechanical design engineer cannot realistically (and economically) expect machine-like accuracy in heavy construction which in the last analysis is built by contractors—usually on a lump sum price basis—with laborers, iron workers and similar rough and ready trades people.

There is an effect of the type of cell usuage; that is—pilot-model, research and development or fundamental research—on the design as it relates to the maximum use of personnel for set-up and maintenance. The "Hot" Cells for fundamental research because of extraordinary variations in their uses are probably best suited to the philosphy of maximum personnel maintenance and set-up. As the operations in a "Hot" Cell become more repetitive over longer periods of time, as for example, thru the research and development, the pilot-model to the production "Hot" Cells then does the swing to less set-up and maintenance by people become more attractive, except that production cells may not be able to economically tolerate remote handling equipment breakdowns. The final decision as to how far to go in replaceing direct maintenance with remote manipulations depends on the designer's evaluation of these three main variables: 1) the proven dependability of the remote handling equipment considered; 2) the danger of contamination to personnel working in the cells; and 3) the effect on the overall operation of the failure of either of the above two maintenance and set-up methods.

A description of a recently completed "Hot" Cell for metallurgical engineering research can serve as an example of a cell complex for the acquirement of fundamental knowledge and for use in early research and development. A general location of the "Hot" Cell Complex for metallurgical research is shown in Fig. 1 where the "Hot" Cell is in the semi-works area

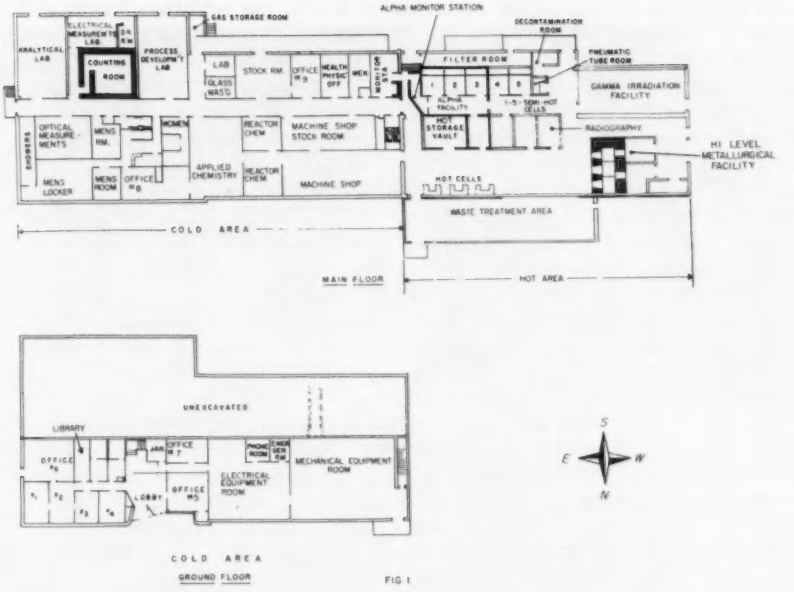


FIG 1

at the west end of the existing Hot Laboratory. A large roll-up door adjoins the yard and provides for efficient use of available space for access and permits handling large irradiated pieces. The cell cross-section and plan is shown in Fig. 2. This cell is designed to handle radioactive material emitting approximately 1,000,000 roentgens per hour of uranium fission products or its equivalent.

There are two items about this layout which are examples of important design criteria. The first is the limitation of "contamination". This is done by subdividing the cell into smaller sections. The second is the step-wise reduction of the degree of contamination. This is done by having separate

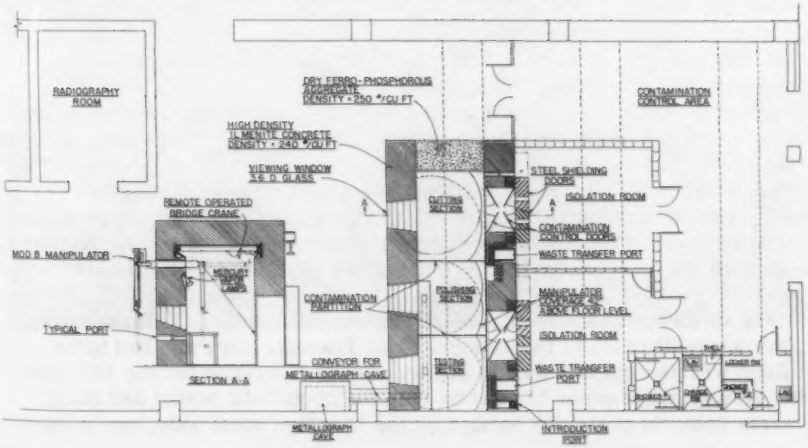


FIG 2

spaces in series for the Alpha containment doors, the isolation rooms and the containment control area between the "Hot" Cells and the "clean" operating area in front of the cell at the manipulators.

The inside dimensions of the cell are 24 feet along the operating face, 7 feet deep and 12 feet high. The front and rear walls are of poured ilmenite aggregate concrete 3 feet thick with a density of 240+ lbs per cubic foot. The ceiling is of the same material 2-1/2 feet thick. The end wall inside the room is a steel container 3 feet out to out and filled with specially graded dry ferrophosphorus fines with a density of 250+ lbs per cubic foot. This wall, shown in Photo A, can be removed if an extension to the cell is needed in the future, and in addition, changes to the cell access can be made in it after temporarily removing the dry ferrophosphorus.

Steel work was prefabricated off-site. Unit sections were built with manipulator ports, window-liners and shielding plug liners in place. The sections were assembled and welded on-site and then the walls poured in the usual way but in batches with ilmenite concrete. Some details can be seen in Photos B and C. The ceiling and roof sections were also prefabricated with access plug liners in place. These were then erected, welded and poured with ilmenite concrete. After completion of the cell proper, the isolation and shower rooms were built using non-shielding concrete blocks. The ceilings of the isolation rooms are made of removable concrete slabs in the area directly in front of the Hot Cell doors. This allows the building overhead bridge crane to be used in the isolation rooms. All surfaces are made decontaminable by keeping them reasonably smooth and coating them with vinyl or expoxy paints. The "Hot" Cell floor is a large stainless steel pan, welded in place.

Three (3) lead glass viewing windows are installed in the operating face of the "Hot" Cell, one for each section. These are oil-filled windows with a shielding value equal to the 240 lb per cubic foot concrete walls. The installation of one of these windows is shown on Photo D.

The gamma ray shielding "Hot" Cell access doors are horizontally biparting and are of steel 16 inches thick and 8 feet high. They weigh approximately 20 tons per set (2 each). They hang from an I-beam on wheeled carriages and a gear and chain arrangement is provided for manual operation. They overlap the opening and no effort is made to seal the edges. The contamination (alpha and other isotope) containment doors which seal the entrance from the cell to the isolation room consists of two sets of gasketed hollow metal doors with built-in windows.

Illumination in the cell is provided by 400 watt color improved mercury vapor lamps, each independently circuited. Four of these lamps are recessed into the shielding wall above each viewing window. Each lamp is fitted with a quick disconnect fitting, requiring only one quarter turn, to facilitate removal by remote handling equipment. 150 watt incandescent lamps provide illumination when personnel are required to work inside. These lamps will also be used for emergency light in case of failure of the mercury vapor lights.

The introduction ports for the entrance of hot samples, filters, tools, etc., are a modification of the Argonne Tool Transfer Lock and had to be built flush with the outside wall in order to leave clearance for the 16" steel doors. A disposable wiper is used to keep the ports both sealed and clean. The waste removal ports are located on the isolation room side, one in each

Figure A

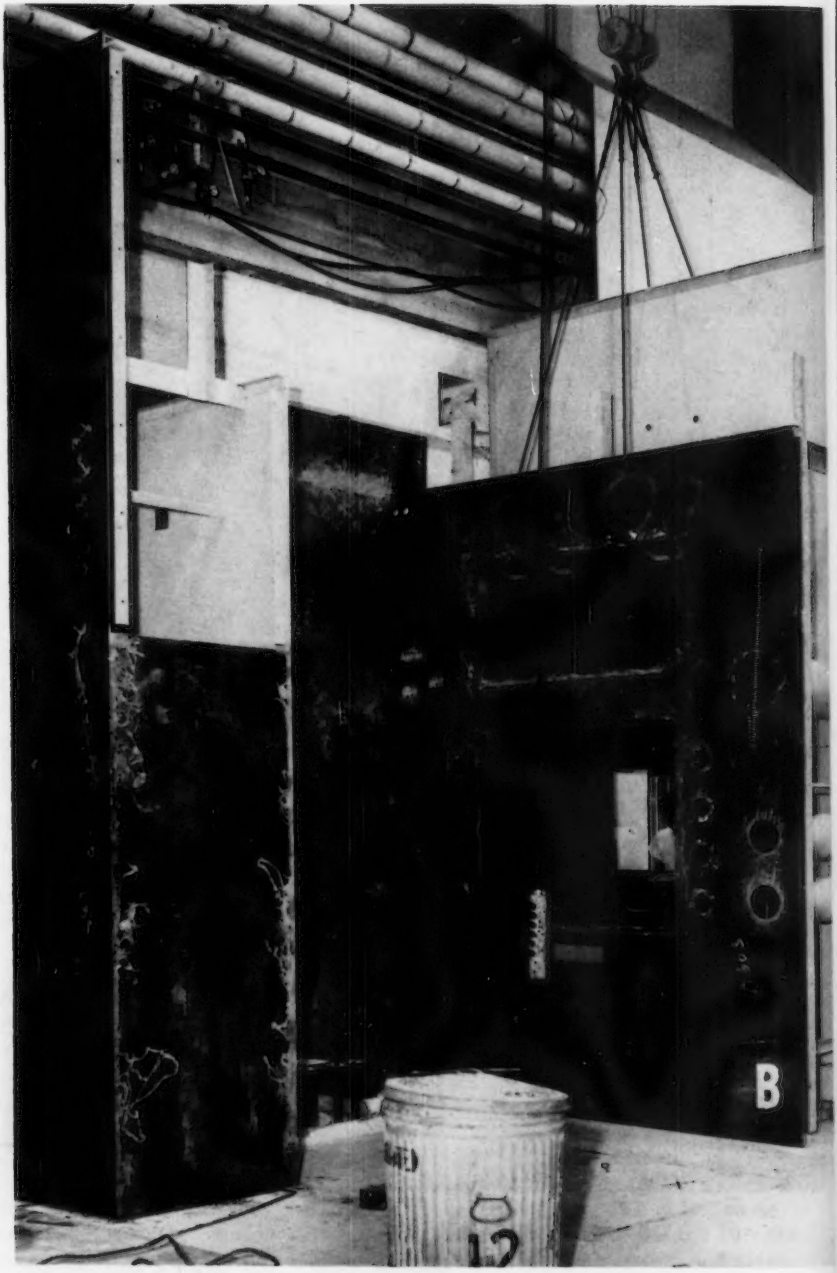


Figure B

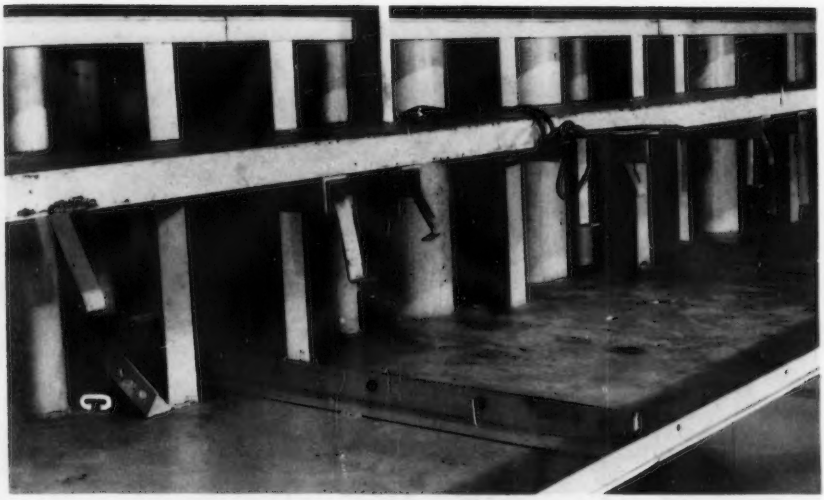

Figure C

room, and are standard weight 14" steel pipe mounted in the cell wall. Shielding is provided by a remotely operated sliding lead door 10" thick. The isolation room end of the port is recessed to leave clearance for the gamma doors, and is machined for two "O" rings.

A shielded waste carrier designed to operate with these waste ports will have a built-in scoop to push the waste can into the cell and withdraw the loaded can into the carrier. The waste can will have a length of 10 mil polyvinyl chloride tubing attached to it. The other end of the tubing will be fastened by means of an "O" ring to the outside end of the waste port. The tube is thus sealed at both ends to serve as a contamination barrier. When the inside shielding door is opened, the waste carrier acts as a shielding door during the withdrawal of the "hot" waste can. After withdrawal the carrier shielding doors are closed on the bag, the carrier is pulled back and a portable commercial heat sealer is used to cut and seal the bag. To introduce a new can, a new bag is slipped over the sealed remnant of the old bag which is removed with a next load as "hot" waste. An effective particle-tight contamination seal is thus maintained at all times.

A pair of Argonne Model 8 manipulators will be mounted above each of the three viewing windows. Each arm will be protected by the latest Argonne designed boot which can be changed without entering the cell. Four of the six arms will have lateral rotation of the slave arm relative to the master arm. Semi-automatic control of angular separation indexing is standard on all six arms. Lead shielding in each arm at the wall liners is equivalent to the "hot" cell wall shielding.

An auxiliary arm mounted on a commercial type boom will be used in the cutting section because of the limited lifting capacity of the Model 8 manipulators. It is operated from a small console by a "joystick" control.

The one-ton, two-speed electric remotely operated crane is bridge-type and will service the cutting section where the heaviest work load is anticipated. It is capable of operating speeds of between 6 inches and 5 feet per minute. It can travel to the other two sections by removal of the upper part of the contamination barrier partitions which divide the cell into three subsections.


Figure D

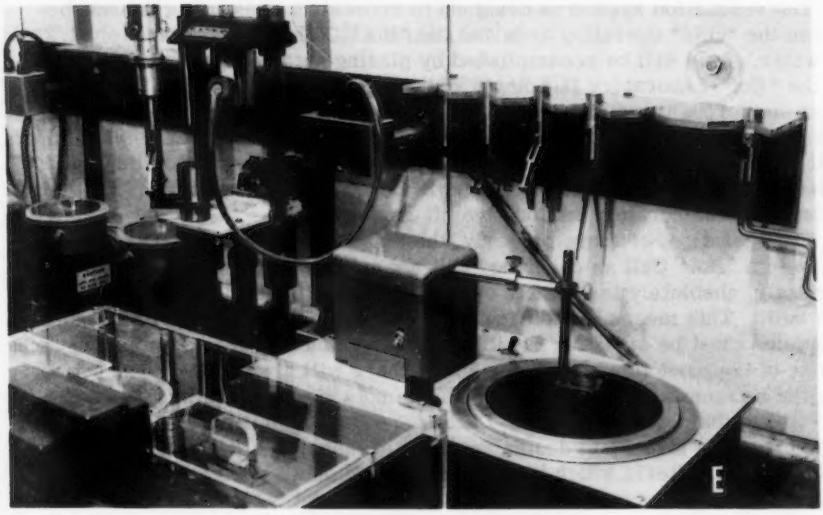

Figure E

The polishing and testing sections will have commercial lift hoists installed on booms to aid the Model 8 manipulators. The booms in all three sections are of the same type in order to allow the hoists or the auxiliary arm to be interchanged if required. A mock-up of some of the remote operated experimental equipment is shown on Photo E.

Minor maintenance and preparations for entry into the cell will be accomplished remotely by means of the Model 8 manipulators and an auxiliary arm. Personnel will use one-piece plastic protective suits. This suit features a separate face mask inside the suit with its own air-demand regulator. This will maintain respiratory protection for the wearer in case of physical damage to the protective suit. The mask is modified to accept a microphone and headset, which can be plugged into the intercom system.

Personnel, properly suited, enter the isolation rooms through gasketed doors at the personnel change room and the door thru the partition between isolation rooms. The activity level in the cell is made as low as possible by removing or storing "hot" material. Modified Electro-Lux vacuum cleaners remotely operated by the manipulators will remove loose contamination. Access to the "Hot" Cell proper is through the gamma shielding doors and the set of gasketed alpha barrier doors. All rooms are fitted with intercom jacks so that personnel can maintain communication at all times.

On leaving the isolation room, personnel use the contaminated shower (No. 1) to remove loose contamination from the suit and a thorough scrub down is done prior to removal of the suit from the person. After removal of the suit, it is surveyed for contamination and hung up in the change room. Personnel then clean up themselves in the clean shower room (No. 2) under a health-physicist's surveillance. The general area of the "Hot" Cell Complex will be under continual health-physics supervision. The "Hot" Cell and isolation rooms will be instrumented to relay general radiation level readings to the operating face of the cell which is in the "cold" area.

The ventilation system is designed to maintain a pressure gradient, between the "cold" operating area and the "Hot" Cells, of approximately 1/2" of water. This will be accomplished by placing automatic sensing devices in the "Hot" Laboratory Building's radioactive off-gas system. Disposable first stage roughing filters in the cell are designed to be introduced through the introduction ports and installed by the Model 8 manipulators. Used filters will be removed through the waste disposal port. Contamination that passes through these roughing filters will be removed by absolute filters in the existing "Hot" Laboratory radioactive off-gas system.

The operation, or more properly, the experimental manipulations that will go on in a "Hot" Cell as described will not only be manifold but more importantly, absolutely impossible of complete specification even after the cells are built. This means that during the planning work the maximum economical provision must be made for flexibility in use. Since in general a human being is one of the most flexibile of machines, there will always be a tendency to use the maximum of people rather than remote control manipulation for set-up and maintenance in "Hot" Cells requiring flexibility. The primary meaning to the structural design engineer of these considerations is that all of the design criteria which he sets up prior to detail design requires that his layout and construction should take into account both the flexibility and limitations of both personnel and remote equipment.

In conclusion, it may be said that the effect on structural design criteria for "Hot" Cells using the philosophy of a maximum of set-up and maintenance by people depends on the design engineer's opinion as to the proven reliability of remote-handling equipment versus the contamination exposure of personnel in the cells as it affects their safety. In general, cells using only proven remote-handling equipment with the operators doing all else results at this time in the simplest layouts and structure because of the smaller amount of mechanical and electrical machinery.

Since the continued development and improvement of remote-handling equipment is unquestionably to be expected, it obviously sets the trend. This trend by definition will tend to draw the now divergent philosophies of operation and design more closely together and will in time possibly eliminate them. It seems reasonable then to say that only proven remote handling equipment should be used on "Hot" Cells used for fundamental research and possibly for production which means that these types would use the maximum of people for the remainder of the work which has to be done inside the cells. This leaves the research-development and pilot-model cells for the field work in the development and research required to perfect the more sophisticated remote handling machinery which might well require less personnel "in-cell" set-up and maintenance in the future.

Journal of the

STRUCTURAL DIVISION

Proceedings of the American Society of Civil Engineers

CONTENTS

DISCUSSION

Page

Design of Long Reinforced Concrete Columns, by B. Broms and I. M. Viest. (Proc. Paper 1694, July, 1958. Prior discussion: 1952. Discussion closed.)
by J. G. MacGregor and C. P. Seiss. . . . . 137

Generalization of the Successive Approximation Method, by Panagiotis D. Moliotis. (Proc. Paper 1816, October, 1958. Prior discussion: 2043. Discussion closed.)
by Panagiotis D. Moliotis (closure) . . . . . 139

Equivalent Systems for the Deflection of Variable Stiffness Members, by D. G. Fertis and E. C. Zobel. (Proc. Paper 1820, October, 1958. Prior discussion: 2043. Discussion closed.)
by D. G. Fertis and E. C. Zobel (closure). . . . . 141

Design of Pier Bent and Rigid Frame by a Computer, by Charles P. C. Tung. (Proc. Paper 1854, November, 1958. Prior discussion: 1952, 2043. Discussion closed.)
by Charles P. C. Tung (closure) . . . . . 143

Biaxially Loaded Reinforced Concrete Columns, by Kuang-Han Chu and Algis Pabarcius. (Proc. Paper 1865, December, 1958. Prior discussion: 1988, 2075. Discussion closed.)
by Kuang-Han Chu and Algis Pabarcius (closure). . . . . 145

Shear Strength of Reinforced Concrete Beams, by Sidney Guralnick. (Proc. Paper 1909, January, 1959. Prior discussion: 2009, 2075. Discussion closed.)
by Sidney A. Guralnick (closure). . . . . 149

(Over)

Note: Paper 2237 is part of the copyrighted Journal of the Structural Division, Proceedings of the American Society of Civil Engineers, Vol. 85, ST 8, October, 1959.

Page

Strength of Rivets and Bolts in Tension, by Munse, Petersen and Chesson. (Proc. Paper 1970, March, 1959. Prior discussion: none. Discussion closed.)
by W. R. Penman and E. F. Ball . . . . . 157

Short Flexible Suspension Bridges for Heavy Trucks, by Sven Olof Asplund. (Proc. Paper 2004, April, 1959. Prior discussion: none. Discussion open.)
by A. A. Eremin. . . . . 159

Analysis of a Two-Column Symmetrical Bents, B. R. Cooke. (Proc. Paper 2037, May, 1959. Prior discussion: none. Discussion open.)
by O. A. Glogau . . . . . 161
by M. L. Pei . . . . . 161
by Michael Jordan . . . . . 162

# DESIGN OF LONG REINFORCED CONCRETE COLUMNS[a]

## Corrections to Discussion by J. G. MacGregor and C. P. Seiss

CORRECTIONS—In Proc. Paper 1952 in the February Journal of the Structural Division, on p. 200 in line 10, please change " . . . equal to 103, 106, and 110 percent, . ." to ". . . equal to 110, 106, and 103 percent, . ."

On p. 203, in line 2 of section 4(b), please change the words "the length effect" to "the effect of sustained high loads."

a. Proc. Paper 1694, July, 1958, by B. Broms and I. M. Viest

# GENERALIZATION OF THE SUCCESSIVE APPROXIMATION METHOD[a]

## Closure by Panagiotis D. Moliotis

PANAGIOTIS D. MOLIOTIS,[1] F. ASCE.—Mr. Perng-FeiGou gives a different way of calculating distribution and carry-over factors using the slope-deflection equations. The calculation of these factors by this well known slope deflection equations is also very interesting.

In the subject paper, in calculating distribution and carry-over factors, an identical route was followed to that used in the classical case of calculating these factors in framed structures with point joints and not small undeformed areas.

It was considered more advisable to follow this route because we are of the opinion that the reader will find it easier to follow a similar method for calculating the distribution and carry-over factors to that used in the classical case.

The whole study aimed in calculating framed structures, whose joints are not points but small undeformed areas, by the method of successive approximations which is used by designers.

a. Proc. Paper 1816, October, 1958, by Panagiotis D. Moliotis.
1. Dr. Civ. Eng., Athens, Greece.

# EQUIVALENT SYSTEMS FOR THE DEFLECTION OF VARIABLE STIFFNESS MEMBERS[a]

Closure by D. G. Fertis and E. C. Zobel

D. G. FERTIS and E. C. ZOBEL[1].—The authors wish to thank Mr. Perng-Fei Gou for his discussion of their article on the exact and approximate methods of equivalent systems for the deflection of variable stiffness members. The authors agree that the steps as outlined by Mr. Perng-Fei Gou, culminating in the equivalent moment diagram, are adequate for the determination of the deflection of a point on the system and that for this deflection, the steps utilizing the equivalent shear diagram and the equivalent beam, may be omitted. However, the authors have found it desirable to utilize the equivalent system for the following reasons:

1) Physical clarification of the problem.

2) Any method may be used to determine the deflection of a point, or, for that matter, the equation of the elastic curve.

3) The equivalent system greatly simplifies the approach to statically indeterminate problems.

4) A moment diagram, constructed by parts, utilizing the loads on the equivalent beam is adaptable for rapid calculation of deflections.

5) The equivalent system may be used as a research tool. For example, the authors have effectively utilized the concept of the equivalent system to solve the natural frequencies of vibration of complex structures. The results of this research have led to a greatly simplified dynamic model.

The authors have found that, in general, the error for deflection calculations using the approximate method of equivalent systems, for a minimum number of concentrated loads, is less than one percent. As a point of interest, the equivalent system has negligible error when applied to vibration studies.

a. Proc. Paper 1820, October, 1958, by D. G. Fertis and E. C. Zobel.
1. Assistant Profs. of Eng. Mechanics, Wayne State Univ., Detroit, Mich.

# DESIGN OF PIER BENT AND RIGID FRAME BY A COMPUTER[a]

## Closure by Charles P. C. Tung

CHARLES P. C. TUNG,[1] M. ASCE.—In answer to the comments of Messrs. Berg and Hoffman concerning the choice of the best method of computation for the computer, the author wishes to quote his statement in full from his original paper:

> "It is generally true for any problem that the best method for manual computation is also the best method for automatic computation. The reason is quite simple. Automatic computation requires initial programming of the problem, and the initial programming is nothing but a form of manual computation in great detail. Adopting the best method for manual computation will make the programming of the particular problem considerably easier."

The author is interested in keeping the programming time of any problem to a minimum. This is a matter of simple economics and, incidentally, also a matter of vital concern to a private engineering firm utilizing electronic computation. As long as a method of computation can achieve the required objective, sophistication or elegance in mathematics should not influence the choice of the method. In the author's opinion, the method using the minimum amount of programming time in the solution of any problem is the best method of computation for the computer.

Most digital computer of medium scale class are basically built for fixed-point operations. For the solution of a system of linear simultaneous equations, floating-point operations are necessary. One of the best methods for the solution of these equations is by means of matrix inversion and matrix-vector multiplication. In general, the floating-point and matrix subroutines are developed and supplied by the computer manufacturers. Relatively, their development is too vast a project to be undertaken by any private engineering firm. In the case of the LGP-30, the manufacturer's floating-point and matrix subroutines consist of approximately 1800 commands. In the author's original program, still using the fixed-point operations, the solution of joint moments is achieved by the use of a moment-distribution subroutine which consists of approximately 300 commands. Should the method of slope deflection be chosen for the solution of joint moments, the 1800-command floating-point and matrix subroutines would have to be incorporated into the program and would occupy a major portion of the memory unit of the computer, thus drastically limiting the capability of a comprehensive program. Again, as Mr. Hoffman pointed out, the slope deflection method would further require a secondary solution

a. Proc. Paper 1854, November, 1958, by Charles P. C. Tung.
1. Super. Engr., King & Gavaris, New York, N. Y.

in order to obtain the joint moments. It is true that computers can solve difficult problems by difficult ways in minutes or even seconds. Nevertheless, one does not have to choose the difficult way to solve a problem just as a challenge to the computer.

Just as a point of information, at the time when the author's original program was written, the LGP-30 manufacturer had not completed the development of the floating-point and matrix subroutines. Now, again, it is a matter of pure simple economics. One does not sit down and tackle the 1800-command subroutines, when one can find a much easier way out with a 300-command subroutine. At least a private consulting engineer cannot afford to. The author finds it extremely difficult to visualize Mr. Berg's metaphor of the method of slope deflection and simultaneous equations as riding over a bridge, and method of moment distribution as riding in a ferry boat. According to the extent of programming required in the two methods, Mr. Berg's picturesque comparisons would seem more appropriate if they were exactly reversed.

Except for the fact that solution of simultaneous equations is required, Mr. Hoffman's method of conjugate beam definitely has its merits. As a matter of fact, the author has used the conjugate beam principle together with Newmark's numerical procedure[1] in a completed program for the solution of stiffnesses, carry-over factors, fixed-end moments, and deflections for members of variable moment of inertia. This program, as mentioned in the author's original paper, was an extension to the design programs of pier bent, rigid frame, and continuous beams.

## REFERENCE

1. "Numerical Procedure for Computing Deflections, Moments and Buckling Loads," by N. M Newmark, Transactions, ASCE, Vol. 108. 1943, pp 1161-1234.

# BIAXIALLY LOADED REINFORCED CONCRETE COLUMNS[a]

## Closure by Kuang-Han Chu and Algis Pabarcius

KUANG-HAN CHU,[1] F. ASCE and ALGIS PABARCIUS,[2] A.M. ASCE.—The authors would like to thank Dr. Au and Mr. Pannell for their discussions. Mr. Pannell's method is very interesting and it is hoped that this method would be treated more fully in a separate paper.

As Dr. Au has rightly pointed out, the main contributions of the authors are (i) to present a thorough analysis of the stress-strain distribution in the inelastic range so that it could be applied to column sections of various shapes and (ii) to clarify the basic criteria of failure of such members. It appears that precisely on these points Mr. Pannell does not agree. Mr. Pannell states: "Since the force of the stress block in bending and compression cannot be defined with any accuracy — and indeed it is difficult to see that it ever be so defined, for stresses are not measurable quantities — then no accurate determination of stress can be obtained from the measured strain." It is true that stresses are not precisely measurable and the stress distribution cannot be defined with accuracy. However, there lies the paradox, the ultimate strain (say 0.003) alone cannot be used to predict the failure load (including moment) by theoretical analysis, unless the stress-strain relationship is known, no matter whether this relationship is real or assumed.

The real trouble in using Whitney's stress block (as Messrs. Pannell, Au and others did) is that this stress block does not represent stress strain relationship. Whitney's block can be related to ultimate strain only when certain empirical coefficients have been determined.

To illustrate the above statements, let us first trace the development of Whitney's stress block for the case of a rectangular section subjected to uniaxial bending. Assume that the stress-strain relationship is trapezoidal. The coefficients $k_1$, $k_2$, $k_u$ as defined in the ASCE-ACI report are as shown in Fig. 1. It has been shown in the report that $k_2/k_1 \approx 0.5$ (almost independent of $\epsilon_u$) and $k_1 = 1 - (0.425f'_c/E_c\epsilon_u)$. Therefore, for $E_c = 1000\, f'_c$ and $\epsilon_u = 0.003$, $= 0.003$, we may use a Whitney's block with $k_1 = 0.858$ (see Fig. 2). However, if $\epsilon_u \neq 0.003$ or if the actual strain $\epsilon < \epsilon_u$ then $k_1 \neq 0.858$. Also note that if the distribution is parabolic than $k_2/k_1 = 0.554$ and $k_1 = 0.78$. It can be seen that the values of $k_1$, $k_2$ depends quite a bit on the stress-strain relationship.

Now consider the case of a circular section. Let us try to replace the trapezoidal stress distribution with a Whitney's stress block of constant

a. Proc. Paper 1865, December, 1958, by Kuang-Han Chu and Algis Pabarcius.
1. Associate Prof. Civ. Eng. Dept., Illinois Inst. of Technology, Chicago, Ill.
2. Instr., Civ. Eng. Dept., Univ. of Illinois, Chicago Div., Chicago, Ill.

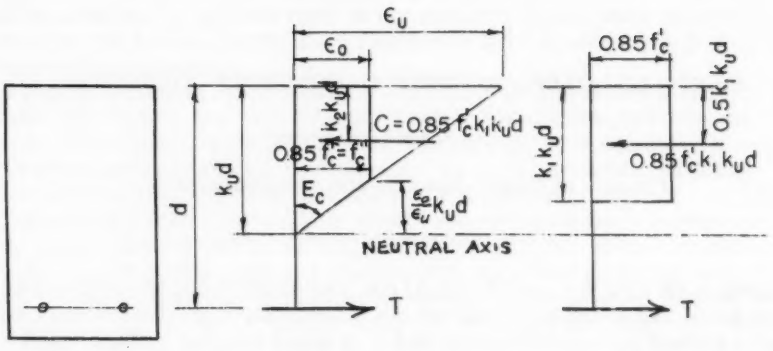


Fig. 1. Trapezoidal Distribution

Fig. 2. Whitney's Stress Block

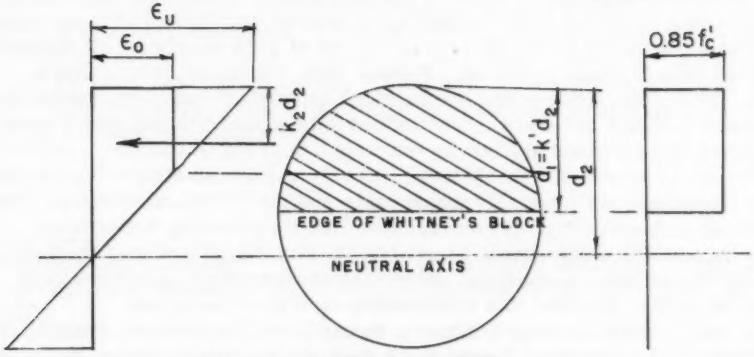


Fig. 3. Circular Sections
Trapezoidal Distribution and Whitney's Block

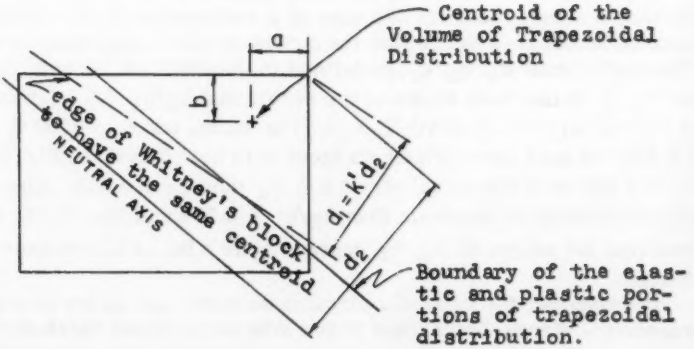


Fig.4. Rectangular Section Subjected to Biaxial Bending.

height (= 0.85 $f'_c$). If $E_c$ = 1000 $f'_c$ and $\epsilon_u$ = 0.003 then obviously (see Fig. 3) ($k' = d_1/d_2$) < ($k_1$ = 0.858) because the part of the volume of the trapezoidal stress distribution contributed by the elastic portion of the distribution in the circular section is more than the corresponding part in the rectangular section. The coefficient $k_2$ which indicates the location of the resultant of the compressive stress of trapezoidal distribution is no longer equal to 0.5 $k_1$ nor does it necessarily correspond to the centroid of the area occupied by the Whitney's block. Therefore in computing the ultimate load for circular sections, many simplifying assumptions were made by Whitney and Hogenstad.(3,4,7)*

A similar difficulty exists in using the Whitney's block for rectangular sections subjected to biaxial bending (see Fig. 4). For example if the stress distribution is trapezoidal, in order to use Au's method with confidence, it is necessary to investigate the following assumptions: (i) If the trapezoidal distribution is to be replaced by a Whitney's block with the same centroid, then their volume would be approximately equal. (ii) The edge of the equivalent Whitney's block would be parallel to the neutral axis. (iii) The coefficient $k' = d_1/d_2$ (see Fig. 4) would be approximately equal to $k_1$ which is derived for uniaxial bending. Special attention should be paid to this assumption (iii) because it relates the Whitney's stress block (as represented by the distance $d_1$) and the ultimate strain (reached in a distance $d_2$). Fortunately as shown by the authors** that with the exception of assumption (ii) in certain cases, the above assumptions are fairly good.

It would be very interesting to learn how Mr. Pannell has related the Whitney's stress block with the ultimate strain. In the author's opinion, this relationship should not be assumed but should be established by certain stress-strain relationships. The author's strongly believe that in order to use the ultimate strain as criteria for failure, either the stress-strain relationship of concrete in compression must be ascertained, or the range of variation of such coefficients as k', $k_1$, $k_2$ etc. must be carefully examined.

*Reference number given in the original article, Proc. Paper 1865.

**Discussion of T. Au's paper, "Ultimate Strength Design of Rectangular Concrete Members Subjected to Unsymmetrical Bending" by Kuang-Han Chu and A. Pabarcius, Journal of the American Concrete Institute, Sept. 1958 p. 1253.

# SHEAR STRENGTH OF REINFORCED CONCRETE BEAMS[a]

## Closure by Sidney A. Guralnick

SIDNEY A. GURALNICK,[1] A.M. ASCE.—The author would like to take this opportunity to thank Messrs. Chu, Warner, Cowan, Goschy and Balazas for the time and effort they have expended in writing discussions of his paper. The comments made in these discussions certainly form a significant contribution to the value of the paper.

Dr. Chu has raised three questions of considerable importance and an attempt to answer them follows.

The first question asked was: "Why is $v'_c$ used to predict the occurrence of the first diagonal tension crack?" In answer to this, although failure in "pure shear" in plain concrete is almost always observed as a "diagonal-tension" rupture, it is correct to use the maximum shear stress, $v'_c$, which corresponds to the failure state of stress to describe same (since $v'_c$ is simply the radius of the pure shear stress circle at failure). As has been stated by Bijlaard(3) and others, the radius of the "pure shear" stress circle must be equal in magnitude to the diameter of the "pure tension" stress circle in plain concrete. However, if a straight-line approximation of the Mohr envelope is adopted, the magnitude of the maximum shear stress at failure for an element subjected to a pure shear state of stress is given by a geometrically-derived relationship which is the author's Eq. 13. The magnitude of $v'_c$ given by this equation is always less than the magnitude of the pure tensile strength, $f'_t$, and Eq. 13 therefore represents a conservative estimate of the pure shear strength of plain concrete (as was demonstrated in Section IV of the paper.)

The second question concerns the author's use of average stresses. The average normal and shear stresses were used in the author's derivations simply because it is impossible at the present state of knowledge to predict the "exact" stresses in the compression zone of the beam after flexural tension and diagonal-tension cracking have occurred. Consequently, recourse was had to the average stresses even though it was recognized that Mohr's circle properly refers to the state of stress at a point. Since in most cases the normal and shear stress distributions are convex outward, there is probably not a great deal of difference between the average and the maximum stress. Furthermore, it is quite likely that the maximum normal stress will occur at a level other than that at which the maximum shear stress occurs. Therefore, the location within the compression zone at which the combination

a. Proc. Paper 1909, January, 1959, by Sidney A. Guralnick.

1. Assistant Prof., Civil Engr. Dept., Illinois Inst. of Technology, Chicago, Ill.

of normal stress and shear stress is such as to cause failure will very probably be one at which either one or both of the stress components are lower than their respective maximum values. Thus the inexactitude inherent in using the average stresses is probably quite low.

The third question raised concerned the applicability of the author's theories to the case of a beam section subjected to a partly elastic and partly inelastic stress distribution. Or, in other words, is the theory applicable if the maximum compressive stress at failure is expected to be somewhere in the range between fifty and one hundred percent of $f'_c$? The author believes that his theory is applicable in such cases if one can correctly compute the quantity $k_u$. As was pointed out by Mr. Warner, it is necessary to use a compatibility condition to obtain an analytical expression for $k_u$. Unfortunately, an explicit compatibility condition to be used in predicting shear strength is yet to be definitively established. If and when such a compatibility relation is established, it can easily be incorporated into the author's theory. In view of the present lack of an explicit compatibility relation, one must somehow estimate $k_u$ when it is expected that the compressive stress at failure will lie in the range between fifty and one hundred percent of $f'_c$. One way to estimate $k_u$ for this case is to assume that the stress in the tension steel is at the yield point and $k_u$ is given by the well-known equation from flexural strength analysis

$$k_u = \frac{1}{k_1 k_3} \cdot \frac{p f_y}{f'_c}$$

in which $k_1$ and $k_3$ are given by Eq. 19. The minimum, and therefore the most conservative value for $k_u$ will result if one uses this procedure. In reviewing the "restrained" beams given in Table-1, the author used a slightly different approach in computing $k_u$. Since large amounts of compression reinforcement were present in all the restrained beams, the most conservative estimate of $k_u$ resulted if one used the following equation to compute $k_u$:

$$k_u = \frac{\epsilon_u}{\epsilon_u + \epsilon_y}$$

in which $\epsilon_y$ is the yield strain of the tensile reinforcement and $\epsilon_u$ is the ultimate compression strain for plain concrete. The value of $\epsilon_u$ was obtained from the equation given by Hognestad, Hanson, and McHenry(11) as:

$$\epsilon_u = 0.004 - \frac{f'_c}{6.5 \times 10^6}$$

The author fully agrees with Mr. Warner that further theoretical and experimental studies are needed in regard to the problem of formulating a rational compatibility condition for shear failure. Furthermore he is acutely aware of the pressing need for studies of the behavior of beams loaded through side stubs since these more closely represent the conditions to be found in actual cast-in-situ structures than do the typical top-surface-loaded laboratory test specimen.

The constructive evaluation of the author's work by Professor Cowan is most appreciated. It is very gratifying that Professor Cowan finds so many

areas of agreement with the author's arguments. The one area of apparent disagreement concerning failure criteria is more one of semantics than one of physical principle. Professor Cowan argues that if the tensile and compressive strength of concrete are two separate physical constants of the material, then two separate failure criteria must be used. In the author's opinion, this is just another way of stating that at least two physical constants are necessary to completely specify the envelope of circles representing failure states of stress (i.e. the "rupture envelope" or "intrinsic curve") and, in the case of plain concrete, these physical constants are the tensile and the compressive strengths. Professor Cowan's dual failure criterion differs from the author's failure criterion only in the details concerning the method of specifying the exact shape of the rupture envelope. Results obtained from either approach should be comparable.

It is unfortunate that Professor Cowan misinterpreted the author's Fig. 7 thus leading him to conclude there was a great physical difference between his and the author's failure criteria. Fig. 7 was deliberately not drawn to scale since its sole purpose was to illustrate the various geometrical quantities and relations used in the development of Eq. 14a. No single fixed value of the angle $\theta$ was used in the author's work (as erroneously assumed by Professor Cowan.) The angle $\theta$ was treated as a perfectly general quantity whose functional relations are given by Eq. 11. Perhaps a more meaningful relation for the angle $\theta$ results if one transforms the second of Eqs. 11 by the substitution $\alpha = -f'_t/f'_c$ to obtain

$$\sin\theta = \frac{1-\alpha}{1+\alpha}$$

From this equation it is obvious that as the ratio of tensile to compressive strength, $\alpha$, decreases angle $\theta$ increases. Thus it is seen that, contrary to Professor Cowan's implications, no significant desparity exists between the author's work and that of Balmer[2] or Richart, Brandtzaeg and Brown.[18] The author apologizes for the typographical error which appears on page 10, reference (54) should be reference (37).

Many thanks are due Messers Goschy and Balazas for their independent verification of the author's Eq. 14a which is so central to his entire theory of shear strength. Their use of the concept of "reduced stress" is very interesting and may have important applications in building code provisions and design procedures if the author's theories gain wider acceptance. It is believed that the questions raised in their remarks are fully answered elsewhere in this discussion.

In view of the questions raised concerning certain of the assumptions made by the author and as check on the validity of his theory, a further analysis is presented of the shear strength of beams reinforced with vertical stirrups. Eq. 36, which is based on an empirical expression developed by Laupa, Siess and Newmark,[31] gives the total shear resistance, $V_{tot}$, of a beam reinforced with vertical stirrups. An analytic expression for $V_{tot}$ which is very similar in form to Eq. 36 may be derived as follows.

Considering the free-body diagram of a portion of a beam reinforced with vertical stirrups shown in Fig. 16, the following assumptions may be made:

1) For the purposes of calculating ultimate strength, only the stirrups crossed by a diagonal-tension crack are effective in contributing to the shear resistance of the beam.

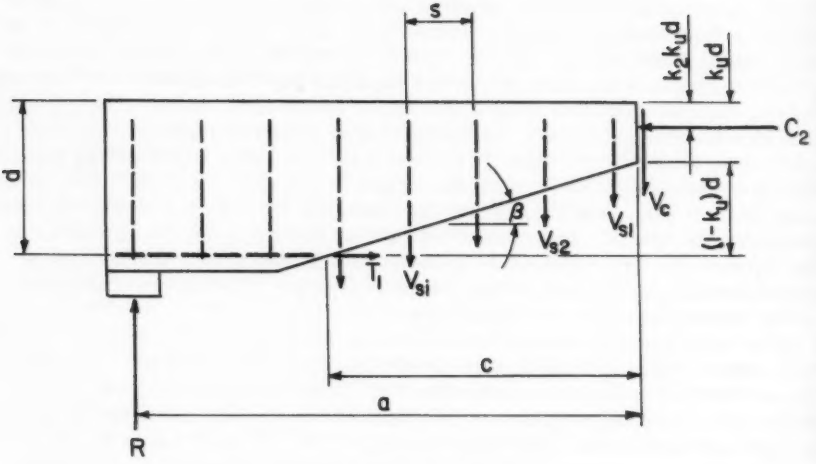


FIGURE 16

2) At failure the stress in the stirrups crossed by a diagonal-tension crack is equal to the yield stress of the steel.

If the free-body diagram shown in Fig. 16 is in equilibrium, then

$$R = V_{tot} = V_c + V_s \tag{38}$$

in which $V_C$ is the contribution to the shear resistance of the concrete and $V_S$ that of the stirrups. $V_S$ may also be written as

$$V_s = \sum_{i=1}^{n} V_{si} = nA_v f_{yw} \tag{39}$$

If the stirrups in the region crossed by a diagonal-tension crack are equally spaced, then

$$n = \frac{c}{s}$$

in which

$$c = (1 - k_u)\, d\, \cot\beta$$

Therefore,

$$n = \frac{(1 - k_u)\, d\, \cot\beta}{s} \tag{40}$$

Substituting n given by Eq. 40 into Eq. 39 an equation for $V_S$ is obtained

$$V_s = \frac{(1 - k_u)\, d\, \cot\beta}{s} A_v f_{yw} \tag{41}$$

or

$$V_s = \left[(1 - k_u)\, bd \cot\beta\right] r f_{yw} \tag{41a}$$

in which

$$r = \frac{A_v}{bs}$$

If the right-hand side of Eq. 41a is multiplied by the ratio $V_c/bk_u dv_c$ which is equal to unity, the equation for $V_S$ becomes

$$V_s = \frac{1 - k_u}{k_u} \cdot \frac{\cot\beta}{v_c}\, r f_{yw} V_c \tag{42}$$

If the angle $\beta$ is less than 45° (the usual case*), cot $\beta$ is greater than unity. Therefore a conservative estimate of $V_S$ results if cot$\beta$ is set equal to unity in Eq. 42. If this is done Eq. 42 becomes

$$V_s = \frac{1 - k_u}{k_u} \cdot \frac{r f_{yw}}{v_c} V_c \tag{43}$$

Substitution of $V_S$ given by Eq. 43 into Eq. 38 yields an equation for the shear resistance of a reinforced concrete beam

$$V_{tot} = \left(1 + \frac{1 - k_u}{k_u} \cdot \frac{r f_{yw}}{v_c}\right) V_c \tag{44}$$

Eq. 44 is seen to be remarkably similar to the empirically-derived Eq. 36

$$V_{tot} = \left(1 + \frac{2 r f_{yw}}{10^3}\right) V_c \tag{36}$$

One obvious advantage of Eq. 44 over Eq. 36 is that it is dimensionally correct.

Eq. 44 may be further simplified by substituting for the ratio $(1 - k_u)/k_u$ the quantity $\gamma$. If this is done Eq. 44 becomes

$$V_{tot} = \left(1 + \gamma \frac{r f_{yw}}{v_c}\right) V_c \tag{45}$$

In the usual case $k_u$ is less than 0.5 and therefore a conservative value for $\gamma$ is unity. In those unusual cases in which $k_u$ exceeds 0.5, Eq. 44 must be used to compute shear resistance. Or, in other words, Eq. 45 may always be used provided that

$$\gamma \leq \frac{1 - k_u}{k_u}$$

or,

$$\gamma \leq 1.0$$

whichever is the smaller.

*It is possible for angle $\beta$ to be greater than 45° but such will be the case if and only if the M/Vd ratio is less than about 2.5.

To demonstrate the validity of Eq. 45, ultimate strengths of the restrained beams reported in Table 2 are compared with values of predicted shear strength. The results of this comparison of test and theory are reported in Table-4. In addition, a comparison of test and theory for four new beam specimens,* whose properties are given in Table-3, are also reported in Table-4. Beams IIA-IM and IID-IM had plain webs while the other ten beams reported in Table-4 had web reinforcement consisting of equallyspaced vertical stirrups.

Table - 3

Properties of Series-M Beam Specimens

| Beam No. | L (ft.) | b* (ins.) | b'** (ins.) | d (ins.) | M/Vd | $f'_c$ (psi) | $f_r$ (psi) | $f_y$ (ksi) | Long. Reinf. | Web Reinf. |
|---|---|---|---|---|---|---|---|---|---|---|
| IIA-1M | 12.0 | 23.0 | 7.0 | 12.55 | 2.87 | 3898 | 390 | 92.2 | 2 - #7, 2 - #6 | |
| IIB-1M | | | | 12.63 | 2.85 | 3237 | 366 | 103.1 | 4 - #5 | #4 @ 3 - 1/2 |
| IIC-1M | | | | 12.46 | 2.89 | 4862 | 455 | 83.7 | 2 - #7, 2 - #10 | |
| IID-1M | | | | 12.55 | 2.87 | 4493 | 461 | 92.2 | 2 - #7, 2 - #6 | #4 @ 3 - 1/2 |

* Flange Width of Tee-Beam

** Stem Width of Tee-Beam

Table - 4

Comparison of Beam Test Results with Theory

| Beam No. | Test Results | | Results of Calculation | | | | | | | | | % Error = $\frac{V_u - V'}{V'} \times 100\%$ |
|---|---|---|---|---|---|---|---|---|---|---|---|---|
| | $V_u$ (kips) | Type Failure | $V_f$ (kips) | $\alpha$ | $k_p$ | $V_c$ (kips) | $\frac{rfyv}{v_s}$ | $\gamma$ | $V_{tot}$ (kips) | Pred. Type Failure | V' (kips) | (%) |
| IIA-1 | 58.0 | DT | 52.53 | 1/20.5 | 5.30 | 16.04 | 2.081 | 0.835 | 43.92 | shear | 43.92 | + 24.3 |
| -2 | 30.8 | DT | 52.44 | 1/16.0 | 4.19 | 15.32 | 0.851 | .814 | 25.94 | shear | 25.94 | + 15.8 |
| IIB-1 | 44.2 | DT | 30.47 | 1/15.8 | 4.03 | 14.29 | 2.406 | .783 | 41.21 | flex. | 30.47 | + 11.1 |
| -2 | 25.4 | DT | 31.39 | 1/15.8 | 4.14 | 14.76 | 0.903 | .783 | 25.20 | shear | 25.20 | + 0.8 |
| IIC-1 | 91.2 | DT | 88.58 | 1/22.7 | 5.99 | 24.81 | 1.293 | .904 | 53.81 | shear | 53.81 | + 41.0 |
| -2 | 40.8 | DT | 92.33 | 1/22.7 | 6.21 | 25.67 | 0.489 | .904 | 37.02 | shear | 37.02 | + 9.3 |
| IID-1 | 71.0 | DT&FT | 55.17 | 1/22.7 | 6.04 | 24.40 | 1.293 | .942 | 54.12 | shear | 54.12 | + 23.8 |
| -2 | 40.5 | DT | 56.33 | 1/22.7 | 6.18 | 24.89 | 0.489 | .942 | 36.36 | shear | 36.36 | + 10.2 |
| IIA-1M | 19.1 | DT | 59.9 | 1/20.0 | 5.73 | 18.24 | | | 18.24 | shear | 18.24 | + 4.5 |
| IIB-1M | 53.3 | FT | 41.2 | 1/17.7 | 5.04 | 17.04 | 2.320 | .984 | 55.94 | flex. | 41.2 | + 22.7 |
| IIC-1M | 22.7 | DT | 93.3 | 1/21.3 | 5.89 | 24.45 | | | 24.45 | shear | 24.45 | - 7.7 |
| IID-1M | 77.9 | FT | 60.6 | 1/19.5 | 5.47 | 23.43 | 1.723 | .931 | 61.01 | flex. | 60.6 | + 22.2 |

*These specimens are designated as series-M beams.

It may be observed in Table 4 that the theory correctly predicts the mode of failure in all but one case. The exception is beam IIB-1 which had a low computed flexural strength, $V_f$. Beams IIB-1M and IID-1M which failed in flexure also had low computed flexural strengths. This underestimation of flexural strength was due to the fact that the tensile reinforcing steel used* had little or no "yield plateau" and entered the strain hardening range almost immediately upon reaching its yield stress. The flexural strength calculations were, of course, simply based on attaining the yield stress in the tensile steel at failure and they did not reflect any extra strength which might occur if tensile steel stresses progressed into the strain hardening range.

Considering all beams other than the three mentioned above, the extreme right-hand column of Table-4 shows that the theory is conservative in all but one case. Furthermore, in six of the beams which failed in shear the percent error between test and theory confined to the range - 7.7% to + 15.8%. In the remaining three beams the percent error is rather high, approximately + 24% in two beams and + 41% in the third beam. Since the theory errs on the conservative side in these cases and since these results may have been affected by errors in experimental technique, it is believed that these last three beams do not cast any serious doubt as to the general validity of the author's theories.

In conclusion the author feels that a promising analytical approach to the problem of predicting the shear strength of reinforced concrete beams has been initiated. Much further analytical and experimental work remains to be done; however, it is believed that at the very least the theories developed herein comprise a rational point of departure for future research.

*All beams were reinforced with high-strength alloy steel deformed bars having a nominal yield point of 80,000 psi.

# STRENGTH OF RIVETS AND BOLTS IN TENSION[a]

Discussion by W. R. Penman and E. F. Ball

W. R. PENMAN[1] and E. F. BALL,[2] F. ASCE.—The authors are to be congratulated on another fine report in a long series dealing with the study of fasteners. It is stated that some design specifications still prohibit the use of structural connections which are subjected to direct tensile loads. We understand that there are now only a few structural specifications which do not sanction the use of rivets and bolts, or either, in connections subject to tension. Bolts in tension probably are used in greater quantities in structures, such as in multi-story buildings, than anywhere else. Multi-story buildings, and others, have used rivets in tension before the event of the high-strength bolt, and are still doing so.

There are many applications of bolts which are used in tension, for example the flange bolts or studs in high-pressure and high-temperature piping systems; cylinder-head studs in engines and many others in use for many years.

It is stated that the cross-sectional area of a driven 3/4" diameter rivet is about 0.518 sq. in. compared to the stress area of a 3/4" bolt being 0.334 sq. in., and that lower strength rivets may develop a load-carrying capacity approaching that of high-strength bolts. This rivet area is based on a 3/4" rivet completely filling a 13/16" hole when hot driven. This condition is only true in cases of very short grip lengths, and even then it is dependent on the human element in driving any particular rivet. Design would require the use of the area of the nominal diameter of the rivet, i.e., 0.442 sq. in. for a 3/4" rivet.

It is noted that nut stripping failure occurred in some of the tests and we feel it should be pointed out that the American Society of Testing Materials took steps in 1957 to increase the nut proof load and that the current A.S.T.M. Spec. A325-58T now requires the minimum nut stripping values to be approximately 25% higher than those of the minimum bolt strength values.

a. Proc. Paper 1970, March, 1959, by Munse, Petersen and Chesson.
1. Bethlehem Steel Co., Bethlehem, Pa.
2. Bethlehem Steel Co., Bethlehem, Pa.

# SHORT FLEXIBLE SUSPENSION BRIDGES FOR HEAVY TRUCKS[a]

## Discussion by A. A. Eremin

A. A. EREMIN,[1] M. ASCE.—The author has stated that heavy truck loading produces a large, around 30 inches, deflection. However, Mr. Asplund stated that the trucks are easily overcoming the resulting heavy grades and also that the truck drivers do not notice the heavy grades. Yet, Mr. Asplund then stated that "the translations and rotations in deck structure need considerable attention."

It would be interesting to know more about the cost of continuous inspection and maintenance of the deck structure, details of their original condition, and the cost of regulating the traffic across the bridge.

For the cast of short span suspension bridges considerable study was made of methods of reducing the live load deflections. In Figs. 30 (a) and (b) are

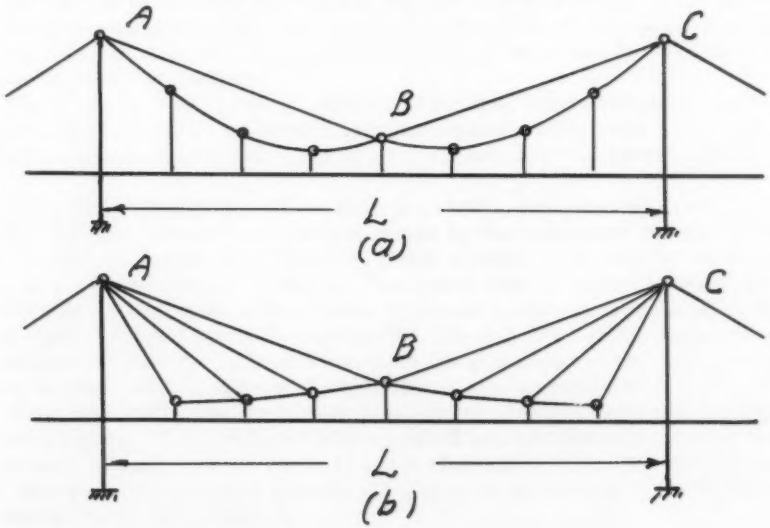


FIG. 30.

By AA Eremin.
8/25/59

a. Proc. Paper 2004, April, 1959, by Sven Olof Asplund.

1. Assoc. Bridge Engr., Bridge Dept., California State Highways, Sacramento, Calif.

shown short span suspension bridges in which the moving live load deflections are reduced by hinges and tie rods. Dead load at hinge B, Figs. 30 (a) and (b) may eliminate the negative live load deflection at that section. Furthermore, the height of towers in the suspension bridges in Figs. 30 (a) and (b) may also be reduced to a minimum.

The economic value of short span suspension bridges is important. Therefore, the author has made a valuable contribution by showing details and design method of a typical suspension bridge used in Swedish hydro-electric plants.

# ANALYSIS OF TWO-COLUMN SYMMETRICAL BENTS[a]

Discussions by O. A. Glogau, M. L. Pei, and Michael Jordan

O. A. GLOGAU[1].—Mr. Cooke has presented an interesting method which has been found very useful in practice. He does not appear to be aware however that an almost identical method was published by N. Naylor in the "Structural Engineer" London, April, 1950.

In addition to the cases dealt with by Mr. Cook, Naylor applied the method to a Vierendeel girder with similar top and bottom chords.

Further papers on this subject have appeared in German publications, the most interesting being one by G. Ehlers and published in "Beton u. Stahlbeton" Jan. 1957. Ehlers shows how a multibay, multistorey frame can be dealt with by an equivalent two column symmetrical bent provided the column stiffnesses are in a certain ratio, which is a function of the beam stiffnesses. This ratio (but not necessarily the sizes of members) must be constant for all storeys. In practice particularly with concrete buildings this ratio can easily be obtained.

There are of course a large number of building frames where an approximate analysis leads to sufficiently accurate results when seen in the light of uncertainties in lateral loads and of other factors such as uneven settlement.

M. L. PEI,[2] M. ASCE.—The author presented some numerical examples of two-column symmetrical bents analysed by the Cantilever Moment Distribution Method of Grinter and Tsao.(1) There appears to be nothing essentially new in the present paper. That the Cantilever Moment Distribution Method is applicable only to symmetrical bents subjected to anti-symmetrical loadings was clearly pointed out by the writer.(2) The extension of the method to unsymmetrical loadings by first separating the given loading to a symmetrical part, together with a numerical example was also pointed out by the writer.(2)

When applicable, the Cantilever Moment Distribution Method is the fastest method known. The popularity of the method will undoubtedly increase with time as it becomes better known to the profession at large. In order to avoid its misuse, it is important to state the following limitations of the Cantilever Moment Distribution Method:

1. The structure must be symmetrical.
2. The loading must be anti-symmetrical.
3. The structure must be a two-column bent, or a two-chord Vierendeel truss. In other words, a section across the structure, taken normal to

a. Proc. Paper 2037, May, 1959, by B. R. Cooke.

1. Ministry of Works, Wellington, N. Z.
2. Associate Prof., The City College of New York, New York, N. Y.

the axis of symmetry, must not cut more than two members of the structure.

The last limitation is inherent in the derivation of the Cantilever Moment Distribution Method. As far as I know, it has never been clearly stated in any published paper before.

## REFERENCES

1. "Joint Translation by Cantilever Moment Distribution," by L. E. Grinter and C. H. Tsao, Transactions, ASCE, Vol. 119, p. 1145, 1954.
2. Discussion of "Joint Translation by Cantilever Moment Distribution," by M. L. Pei, Transactions, ASCE Vol. 119, 1954, p. 1208.

MICHAEL JORDAN,[1] A.M. ASCE.—One of the examples in the paper treats the problem of applying the Cantilever Moment Distribution method to bents having variable moments of inertia. The author determines the modified stiffness by equating the M/EI diagram equal to unity. Where the members are haunched or otherwise tapered the expression for the area under the M/EI diagram will become more involved.

A method for determining the modified stiffness of any member can be developed using only the ordinary Moment Distribution constants. Let $K'_{AB}$ equal the modified stiffness of member AB.

The following relationship is well known.

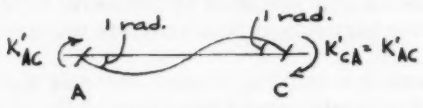


$$\frac{K'_{AC}}{K_{AC}} = 1 + C_{AC}$$

A similar relationship exists for the columns.

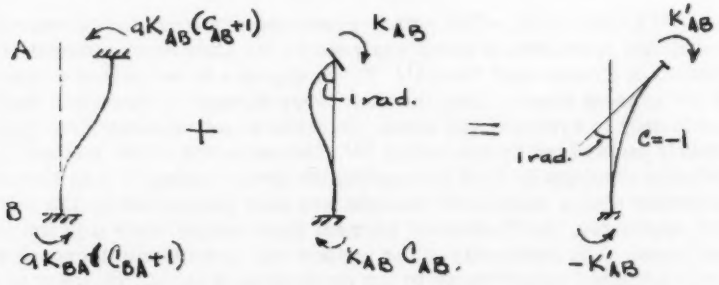


At A: $K'_{AB} = -aK_{AB}(C_{AB}+1) + K_{AB}$

At B: $-K'_{AB} = -aK_{BA}(C_{BA}+1) + K_{AB}C_{AB}$

Since $K_{AB}C_{AB} = K_{BA}C_{BA}$

1. Designer, H. M. O'Neil Co., Oakland, Calif.

$$a = \frac{1 + C_{AB}}{2C_{AB} + 1 + \frac{K_{BA}}{K_{AB}}}$$

So:

$$\boxed{\frac{K'_{AB}}{K_{AB}} = 1 - a(C_{AB} + 1)}$$

The coefficient "a" can also be used to determine fixed end moments for a given Story Moment, $M_{St}$.

$$M_{fAB} = a \cdot \frac{M_{St}}{2}$$

$$M_{fBA} = (1-a)\frac{M_{St}}{2}$$

## PROCEEDINGS PAPERS

The technical papers published in the past year are identified by number below. Technical-division sponsorship is indicated by an abbreviation at the end of each Paper Number, the symbols referring to: Air Transport (AT), City Planning (CP), Construction (CO), Engineering Mechanics (EM), Highway (HW), Hydraulics (HY), Irrigation and Drainage (IR), Pipeline (PL), Power (PO), Sanitary Engineering (SA), Soil Mechanics and Foundations (SM), Structural (ST), Surveying and Mapping (SU), and Waterways and Harbors (WW), divisions. Papers sponsored by the Department of Conditions of Practice are identified by the symbols (PP). For titles and order coupons, refer to the appropriate issue of "Civil Engineering." Beginning with Volume 82 (January 1956) papers were published in Journals of the various Technical Divisions. To locate papers in the Journals, the symbols after the paper number are followed by a numeral designating the issue of a particular Journal in which the paper appeared. For example, Paper 1859 is identified as 1859 (HY7) which indicates that the paper is contained in the seventh issue of the Journal of the Hydraulics Division during 1958.

### VOLUME 84 (1958)

OCTOBER: 1790(EM4), 1791(EM4), 1792(EM4), 1793(EM4), 1794(EM4), 1795(HW3), 1796(HW3), 1797(HW3), 1798(HW3), 1799(HW3), 1800(HW3), 1801(HW3), 1802(HW3), 1803(HW3), 1804(HW3), 1805(HW3), 1806(HY5), 1807(HY5), 1808(HY5), 1809(HY5), 1810(HY5), 1811(HY5), 1812(SM4), 1813(SM4), 1814(ST6), 1815(ST6), 1816(ST6), 1817(ST6), 1818(ST6), 1819(ST6), 1820(ST6), 1821(ST6), 1822(EM4), 1823(PO5), 1824(SM4), 1825(SM4), 1826(SM4), 1827(ST6)[c], 1828(SM4)[c], 1829(HW3)[c], 1830(PO5)[c], 1831(EM4)[c], 1832(HY5)[c].

NOVEMBER: 1833(HY6), 1834(HY6), 1835(SA6), 1836(ST7), 1837(ST7), 1838(ST7), 1839(ST7), 1840(ST7), 1841(ST7), 1842(SU3), 1843(SU3), 1844(SU3), 1845(SU3), 1846(SU3), 1847(SA6), 1848(SA6), 1849(SA6), 1850 (SA6), 1851(SA6), 1852(SA6), 1853(SA6), 1854(ST7), 1855(SA6)[c], 1856(HY6)[c], 1857(ST7)[c], 1858(SU3)[c].

DECEMBER: 1859(HY7), 1860(IR4), 1861(IR4), 1862(IR4), 1863(SM5), 1864(SM5), 1865(ST8), 1866(ST8), 1867 (ST8), 1868(PP1), 1869(PP1), 1870(PP1), 1871(PP1), 1872(PP1), 1873(WW5), 1874(WW5), 1875(WW5), 1876 (WW5), 1877(CP2), 1878(ST8), 1879(ST8), 1880(HY7)[c], 1881(SM5)[c], 1882(ST8)[c], 1883(PP1)[c], 1884(WW5)[c], 1885(CP2)[c], 1886(PO6), 1887(PO6), 1888(PO6), 1889(PO6), 1890(HY7), 1891(PP1).

### VOLUME 85 (1959)

JANUARY: 1892(AT1), 1893(AT1), 1894(EM1), 1895(EM1), 1896(EM1), 1897(EM1), 1898(EM1), 1899(HW1), 1900(HW1), 1901(HY1), 1902(HY1), 1903(HY1), 1904(HY1), 1905(PL1), 1906(PL1), 1907(PL1), 1908(PL1), 1909(ST1), 1910(ST1), 1911(ST1), 1912(ST1), 1913(ST1), 1914(ST1), 1915(ST1), 1916(AT1)[c], 1917(EM1)[c], 1918(HW1)[c], 1919(HY1)[c], 1920(PL1)[c], 1921(SA1)[c], 1922(ST1)[c], 1923(EM1), 1924(HW1), 1925(HW1), 1926 (PL1), 1927(HW), 1928(HW1), 1929(SA1), 1930(SA1), 1931(SA1), 1932(SA1).

FEBRUARY: 1933(HY2), 1934(HY2), 1935(HY2), 1936(SM1), 1937(SM1), 1938(ST2), 1939(ST2), 1940(ST2), 1941(ST2), 1942(ST2), 1943(ST2), 1944(ST2), 1945(HY2), 1946(PO1), 1947(PO1), 1948(PO1), 1949(PO1), 1950(HY2)[c], 1951(SM1)[c], 1952(ST2)[c], 1953(PO1)[c], 1954(CO1), 1955(CO1),1956(CO1),1957(CO1), 1958(CO1), 1959(CO1).

MARCH: 1960(HY3), 1961(HY3), 1962(HY3), 1963(IR1), 1964(IR1), 1965(IR1), 1966(IR1), 1967(SA2), 1968(SA2), 1969(ST3), 1970(ST3), 1971(ST3), 1972(ST3), 1973(ST3), 1974(ST3), 1975(ST3), 1976(WW1), 1977(WW1), 1978(WW1), 1979(WW1), 1980(WW1), 1981(WW1), 1982(WW1), 1983(WW1), 1984(SA2), 1985(SA2)[c], 1986 (IR1)[c], 1987(WW1)[c], 1988(ST3)[c], 1989(HY3)[c].

APRIL: 1990(EM2), 1991(EM2), 1992(EM2), 1993(HW2), 1994(HY4), 1995(HY4), 1996(HY4), 1997(HY4), 1998 (SM2), 1999(SM2), 2000(SM2), 2001(SM2), 2002(ST4), 2003(ST4), 2004(ST4), 2005(ST4), 2006(PO2), 2007 (HW2)[c], 2008(EM2)[c], 2009(ST4)[c], 2010(SM2)[c], 2011(SM2)[c], 2012(HY4)[c], 2013(PO2)[c].

MAY: 2014(AT2), 2015(AT2), 2016(AT2), 2017(HY5), 2018(HY5), 2019(HY5), 2020(HY5), 2021(HY5), 2022(HY5), 2023(PL2), 2024(PL2), 2025(PL2), 2026(PP1), 2027(PP1), 2028(PP1), 2029(PP1), 2030(SA3), 2031(SA3), 2032(SA3), 2033(SA3), 2034(ST5), 2035(ST5), 2036(ST5), 2037(ST5), 2038(PL2), 2039(PL2), 2040(AT2)[c]. 2041(PL2)[c], 2042(PP1)[c], 2043(ST5)[c], 2044(SA3)[c], 2045(HY5)[c], 2046(PP1), 2047(PP1).

JUNE: 2048(CP1), 2049(CP1), 2050(CP1), 2051(CP1), 2052(CP1), 2053(CP1), 2054(CP1), 2055(CP1), 2056 (HY6), 2057(HY6), 2058(HY6), 2059(IR2), 2060(IR2), 2061(PO3), 2062(SM3), 2063(SM3), 2064(SM3), 2065 (ST6), 2066(WW2), 2067(WW2), 2068(WW2), 2069(WW2), 2070(WW2), 2071(WW2), 2072(CP1)[c], 2073(IR2)[c], 2074(PO3)[c], 2075(ST6)[c], 2076(HY6)[c], 2077(SM3)[c], 2078(WW2)[c].

JULY: 2079(HY7), 2080(HY7), 2081(HY7), 2082(HY7), 2083(HY7), 2084(HY7), 2085(HY7), 2086(SA4), 2087 (SA4), 2088(SA4), 2089(SA4), 2090(SA4), 2091(EM3), 2092(EM3), 2093(EM3), 2094(EM3), 2095(EM3), 2096 (EM3), 2097(HY7)[c], 2098(SA4)[c], 2099(EM3)[c], 2100(AT3), 2101(AT3), 2102(AT3), 2103(AT3),2104(AT3), 2105(AT3), 2106(AT3), 2107(AT3), 2108(AT3), 2109(AT3), 2110(AT3), 2111(AT3), 2112(AT3),2113(AT3), 2114(AT3), 2115(AT3), 2116(AT3), 2117(AT3), 2118(AT3), 2119(AT3), 2120(AT3), 2121(AT3),2122(AT3), 2123(AT3), 2124(AT3), 2125(AT3).

AUGUST: 2126(HY8), 2127(HY8), 2128(HY8), 2129(HY8), 2130(PO4), 2131(PO4), 2132(PO4), 2133(PO4),2134 (SM4), 2135(SM4), 2136(SM4), 2137(SM4), 2138(HY8)[c], 2139(PO4)[c] 2140(SM4)[c].

SEPTEMBER: 2141(CO2),2142(CO2),2143(CO2),2144(HW3),2145(HW3), 2146(HW3), 2147(HY9), 2148(HY9), 2149(HY9),2150(HY9),2151(IR3), 2152(ST7)[c], 2153(IR3), 2154(IR3), 2155(IR3), 2156(IR3), 2157(IR3), 2158 (IR3),2159(IR3),2160(IR3),2161(SA5),2162(SA5),2163(ST7),2164(ST7), 2165(SU1), 2166(SU1),2167(WW3), 2168(WW3), 2169(WW3), 2170(WW3), 2171(WW3), 2172(WW3), 2173(WW3), 2174(WW3), 2175(WW3), 2176 (WW3), 2177(WW3), 2178(CO2)[c], 2179(IR3)[c], 2180(HW3)[c], 2181(SA5)[c], 2182(HY9)[c], 2183(SU1)[c], 2184 (WW3)[c], 2185(PP2)[c], 2186(ST7)[c], 2187(PP2), 2188(PP2).

OCTOBER: 2189(AT4), 2190(AT4), 2191(AT4), 2192(AT4), 2193(AT4), 2194(EM4), 2195(EM4), 2196(EM4), 2197(EM4), 2198(EM4), 2199(EM4), 2200(HY10), 2201(HY10), 2202(HY10), 2203(PL3), 2204(PL3), 2205 (PL3), 2206(PO5), 2207(PO5), 2208(PO5), 2209(PO5), 2210(SM5), 2211(SM5), 2212(SM5), 2213(SM5), 2214 (SM5), 2215(SM5), 2216(SM5), 2217(SM5), 2218(ST8), 2219(ST8), 2220(EM4), 2221(ST8), 2222(ST8), 2223 (ST8), 2224(HY10), 2225(HY10), 2226(PO5), 2227(PO5), 2228(PO5), 2229(ST8), 2230(EM4), 2231(EM4), 2232(AT4)[c], 2233(PL3)[c], 2234(EM4)[c], 2235(HY10)[c], 2236(SM5)[c], 2237(ST8)[c], 2238(PO5)[c], 2239(ST8), 2240 (PL3).

c. Discussion of several papers, grouped by divisions.

# AMERICAN SOCIETY OF CIVIL ENGINEERS

## OFFICERS FOR 1959

### PRESIDENT

FRANCIS S. FRIEL

### VICE-PRESIDENTS

*Term expires October, 1959:*
WALDO G. BOWMAN
SAMUEL B. MORRIS

*Term expires October, 1960:*
PAUL L. HOLLAND
LLOYD D. KNAPP

### DIRECTORS

*Term expires October, 1959:*
CLINTON D. HANOVER, Jr.
E. LELAND DURKEE
HOWARD F. PECKWORTH
FINLEY B. LAVERTY
WILLIAM J. HEDLEY
RANDLE B. ALEXANDER

*Term expires October, 1960:*
PHILIP C. RUTLEDGE
WESTON S. EVANS
TILTON E. SHELBURNE
CRAIG P. HAZELET
DONALD H. MATTERN
JOHN E. RINNE

*Term expires October, 1961:*
THOMAS J. FRATAR
EARL F. O'BRIEN
DANIEL B. VENTRES
CHARLES W. BRITZIUS
WAYNE G. O'HARRA
FRED H. RHODES, JR.
N. T. VEATCH

### PAST PRESIDENTS

*Members of the Board*

MASON G. LOCKWOOD

LOUIS R. HOWSON

---

### EXECUTIVE SECRETARY

WILLIAM H. WISELY

### ASSISTANT SECRETARY

E. LAWRENCE CHANDLER

### ASSISTANT TREASURER

ENOCH R. NEEDLES

---

# PROCEEDINGS OF THE SOCIETY

HAROLD T. LARSEN
*Manager of Technical Publications*

PAUL A. PARISI
*Editor of Technical Publications*

MARVIN SCHECHTER
*Assistant Editor of Technical Publications*

---

### COMMITTEE ON PUBLICATIONS

HOWARD F. PECKWORTH, *Chairman*

PHILIP C. RUTLEDGE, *Vice-Chairman*

E. LELAND DURKEE
TILTON E. SHELBURNE
CHARLES W. BRITZIUS
FRED H. RHODES, JR.